



BÁRBARA OLINDA NARDIS

**CATION-MODIFIED BIOCHARS TO REMOVE PHOSPHATE
FROM AQUEOUS SOLUTION AND THEIR AGRONOMIC
VALUE**

LAVRAS – MG

2020

BÁRBARA OLINDA NARDIS

**CATION-MODIFIED BIOCHARS TO REMOVE PHOSPHATE FROM AQUEOUS
SOLUTION AND THEIR AGRONOMIC VALUE**

Thesis presented to the Federal University of Lavras, as part of the requirements of the graduate program in Soil Science, area of concentration in Soil Fertility and Plant Nutrition, to earn the title of Doctor.

Prof. Dr. Leônidas Carrijo Azevedo Melo

Advisor

Prof. Dr. Luiz Roberto Guimarães Guilherme

Co-advisor

LAVRAS-MG

2020

**Ficha catalográfica elaborada pelo Sistema de Geração de Ficha Catalográfica da Biblioteca
Universitária da UFLA, com dados informados pelo(a) próprio(a) autor(a).**

Nardis, Bárbara Olinda.

Cation-modified biochars to remove phosphate from aqueous
solution and their agronomic value / Bárbara Olinda Nardis. - 2020.
118 p. : il.

Orientador(a): Leônidas Carrijo Azevedo Melo.

Coorientador(a): Luiz Roberto Guimarães Guilherme.

Tese (doutorado) - Universidade Federal de Lavras, 2020.

Bibliografia.

1. Recovery phosphorus. 2. engineered-biochar. 3. modified
biochar. I. Melo, Leônidas Carrijo Azevedo. II. Guilherme, Luiz
Roberto Guimarães. III. Título.

BÁRBARA OLINDA NARDIS

**CATION-MODIFIED BIOCHARS TO REMOVE PHOSPHATE FROM AQUEOUS
SOLUTION AND THEIR AGRONOMIC VALUE**

Thesis presented to the Federal University of Lavras, as part of the requirements of the graduate program in Soil Science, area of concentration in Soil Fertility and Plant Nutrition, to earn the title of Doctor.

APPROVED in 28 August 2020.

Dr. Carlos Alberto Silva	UFLA
Dr. Guilherme Lopes	UFLA
Dr. Jairo Tronto	UFV
Dr. Luís Reynaldo Ferracciú Alleoni	ESALQ/USP

Dr. Leônidas Carrijo Azevedo Melo
Advisor

**LAVRAS – MG
2020**

*Aos meus pais, Wilian e Léia, aos irmãos Kika e Juninho, á minha sobrinha Sophie às avós
Célia e Olinda (in memoria).*

Dedico

AGRADECIMENTOS

Agradeço primeiramente a Deus por ter iluminado o meu caminho, não ter me deixado desistir nos momentos difíceis e me mostrar que quando há fé, perseverança e trabalho a vitória é certa.

À UFLA, instituição a qual tenho muito orgulho de ter feito parte, pela minha formação acadêmica e toda a estrutura necessária para que eu pudesse realizar a pesquisa. Ao Programa de Pós-Graduação em Ciência do Solo e a todos os professores que contribuíram para a minha formação como profissional e como pessoa. À Coordenação de Aperfeiçoamento de Pessoal de Nível Superior (CAPES) pela concessão da bolsa de doutorado. Ao Conselho Nacional de Desenvolvimento Científico e Tecnológico (CNPq) e à Fundação de Apoio à Pesquisa de Minas Gerais (FAPEMIG) pelo subsídio financeiro.

Ao meu orientador professor Leônidas Melo, pelo apoio, paciência, generosidade e colaboração em todos os momentos. Professor, foi um prazer tê-lo como orientador e muito obrigado pelas inúmeras lições. Agradeço também a Patrícia e João Gabriel pela amizade e carinho, vocês são meu exemplo profissional e pessoal.

Aos membros da banca examinadora, composta Dr. Carlos Alberto Silva, Dr. Guilherme Lopes, Dr. Jairo Tronto, Dr. Luís Alleoni e Dr. Leônidas Melo pela disponibilidade para participar, pelas contribuições dadas e pela extrema competência na avaliação desta tese. Ao meu co-orientador Bebeto pela ajuda sempre que solicitado e por todo incentivo durante esse período.

Agradeço muito ao professor Alfredão (*in memoria*) pelo carinho, amizade e por ter tido a oportunidade de aprender tanto com o senhor. Obrigada por todos os momentos que nos incentivou a buscarmos o conhecimento e darmos o melhor de nós.

A todo corpo docente do DCS-UFLA por todos os ensinamentos dentro e fora da sala de aula. Aos funcionários do DCS - Mari, Lívia, Geila, Roberto, João Gualberto, Alexandre, José Roberto (Pezão), Márcio, Humberto, Carlinhos, Téo e Dulce pela amizade, espírito de solidariedade, presteza e contribuição na realização das análises, e às secretárias Dirce, Maria Alice, Riqueline e Regina que, sempre atenciosas e cordiais, fazem um eficiente trabalho.

Agradeço imensamente o professor Dean Hesterberg por toda ajuda e tudo que aprendi com você. E a North Carolina State University por terem me recebido com muito carinho e pela

experiência maravilhosa de conhecer outra cultura. Aos amigos que fiz nesse período e que me acolheram com muito carinho Juliana, Rafael, Jú, Thais e Pedro.

Aos meus pais, Wilian e Léia que por muitas vezes deixaram de realizar seus sonhos para que eu pudesse concretizar os meus, pelo amor incondicional, pelos ensinamentos e conselhos valiosos e por acreditarem sempre em mim. Agradeço, também, aos meus irmãos Kika e Juninho pelo apoio e incentivo. Minha sobrinha que é o amor da minha vida Sophie por alegrar meus dias. Minha cunhada Marcella, por toda torcida e apoio. Às minhas tias e tios, primos e primas, pela contribuição que deram de alguma maneira para minha formação, especialmente à minha vizinha Célia pelo carinho e amor.

Ao meu marido Fabrício, pelo amor, apoio e companheirismo dedicados a mim e por participar dos momentos mais importantes da minha vida. Obrigada por me acalmar quando me desesperava e por sempre me incentivar a buscar o meu melhor. Agradeço, também, a minha sogra pela torcida e amizade.

A todos os meus amigos, que sempre levarei no coração. Em especial Lari, Thalitinha, Padovani, Ana Cláudia, Mari, Dida, Thalita, Gabi, Kelly, Keyla, Anelisa, Ana Luisa, Vinícius, Carol, Luana, Gislayne, Maria Cecília, Angélica, Uidemar e Abraão. Às amigas Lúcia e Helen por tornarem meu convívio cada dia mais agradável, vocês são demais. Aos meus irmãos do MUR, em especial àqueles no qual pude servir ao lado no GPP Fê, Dui, Maria Rita, Larissa, Bianca, Rafa, Guilherme, Lermem, Mabel e suas crianças, Pacelli, Saulinho, Erica, Maju, Joyce e Alice. Também agradeço a todos os meus amigos do GETAFS - Jefferson, Cris, Aline, Evanise, Alvaro, Isabella, Renato, Dehon, Gustavo e Ivan por toda ajuda, risadas e momentos que nunca serão esquecidos. Aos colegas da salinha e do DCS Soraya, Flávia, Franklin, Damy, Fábio, Sara, Samara, Corguinha, Cyntia, Bruno, Ferreira, Anita, Serginho, Monna Lysa, Aline, Fran, Márcio, Jaqueline, Mariana, Marisângela, César, Leonardo, Gilson, Ediu.

Aos meus pupilos e companheiros do NECS por toda confiança, aprendizado e o oportunidade de poder crescer junto com vocês, em especial João Renato, Mariany, Maria Vitória, Wesley, Thiago, Amanda, Alan, Arthur, Pará, Bia e tantos outros que passaram por esse núcleo maravilhoso.

De modo geral, agradeço a todos que me ajudaram na realização deste sonho, e peço desculpas àqueles cujos nomes não citei, pois não são menos importantes. Enfim, a todos que, direta e indiretamente, contribuíram para a conclusão desta importante caminhada.

EPÍGRAFE

Sonhem, sonhem alto [...]
O que torna um sonho irrealizável
Não é o sonho em si.
Mas a inércia de quem sonha.
Não sejam inertes!
Aldredo Scheid Lopes

RESUMO GERAL

A recuperação de fósforo (P) a partir de resíduos e águas residuárias é uma necessidade crescente no cenário atual. Nesse contexto, o uso de biocarvão modificado com cátions como adsorventes é de suma relevância. Tal tecnologia de modificação de biochar pode ser empregada a partir de diversas matérias-primas e deve ser estudada. Os objetivos desse trabalho foram: i) estudar diferentes biomassas impregnadas com magnésio (Mg^{2+}) para recuperar P de solução aquosa e seu potencial uso como fertilizante; ii) avaliar a impregnação com cátions (Mg^{2+} , Fe^{3+} e Al^{3+}) e métodos de produção (forno mufla e forno vertical com fluxo de N_2) na adsorção de P e características físicas e químicas dos biocarvões; e iii) realizar a especiação de P adsorvida no biochar modificado com cátions, usando a espectroscopia de absorção de raios X (XAS). No primeiro estudo, biocarvões foram produzidos por pirólise lenta a $500\text{ }^\circ\text{C}$ a partir de cama de frango (BCF), esterco de suínos (BES) e lodo de esgoto (BLE), impregnados com $\pm 10\%$ de magnésio Mg^{2+} no biocarvão. Esses materiais foram caracterizados e a capacidade de sorver P foi estudada. Posteriormente, avaliou-se a eficiência dos biocarvões em reter e liberar o P. BES e BCF impregnados com Mg e carregados com P apresentaram potencial para serem reutilizados como fertilizantes fosfatados; suas eficiências foram iguais ou superiores ao TSP no cultivo de milho em curto prazo, além de melhorar a fertilidade do solo para novos cultivos. Em outro estudo, o esterco de suíno foi impregnado com $\pm 20\%$ de Mg^{2+} , alumínio (Al^{3+}) e ferro (Fe^{3+}) e produzido sob dois métodos de preparo (forno mufla e forno vertical sob fluxo de N_2). Foi realizada uma caracterização físico-química detalhada e foi feito um estudo da capacidade de adsorção e liberação de P a partir de solução aquosa. O BES impregnado com 20% de Mg e produzido em forno mufla apresentou a maior sorção de P (231 mg g^{-1} , isoterma de SIPS) quando comparado aos materiais impregnados com Al e Fe. O biocarvão modificado com Fe apresentou a menor capacidade de adsorção de P, não possibilitando a modelagem da adsorção. Os métodos de produção (mufla - baixo O_2 ou forno sob N_2) não tiveram influência significativa nas características que regem a adsorção, como grupos funcionais, área superficial, quantidade e tamanho dos poros e formação de minerais. Por fim, os biocarvões modificados com cátions e carregados com P foram analisados por espectroscopia de absorção de raios X na região próxima à borda de absorção do P (XANES). No biocarvão não impregnado com cátions, os fosfatos de cálcio (P-Ca) foram as principais espécies químicas, predominando a hidroxiapatita. Já nos biocarvões impregnados com Al houve predomínio de compostos P-Al e o mesmo foi observado para Fe, ou seja, predominaram as espécies de P-Fe. Por outro lado, para o biocarvão impregnado com Mg, foram identificadas as espécies de P-Mg, mas predominaram as espécies de P-Ca devido à quantidade de Ca no esterco de suíno e à facilidade de precipitação dos compostos P-Ca. O biocarvão modificado com Mg é mais recomendado para tratamento terciário para remoção de P em estações de tratamento de esgoto, devido à sua alevada capacidade de adsorção de P e potencial de desempenho como fertilizante fosfatado superior às fontes solúveis convencionais.

Palavras-chave: Recuperação de fósforo. Uso na agricultura. Fertilizante fosfatado. Caracterização. P-XANES. Biocarvão.

GENERAL ABSTRACT

Phosphorus (P) recovery from waste and wastewater is a growing need in the current and future scenarios. The emergence of adsorbents such as cation-modified biochar is a technology that can be used from different feedstocks. The objectives of this work were: i) to study different biomasses impregnated with magnesium (Mg^{2+}) to recover P from aqueous solution and its potential as a fertilizer; ii) to evaluate the impregnation with different cations (Mg^{2+} , Fe^{3+} and Al^{3+}) and production pyrolysis condition (muffle furnace and vertical furnace with N_2 flow) in the adsorption of P and physical and chemical characteristics of the biochars; and iii) to evaluate the speciation of P adsorbed in the cation-modified biochar, using X-ray absorption spectroscopy (XANES). In the first study, biochars were produced by slow pyrolysis at 500 °C from poultry litter (PLB), pig manure (PMB) and sewage sludge (SSB), impregnated with $\pm 10\%$ magnesium Mg^{2+} in the biochar. They were characterized and their adsorption capacity studied. Subsequently, the efficiency of biochars in retaining and releasing P was evaluated. The main results show that PMB and PLB impregnated with Mg and loaded with P had the potential to be reused as phosphate fertilizers; their efficiencies were equal to or greater than TSP in the short-term cultivation of maize, in addition to improving soil fertility for other cropping cycles. In another study, pig manure was impregnated with $\pm 20\%$ Mg^{2+} , aluminum (Al^{3+}) and iron (Fe^{3+}) and produced under two pyrolysis condition of preparation (muffle furnace and vertical furnace under N_2 flow). A detailed physical-chemical characterization was carried out and a study was made of the adsorption and release capacity of P from aqueous solution. PMB impregnated with 20% Mg and produced in a muffle furnace showed the highest adsorption of P (231 mg g^{-1} , SIPS isotherm) when compared to materials impregnated with Al and Fe. The biochar modified with Fe showed the lowest adsorption capacity of P not allowing the modeling of adsorption. The pyrolysis condition (muffle - low O_2 or furnace under N_2) had no significant influence on the characteristics that govern adsorption, such as functional groups, surface area, quantity and size of pores and formation of minerals. Finally, in another study the biochars modified with cations and loaded with P were analyzed by X-ray absorption near edge structure (XANES). The study indicated that in biochar not impregnated with cations, calcium phosphates (P-Ca) were the main chemical species, with a predominance of hydroxyapatite. In the biochar impregnated with Al, there was a predominance of P-Al compounds and the same was observed for Fe, that is, the species of P-Fe predominated. On the other hand, for the biochar impregnated with Mg, P-Mg species were identified, but the P-Ca species predominated due to the amount of Ca in the pig manure and the trend of precipitation of the P-Ca compounds over P-Mg compounds. The biochar modified with Mg is more recommended for tertiary treatment to remove P in sewage treatment plants, due to its high P adsorption capacity and performance potential as a phosphate fertilizer superior to conventional soluble sources.

Keywords: Phosphorus recovery. Use in agriculture. Phosphate fertilizer. Characterization. P-XANES. Biochar.

SUMMARY

LIST OF ABBREVIATIONS	11
FIRST PART	12
GENERAL INTRODUCTION	12
REFERENCES	14
SECOND PART – ARTICLES	16
CHAPTER 1	16
Phosphorus recover using magnesium-enriched biochar and its potential use as fertilizer	17
CHAPTER 2	52
Production of engineered-biochar under different pyrolysis conditions for phosphorus removal from aqueous solution	53
CHAPTER 3	94
Phosphorus removal from aqueous solution using cation-modified biochars and its speciation using P K-edge XANES spectroscopy	95
CONCLUDING REMARKS	117

LIST OF ABBREVIATIONS

- ANOVA - Analysis of variance
- ADP - Adenosine diphosphate
- ATP- adenosine triphosphate
- BET - Brunauer–Emmett–Teller method
- CAPES - Coordination for the Improvement of Higher Education Personnel
- CETENE - Northeast Strategic Technologies Center
- CNPq - National Council for Scientific and Technological Development
- EC- Electrical conductivity
- EDX- Energy-dispersive X-ray
- ESPP - European Sustainable Phosphorus Platform
- FAPEMIG - Foundation for Research of the State of Minas Gerais
- FTIR - Fourier transform infrared
- ICP-OES - Optical Emission Spectroscopy and Inductively Coupled Plasma
- LCF - Linear Combination Fitting
- LNLS - Brazilian Synchrotron Light Laboratory
- PLB - Poultry litter
- PMB - Pig manure
- PZC - Point of zero charge
- S_{BET} - Surface area method
- SEM - Scanning electron microscopy
- SSB - Sewage sludge
- SXS - Beamline X-Ray Absorption and Photoelectron Spectroscopy in the region of soft X-rays
- TOC - Total organic carbon
- TSP- Triple superphosphate
- XAS - X-ray absorption spectroscopy
- XANES - X-ray Absorption Near Edge Structure
- XRD - X-ray diffraction

FIRST PART

GENERAL INTRODUCTION

Phosphorus (P) is a nutrient for plants and animals. However, it can also cause a negative impact on the environment due to the excessive use of fertilizers, which through runoff or leaching can reach water bodies and cause eutrophication. The main source of P for fertilizer production is phosphate rocks, which are a finite resource. Thus, it is estimated that the demand for P fertilizers may exceed extraction in the next 100 to 120 years (called “peak P”), so there is a need to recycle this nutrient from other sources (CORDELL et al., 2009), such as organic waste, sewage sludge, P-rich wastewaters, etc.

The main existing technologies to recycle P from wastewater are precipitation, adsorption, and biological removal. Precipitation is widely used, and P can be precipitated in the form of struvite ($\text{MgNH}_4\text{PO}_4 \cdot 6\text{H}_2\text{O}$). Adsorption is considered to be the most effective method due to its high selectivity, easy operation, compact installations and reuse of the adsorbent (XIONG et al., 2011; LALLEY et al., 2015; LOGANATHAN et al., 2014).

A number of materials are used to adsorb P, such as montmorillonite (CHANG et al., 2016), zeolites (JIANG et al., 2013), pumice (KARIMAIAAN et al., 2013), iron oxides (GIMÉNEZ et al., 2007), red mud (YE et al., 2015), coir pith (KRISHNAN & HARIDAS, 2008), ash from coal burning in power plants (AGYEI, STRYDOM & POTGIETER, 2002; CHEN et al., 2007; CHO, OH & KIM, 2005), steel slag (BOUJELBEN et al., 2008), etc. Other materials used as adsorbent are biochars from different residues, which can adsorb toxic elements and nutrients (e.g. P). The main advantages of biochars are low cost to obtain, reuse of waste, good stability in the environment, high porosity, easy preparation and operation (TAN et al., 2015; JEONG, DODLA & WANG, 2016). They can also influence the cycling of nutrients acting on the biological, physical and chemical processes of the soil (LAIRD et al., 2010; BIEDERMAN & HARPOLE, 2013).

Negative charges predominate on the biochar surface due to the high pH value and the presence of oxygenated groups, which results in a low recovery capacity of P (H_2PO_4^- or HPO_4^{2-}) from aqueous solutions (ZENG et al., 2013; TAKAYA et al., 2016; SHEPHERD et al., 2017). An interesting alternative to improve the P removal capacity is the impregnation with cations in the feedstock and subsequent pyrolysis or post-pyrolysis treatment. This creates cationic

bridges and substantially increases the adsorption capacity of P from wastewater, and can still be used later as a fertilizer (LI et al., 2016).

The most used cations for the treatment of biochar aiming to retain phosphate are magnesium (Mg^{2+}), iron (Fe^{2+}), and aluminum (Al^{3+}). Mg^{2+} has been the most used cation because it is a nutrient that can be added to the soil together with P (TAYAKA et al., 2016; LI et al., 2016; CUI et al., 2016; JUNG & AHN, 2016), followed by Fe^{2+} (YANG et al., 2018; CAI et al., 2017), and by Al^{3+} (ZHANG et al., 2012; WAN et al., 2017; NOVAIS et al., 2018). It is desirable that the adsorbed phosphate be desorbed in synchrony with the nutrient plant demand, so that the material has the potential to act as an enhanced efficiency fertilizer. Thus, it is important to know the chemical phosphate species formed after adsorption.

X-ray absorption spectroscopy (XAS) at the K edge using synchrotron light is a very powerful technique for understanding P speciation in soils and other environmental matrices, mainly using the XANES regions of the spectrum (HESTERBERG, MCNULTY & THIEME, 2017; SANTOS, HESTERBERG & ALLEONI, 2017). For example, using this technique it was possible to observe the formation of poorly soluble P species (e.g. apatite) in biochar produced at high pyrolysis temperature ($> 600\text{ }^{\circ}C$) (BRUNN et al., 2017). However, despite the widespread use of metal-modified biochars for P recovery by adsorption in recent years, to date, no study has evaluated the P species formed using the XANES technique, nor correlated such chemical species with their agronomic efficiency, which was carried out in this thesis.

The objective of the first chapter is to produce biochars from poultry litter, pig manure and sewage sludge impregnated with Mg^{2+} and verify their ability to remove phosphate from aqueous solution. In addition, evaluate the subsequent release of the adsorbed phosphate and study its use as a fertilizer. The second chapter aimed to study the effect of impregnation with different cations (Mg^{2+} , Fe^{3+} and Al^{3+}) and pyrolysis conditions (furnace with N_2 flow and muffle furnace) on the physicochemical characteristics of biochars and P. adsorption. The third chapter aims to study speciation using absorption spectroscopy and X-rays in modified biochars, in order to understand their behavior when used as fertilizers.

REFERENCES

- AGYEI, N. M.; STRYDOM, C. A.; POTGIETER, J. H. The removal of phosphate ions from aqueous solution by fly ash, slag, ordinary Portland cement and related blends. **Cement and concrete research**, v. 32, n. 12, p. 1889–1897, 2002.
- BIEDERMAN, L. A.; STANLEY HARPOLE, W. Biochar and its effects on plant productivity and nutrient cycling: A meta-analysis. **GCB Bioenergy**, v. 5, n. 2, p. 202–214, 2013.
- BOUJELBEN, N. et al. Phosphorus removal from aqueous solution using iron coated natural and engineered sorbents. **Journal of Hazardous Materials**, v. 151, n. 1, p. 103–110, 2008.
- CAI, R. et al. Phosphate reclaim from simulated and real eutrophic water by magnetic biochar derived from water hyacinth. **Journal of Environmental Management**, v. 187, p. 212–219, 2017.
- CHANG, J. et al. Adsorption of methylene blue onto Fe₃O₄/activated montmorillonite nanocomposite. **Applied Clay Science**, v. 119, p. 132–140, 2016.
- CHEN, J. et al. Phosphate immobilization from aqueous solution by fly ashes in relation to their composition. **Journal of Hazardous Materials**, v. 139, n. 2, p. 293–300, 2007.
- CHO, H.; OH, D.; KIM, K. A study on removal characteristics of heavy metals from aqueous solution by fly ash. **Journal of Hazardous Materials**, v. 127, n. 1–3, p. 187–195, dez. 2005.
- CORDELL, D.; DRANGERT, J. O.; WHITE, S. The story of phosphorus: Global food security and food for thought. **Global Environmental Change**, v. 19, n. 2, p. 292–305, 2009.
- CUI, X. et al. Removal of phosphate from aqueous solution using magnesium-alginate/chitosan modified biochar microspheres derived from *Thalia dealbata*. **Bioresource Technology**, v. 218, p. 1123–1132, 2016.
- GIMÉNEZ, J. et al. Arsenic sorption onto natural hematite, magnetite, and goethite. **Journal of Hazardous Materials**, v. 141, n. 3, p. 575–580, mar. 2007.
- HESTERBERG, D.; MCNULTY, I.; THIEME, J. Speciation of Soil Phosphorus Assessed by XANES Spectroscopy at Different Spatial Scales. **Journal of Environment Quality**, v. 46, n. 6, p. 1190, 2017.
- JIANG, C. et al. Adsorptive removal of phosphorus from aqueous solution using sponge iron and zeolite. **Journal of Colloid and Interface Science**, v. 402, p. 246–252, 2013.
- JUNG, K. W. et al. Fabrication of porosity-enhanced MgO/biochar for removal of phosphate from aqueous solution: Application of a novel combined electrochemical modification method. **Bioresource Technology**, v. 200, n. April 2016, p. 1029–1032, 2016.
- KARIMAIAN, K. A. et al. Retention of phosphorous ions on natural and engineered waste pumice: Characterization, equilibrium, competing ions, regeneration, kinetic, equilibrium and thermodynamic study. **Applied Surface Science**, v. 284, p. 419–431, 2013.
- KRISHNAN, K. A.; HARIDAS, A. Removal of phosphate from aqueous solutions and

sewage using natural and surface modified coir pith. **Journal of Hazardous Materials**, v. 152, n. 2, p. 527–535, 2008.

LAIRD, D. A. et al. Impact of biochar amendments on the quality of a typical Midwestern agricultural soil. **Geoderma**, v. 158, n. 3–4, p. 443–449, 2010.

LALLEY, J. et al. Phosphate removal using modified Bayoxide® E33 adsorption media. **Environ. Sci.: Water Res. Technol.**, v. 1, n. 1, p. 96–107, 2015.

LI, R. et al. Recovery of phosphate from aqueous solution by magnesium oxide decorated magnetic biochar and its potential as phosphate-based fertilizer substitute. **Bioresource Technology**, v. 215, p. 209–214, 2016.

LOGANATHAN, P. et al. Removal and Recovery of Phosphate From Water Using Sorption. **Critical Reviews in Environmental Science and Technology**, v. 44, n. September 2015, p. 847–907, 2014.

NOVAIS, S. V. et al. Poultry manure and sugarcane straw biochars modified with MgCl₂ for phosphorus adsorption. **Journal of Environmental Management**, v. 214, p. 36–44, 2018.

SANTOS, S. R.; HESTERBERG, D.; ALLEONI, L. R. F. Phosphate Speciation and Citrate-Induced Mobilization of P in an Acric Oxisol. **Communications in Soil Science and Plant Analysis**, v. 48, n. 17, p. 1977–1988, 2017.

SHEPHERD, J. G. et al. Biochar and enhanced phosphate capture: Mapping mechanisms to functional properties. **Chemosphere**, v. 179, p. 57–74, 2017.

TAKAYA, C. A. et al. Phosphate and ammonium sorption capacity of biochar and hydrochar from different wastes. **Chemosphere**, v. 145, p. 518–527, 2016.

TAN, X. et al. Application of biochar for the removal of pollutants from aqueous solutions. **Chemosphere**, v. 125, p. 70–85, 2015.

WAN, S. et al. Journal of Industrial and Engineering Chemistry Functionalizing biochar with Mg – Al and Mg – Fe layered double hydroxides for removal of phosphate from aqueous solutions. **Journal of Industrial and Engineering Chemistry**, v. 47, p. 246–253, 2017.

XIONG, J. et al. Phosphate removal from solution using powdered freshwater mussel shells. **Desalination**, v. 276, n. 1–3, p. 317–321, 2011.

YANG, Q. et al. Effectiveness and mechanisms of phosphate adsorption on iron-modified biochars derived from waste activated sludge. **Bioresource Technology**, v. 247, n. August 2017, p. 537–544, 2018.

YE, J. et al. Interaction between phosphate and acid-activated neutralized red mud during adsorption process. **Applied Surface Science**, v. 356, p. 128–134, 2015.

ZENG, Z. et al. Sorption of ammonium and phosphate from aqueous solution by biochar derived from phytoremediation plants. **J Zhejiang Univ-Sci B (Biomed & Biotechnol)**, v. 14, n. 12, p. 1152–1161, 2013.

SECOND PART – ARTICLES

CHAPTER 1

Phosphorus recover using magnesium-enriched biochar and its potential use as fertilizer

(Article published in Archives of Agronomy and Soil Science)

DOI: <https://doi.org/10.1080/03650340.2020.1771699>

Phosphorus recover using magnesium-enriched biochar and its potential use as fertilizer

Bárbara Olinda Nardis^a, Jefferson Santana da Silva Carneiro^a, Isabella Marques Gonçalves de Souza^b, Renato Gonçalves de Barros^a, Leônidas Carrijo Azevedo Melo^{a*}

^aSoil Science Department, Federal University of Lavras, Lavras, Minas Gerais, Brazil;

^bChemistry Department, Federal University of Lavras, Lavras, Minas Gerais, Brazil

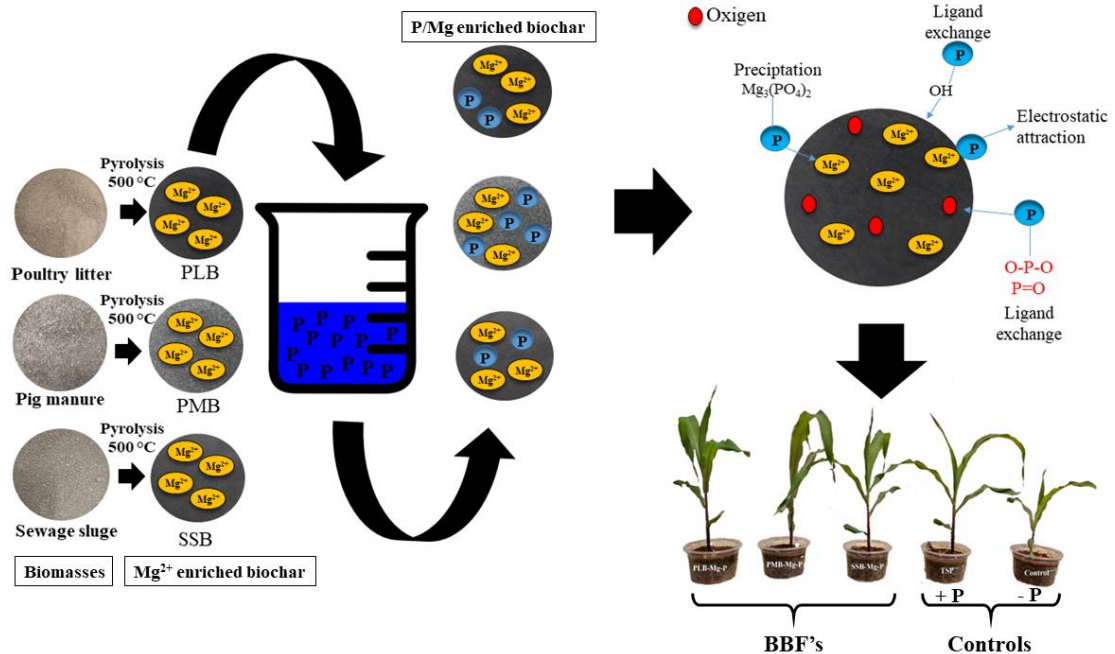
CONTACT: Leônidas Carrijo Azevedo Melo, Soil Science Department, Federal University of Lavras, Lavras, Minas Gerais, Brazil, E-mail: leonidas.melo@ufla.br

Abstract

Phosphorus (P) recovery from wastewater using biochar is an alternative to P recycle and reuse. However, the impregnation of cations for biochar production is needed to enhance P removal. We aimed at studying the P adsorption and release capacity of biochar enriched with magnesium (Mg^{2+}) and its potential use as fertilizer. Biochars were produced from poultry litter (PLB), pig manure (PMB), and sewage sludge (SSB) impregnated with $MgCl_2$. Characterization comprised pH, electrical conductivity, total nutrient content, moisture and ash contents, FTIR, XRD, Raman, and SEM-EDX. Phosphorus adsorption isotherms by biochars were obtained and P desorption was also studied. A pot experiment with maize in an Oxisol was performed with the P-loaded biochars, triple superphosphate - TSP (positive control) and no P application (negative control). PMB showed the highest P adsorption (68.0 mg g^{-1}). The main mechanisms of P removal were through precipitation with cations, ligand exchange reactions and electrostatic attraction on the biochar surface. The P-loaded biochars promoted plant growth and accumulation of P in maize, which was similar or greater than TSP. In conclusion, Mg-impregnated biochar is a sustainable option to add value to organic residues and to recycle P to be reused as enhanced efficiency fertilizer.

Keywords: phosphorus recycling, phosphate, organomineral, biochar-based fertilizer

Graphical abstract



Introduction

Phosphorus (P) is an essential element for living organisms, but its sources are finite, scarce and there is no substitute (Cordell 2008). Population growth causes an increased demand for food production and, consequently, for phosphate fertilizers, which might cause exhaustion of the easily mineable P reserves in the near future (Iwaniec et al., 2016). Therefore, P recycling will be increasingly important to support agriculture production and to reduce environmental pollution pressure. A great amount of P loss occurs via improper waste or wastewater disposal, which along with nitrogen (N), can cause eutrophication in water bodies (Ucker et al., 2012). Therefore, there is an urgent need to recover P and reuse it safely as a fertilizer.

Phosphate rocks are the main P sources processed in the fertilizer industries, which generally promote acid solubilization for producing highly water-soluble fertilizers. Tropical soils, such as most Brazilian agricultural soils, are highly weathered and the clay fraction is dominated by kaolinite, and Fe and Al oxyhydroxides, which have high P fixing capacity, causing low P use efficiency of the soluble sources (Roy et al. 2016). It is estimated that the intensification of agricultural production in the tropics (especially in Brazil) should substantially increase the demand for phosphate fertilizers in the coming decades (Roy et al. 2016; Withers et al. 2018). In addition, in Brazil, about 50% of industrial phosphate is imported

and the country does not have a well-developed P recycling system, which increases the pressure on government agencies and industries on this environmental demand.

In this scenario, it is essential to develop technologies for P recovery, with special emphasis on precipitation and adsorption techniques. P recovery from wastewater and other matrices by adsorption using biochar has gained attention lately (Trazzi et al. 2016; Yin et al. 2018; Vikrant et al. 2018; Takaya et al. 2016; Cai et al. 2017; Li et al. 2016; Sheperd et al. 2016; Cui et al. 2016). Biochar is the solid product of the pyrolysis of organic waste and has several environmental applications (Lehmann and Stephen 2015). The main advantages of biochar are the possibility of recycling residues, high stability in the environment, high porosity, and relatively easy preparation and operation (Tan et al. 2015; Jeong et al. 2016).

The biochar surface is dominated by negative charges due to the high pH and the presence of oxygenated groups, which results in low P adsorption capacity of phosphate ions (H_2PO_4^- or HPO_4^{2-}) from aqueous solution (Zeng et al. 2013; Takaya et al. 2016; Shepherd et al. 2016). An interesting alternative to improve the adsorption capacity of biochar is the impregnation of magnesium (Mg^{2+}) in the raw material for subsequent pyrolysis. Addition of Mg^{2+} creates cationic bridges, which can substantially increase the adsorption capacity of P from wastewater with further potential to be used as fertilizer (Li et al. 2016). To date, few studies have used this approach (Li et al. 2016; Cui et al. 2016; Novais et al. 2018; Yin et al. 2018) and none has been tested as a fertilizer in tropical soils, which are naturally poor in nutrients, especially P and Mg (Lopes & Guilherme 2016).

Yao et al. (2013) studied tomato leaves grown in a peat-based medium enriched with Ca and Mg, converted them into engineered biochar and observed that biochar enriched with Mg was more efficient on the P removal from aqueous solution. Akgül et al. (2019) also observed that Mg-impregnated biochar was the most efficient composite to adsorb P, as compared with those impregnated with Fe, Mn and Al. Recently, Zhu et al. (2020) showed that conversion of MgCl_2 -impregnated corn stalks into biochar promoted the formation of pores and decomposed into MgO nanoparticles, which adsorb PO_4^{3-} mainly by rapid binding on the external surface and the slow diffusion of adsorbed phosphate into the biochar interior. They described the processes involved in the phosphate removal as electrostatic attraction to MgOH^+ sites followed by precipitation to form $\text{Mg}_3(\text{PO}_4)_2$ and MgHPO_4 .

Residues such as poultry litter, pig manure, and sewage sludge are of special interest for testing as raw material for biochar production to use as P adsorbents, due to their high

production in Brazil, reaching 15 million tons per year (Pinto et al. 2014; Dalólio et al. 2017; Agência Nacional das Águas 2017). These residues are associated with wastewater generation, which is challenging in terms of treatment and final disposal since they are often disposed in landfills, causing losses of P and other nutrients. Therefore, more studies are needed, focusing on developing alternatives for recycling and adding value to these materials.

This study aimed to produce Mg-impregnated biochar from poultry litter, pig manure, and sewage sludge for phosphate adsorption from aqueous solution and to evaluate its potential use as fertilizer in a P-fixing tropical soil. With this approach, a sustainable technology to recover P is proposed to reuse waste and to produce enhanced fertilizer for plant growth.

Material and methods

Biochar preparation

Poultry litter was collected in farms near Lavras, Minas Gerais state, Brazil. Pig manure was collected in the swine sector and sewage sludge in the sewage treatment plant, both located at the Federal University of Lavras. The biomasses were oven dried at 50 °C until constant weight, ground in a mill equipped with a 10-mesh sieve (<0.25 mm). Later, the biomasses were impregnated with magnesium chloride (MgCl₂) solution aiming to reach ~10% of Mg in the biochar. This Mg concentration was based in other studies that have showed great performances of biochar on P adsorption in this range of Mg concentration (Li et al. 2016; Novais et al. 2018) and also aiming its final use as a fertilizer (Lustosa Filho et al. 2020). For this, 50 g of each biomass were mixed with 500 mL of 2.67 mol L⁻¹ MgCl₂ solution. Subsequently, the mixture was shaken for 24 h at 120 oscillations per minute in a shaker (TE 240/1 Tecnal) and oven dried at 80 °C.

For the production of biochars, the biomasses with and without Mg²⁺ impregnation were accommodated in porcelain crucibles, which were overlapped to prevent O₂ flow and allow pyrolysis (Bekiaris et al., 2016). The process was carried in a muffle furnace at a heating rate of 10 °C min⁻¹ to reach 500 °C, which was maintained for 2 h (Lustosa Filho et al., 2017). After pyrolysis, the samples were slowly cooled to room temperature, ground in a porcelain mortar, and sieved to <0.25 mm. After processing, six biochars were produced: poultry litter biochar (PLB), pig manure biochar (PMB), sewage sludge biochar (SSB), poultry litter biochar

impregnated with MgCl_2 (PLB-Mg), pig manure biochar impregnated with MgCl_2 (PMB-Mg), and sewage sludge biochar impregnated with MgCl_2 (SSB-Mg).

Biochar characterization

Electrical conductivity (EC) and pH were determined in triplicate according to Singh et al. (2017). The ash and moisture contents of the biochars were evaluated by the standard method ASTM D1762-84 (ASTM 2007). Total Mg and P contents were determined according to Enders and Lehmann (2012). The contents of the tubes were filtered in membranes ($<0.45 \mu\text{m}$) and the elements were quantified by ICP-OES. The C content was determined in an elemental analyzer (model Vario TOC cube, Elementar, Germany).

The microscopic features and morphology were characterized using a field emission gun scanning electron microscopy (Zeiss EVO 50.) equipped with an energy-dispersive X-ray (EDX) spectroscopy (IXRF Systems 500 Digital Processing). X-ray diffraction (XRD) analysis was also carried out to identify any crystallographic structure in the samples using a $\text{CuK}\alpha$ radiation ($\lambda = 0.1540 \text{ nm}$), operated at 30 kV and 15 mA, with Ni filter for $\text{K}\beta$ suppression, and detection with a scintillator of NaI and Be window. Fourier transform infrared (FTIR) spectroscopy were recorded using a Digilab Excalibur spectrometer with a spectral range of $4000 - 400 \text{ cm}^{-1}$ with 32 scans and 4 cm^{-1} resolutions. Analyses were performed on the pristine and Mg-impregnated biochars after P adsorption. Raman analysis was performed with a LabRAM HR Evolution spectrometer. The statistical analysis and the data were analyzed by determining the area ratio between the D and G bands (I_D/I_G) as described in the supplementary information.

Adsorption isotherms

Batch adsorption study was performed as described by Li et al. (2016) with modifications. In triplicate, 100 mg of biochar samples were placed in 50-mL polypropylene tubes and 20 mL of phosphate solution (obtained from a stock solution of 1000 mg L^{-1} of KH_2PO_4) were added (5.0 g L^{-1} adsorbent dose) with the following concentrations: 5, 10, 20, 50, 100, 200, 300, 400, and 500 mg L^{-1} , which were prepared using 0.01 mol L^{-1} $\text{Ca}(\text{NO}_3)_2$ background solution. The mixture was stirred for 30 min at 120 oscillations per minute and the

pH was adjusted to 4.0 with 0.1 mol L⁻¹ HCl solution and stirred for another 24 hours at room temperature. After this period, the equilibrium pH was recorded and extracts were filtrate in membranes (<0.45 μm, Millex HP). The concentration of P at equilibrium solution was measured by ICP-OES.

The adsorption capacity (Q_e) of the different biochars was calculated by mass balance as expressed by equation (1):

$$Q_e \text{ (mg g}^{-1}\text{)} = \frac{V(C_i - C_e)}{m} \quad (1)$$

where V is the volume of solution (L), C_i and C_e are the initial and equilibrium P concentrations (mg L⁻¹), respectively, and m is the biochar (adsorbent) mass (g). The data obtained were adjusted to Langmuir and Freundlich isotherm models as described in the supplementary information.

Desorption study

For the desorption study, the procedure described by Li et al. (2016) was followed with modifications. A total of 200 mg of biochar was used, in which 40 mL of KH₂PO₄ solution containing 300 mg L⁻¹ of P were added, and the mixture was properly shaken on a shaker at 120 rpm for 24 hours. After adsorption, the P-loaded adsorbent was separated from the solution through centrifugation (1,957 g) and the supernatant was analyzed for P by ICP-OES. The amount of adsorbed P was calculated. For desorption, three solutions were tested by adding into the tubes, separately, 20 mL of deionized water, 2% citric acid and Mehlich-1 solution (0.025 mol L⁻¹ de H₂SO₄ + 0.05 mol L⁻¹ de HCl), which were shaken for another 4 hours. After, the supernatant was filtered in blue band filter and P was measured by ICP-OES. The amount of desorbed P was calculated. The desorption rate was calculated by dividing the desorbed amount by the adsorbed amount.

Pot experiments

Soil sample of an Oxisol (Rhodic Hapludox) was collected in Lavras, Minas Gerais, Brazil (915 m altitude, 21°13'34" S and 44°58'31" W) in the subsoil layer (40 - 60 cm) of a

small fragment forest. Samples were air-dried and passed through a 2-mm sieve for chemical and physical soil characterization, then it was fertilized as described in the supplementary information.

Three P-loaded biochars (PLB-Mg, PMB-Mg, and SSB-Mg) were applied aiming to supply 200 mg kg⁻¹ of P, which is the recommended amount for pot experiments (Novais et al. 1991). Pots with triple superphosphate (TSP) and without P addition were carried out as positive and negative controls, respectively. The experiment was set up as a completely randomized design with four replicates. Then, three seeds of maize were sown per pot and five days after germination only one plant was left and cultivated up to 21 days. After the growth period, plant heights and stem diameter were recorded, and plants were harvested. Shoots were collected and oven dried for 72 hours at 65 °C, dry mass production was recorded, and plant material was ground to determine macro and micronutrient contents by ICP-OES, after nitric-perchloric acid digestion (Malavolta et al. 1997). After cultivation, soil from each pot was air-dried, sieved (< 2 mm), and analyzed for pH, available Mg by 1 mol L⁻¹ KCl extractor and P by using the anion-exchange resin (Raij et al. 1986) and Mehlich-1 solution (Mehlich 1953).

Statistical analysis

Normality was analyzed using the Shapiro Wilk test (Shapiro & Wilk 1965), and homoscedasticity was verified using the variance equation test (or the Levene test) (Brown & Forsythe 1974). The data were subjected to analysis of variance (ANOVA) and, when significant ($p < 0.05$), the means were compared by the Tukey test at $p < 0.05$ using the ExpDes.pt package (Ferreira et al., 2011). The Pearson correlation (r) was performed to verify the relationship between P-uptake by plants and the P extracted by Mehlich-1 and anion exchange resin. All analysis was done in software R 3.4.1. (R Core Team 2017).

Results and discussion

Characterization of adsorbents

The properties of the biochars before and after of impregnated with Mg are shown in Table 1. The highest ash contents were observed in the SSB (80.3%) and SSB-Mg (66.9%), followed by PMB (53.9%); PLB (46.1%); PLB-Mg (42.2%) and PMB-Mg (39.7%). The highest ash content in SSB-Mg is due to the composition of this biomass, which is composed

mainly of Al, Fe, and Si (Table S1) that are concentrated during pyrolysis. The ash contents found in the biochar samples in this study are in the same range of those found in other studies with similar biomasses (Novais et al. 2018; Tsai et al. 2012). Variation in biochar ash contents are due to differences in the composition of biomasses, location of collection, and pyrolysis temperature (Domingues et al., 2017). The moisture of the biochars ranged from 1.55 to 19.9%. The pH of the biochars was higher for PLB and PLB-Mg, followed by PMB and PMB-Mg and SSB and SSB-Mg. The lowest pH value for SSB is due to lower levels of basic cations (e.g. Ca^{2+} , Mg^{2+} , and K^+) and higher levels of acid cations (e.g. Fe^{2+} and Al^{3+}). EC followed the same trend of the ash content since they are closely related due to salts dissolution.

Table 1. Properties of biochars from poultry litter (PLB), pig manure (PMB) and sewage sludge (SSB) impregnated with Mg^{2+} .

Properties	Biochar					
	PLB	PLB-Mg	PMB	PMB-Mg	SSB	SSB-Mg
Ash (%)	46.1±0.19	42.2±0.69	53.9±5.75	39.7±0.29	80.3±0.22	66.9±0.65
Moisture (%)	4.54±0.36	19.9±1.86	3.44±0.48	16.7±0.60	1.55±0.07	13.5±0.75
pH (H ₂ O)	10.7±0.02	9.93±0.01	8.02±0.11	9.84±0.01	5.55±0.02	8.45±0.08
EC (mS cm ⁻¹)	12.6±0.20	31.9±0.17	0.33±0.00	27.9±0.12	1.65±0.04	39.7±0.10
C (%)	40.9±0.94	26.9±0.18	44.7±0.41	23.7±0.64	10.6±0.11	5.6±0.05
Mg (g kg ⁻¹)	14.1±0.41	90.1±2.12	3.25±0.06	101±2.80	3.67±0.06	98.8±3.00
P (g kg ⁻¹)	36.1±1.49	19.3±0.31	10.69±0.45	4.26±0.29	6.76±0.14	3.58±0.05
Ca (g kg ⁻¹)	56.8±2.04	29.4±0.68	26.5±0.24	10.8±0.07	11.3±0.34	7.45±0.25

The highest C content was observed in non-impregnated biochars, since impregnation is the addition of salts that makes the biochar more mineral, thus reducing the C content (Table 1). Agrafioti et al. (2013) also found low C contents (6.0-14.4%) in sewage sludge biochar samples prepared at 500 °C, which was attributed to increased volatilization of this element during pyrolysis. The higher C content in biochars is linked to the formation of aromatic groups and also the greater resistance of biochar to microbial degradation (Domingues et al., 2017).. The P content in PLB-Mg was four times greater than PMB-Mg and five times greater than SSB-Mg, showing higher potential of supplying P as a fertilizer. However, P release rate is greatly reduced in biochar as compared to its original feedstock (Liang et al. 2014).

Adsorption isotherm and desorption

Phosphorus adsorption isotherms as well as the fitting of Langmuir and Freundlich models for the Mg-impregnated biochars are shown in Fig 1. Both models could describe the P

isotherm data well and, in general, the Langmuir model fitted better (R^2 of 0.94–0.98) than the Freundlich model (R^2 of 0.86–0.99) (Table 2). The maximum P sorption capacity (q_m) as estimated by the Langmuir model was 34.5, 68.0, and 28.1 mg g^{-1} for PLB-Mg, PMB-Mg, and SSB-Mg, respectively (Table 2).

Table 2. Constants and correlation coefficients of Langmuir and Freundlich models for the sorption of P in biochar impregnated with Mg^{2+} .

Langmuir			
Biochar	$q_m(\text{mg g}^{-1})$	$K_L (\text{L mg}^{-1})$	R^2
PLB-Mg	34.5	0.064	0.94
PMB-Mg	68.0	0.063	0.96
SSB-Mg	28.1	0.071	0.98
Freundlich			
Biochar	$K_F (\text{mg g}^{-1})$	n	R^2
PLB-Mg	2.68	1.84	0.86
PMB-Mg	4.37	1.59	0.90
SSB-Mg	3.34	2.48	0.99

PLB-Mg: poultry litter biochar with 10% of Mg, PMB-Mg: pig manure biochar with 10% of Mg, SSB-Mg: sewage sludge biochar with 10% of Mg.

The best fit of the isotherm data to the Langmuir model indicates predominance of monolayer adsorption, while the Freundlich model is used to describe chemisorption on a heterogeneous surface (Vikrant et al., 2018). The Langmuir constant (K_L) represents the adsorbed adsorbent-binding energy and the Freundlich constant is related to the adsorption capacity in multilayers, while n is related to the adsorption intensity (Luo et al., 2016). There is a qualitative relation between the parameter n and the distribution of adsorption sites, when the n value equals the unit all the energy adsorption sites are equivalent, and the Langmuir model is better suited. However, when $n \neq 1$ the distribution of the energy sites tends to vary with the adsorption density (Meroufel et al., 2013). Thus, the higher the n value the greater the heterogeneity of the adsorption sites. The highest n value was observed in SSB-Mg and the Freundlich model fitted better the data ($R^2 = 0.99$) and showed the lowest q_m value (28.1 mg g^{-1} of P) of the three biochars (Table 2). Conversely, PLB-Mg and PMB-Mg presented lower n values and higher q_m values as compared to SSB-Mg, being better fitted to the Langmuir model ($R^2 = 0.94$ and $R^2 = 0.96$). These results suggest that adsorptions probably took place mainly as monolayers and are better distributed on the biochar surface, although other process such as surface precipitation might have occurred as well. Despite the lowest adsorption capacity of the

SSB-Mg, the qualitative adsorption parameters suggest a high-affinity of P adsorption, which increases its retention in the biochar matrix and might reduce its fertilizer potential.

The most commonly employed cations to enhance biochar P adsorption capacity are Mg, Al, Ca, and Fe. Yin et al. (2018) performed a study using soybean straw biochar impregnated with these four cations and they concluded that Mg has the highest P sorption capacity and, thus, it is indicated to tailor biochar for this specific purpose. The values of q_m found in this study were within the range normally found in the literature for these types of materials (Table 3). However, it demonstrates clearly that the biomass and the pyrolysis temperature greatly affect the P adsorption capacity. Moreover, variations in the maximum adsorption capacity of the cation-impregnated biochar materials can be as high as two orders of magnitude.

Table 3. Summary of the Langmuir maximum adsorption capacity of phosphate by different adsorbents from aqueous solution.

Biomass	Pyrolysis temperature	Q_m (mg g ⁻¹)	Modifier	References
Peanut shells	700 °C	6.79	-	Jung et al. 2015
Raw cypress sawdust	500 °C	58.82	MgCl ₂ .6H ₂ O	Haddad et al. 2017
Holm Oak	650 °C	64.6	MgCl ₂ .6H ₂ O	Takaya et al. 2016
<i>Thalia dealbata</i>	450 °C	46.56	MgCl ₂ -alginate	Cui et al. 2016
Water hyacinth	450 °C	5.07	Iron oxide	Cai et al. 2017
Orange peel powder	700 °C	1.24	FeCl ₃ and FeCl ₂	Chen et al. 2011
Sewage sludge	600 °C	153.85	CaCl ₂	Saadat et al. 2018
Oak	500 °C	46.37	Lanthanum	Wang et al. 2016
Poultry litter	500 °C	34.5	MgCl ₂	This study
Pig manure	500 °C	68.0	MgCl ₂	This study
Sewage sludge	500 °C	28.1	MgCl ₂	This study

Q_m : maximum adsorption capacity of phosphate

Most studies in the literature only evaluate the P adsorption capacity of the modified biochars and highlight their capacity to remove P from aqueous solution. However, it is of primary importance to study the P desorption profile of such materials to evaluate their potential fertilizer value. Therefore, we evaluated the P desorption in the biochars using distilled water, 2% citric acid and Mehlich-1 solution (Fig 1d). The water-soluble P represents the readily available fraction either for plant uptake or leaching, depending on the soil conditions, while the citric acid and Mehlich-1 solutions represent the potentially plant available P fraction since plants usually acidify the rhizosphere and solubilize P (Li et al., 2008). For all extractors, P-loaded PMB-Mg presented higher desorption value followed by P-loaded PLB-Mg and P-loaded SSB-Mg. Mehlich-1 solution caused the highest desorption values (28.0 and 28.6%) for

PLB-Mg and PMB-Mg, while 2% citric acid desorb more P in the SSB-Mg (8.7%). Generally, the lowest desorption values indicate that there is a strong interaction between adsorbent and adsorbate (Li et al. 2016). The P extraction in water was 1.5% for PMB-Mg, 1.3% for PLB-Mg, and 0.7% for SSB-Mg, which indicate that only a small P fraction is readily available and this can be positive for application in highly P-fixing soils (Lustosa Filho et al., 2017). The low P desorption in water is due to the very mild extraction as compared to the high P binding energy in such surface types (Novais et al., 2018). Thus, an actual plant growth test is needed to confirm their potential fertilizer value and to compare with conventional fertilizers.

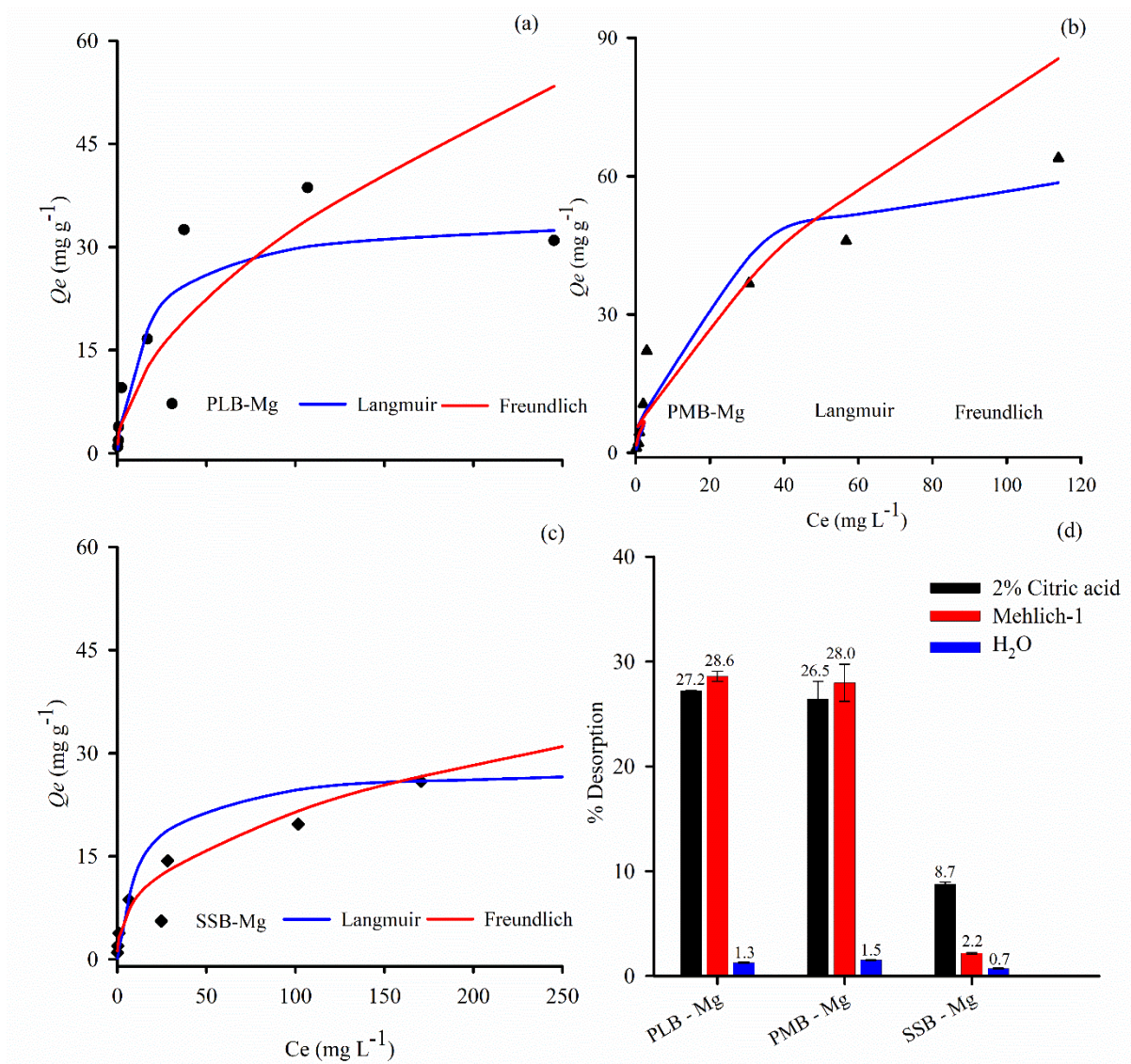


Figure 1. Phosphorus adsorption isotherms (a, b and c) and percentage of desorption (d) in biochar samples impregnated with Mg^{2+}

Notes: Error bars represent the standard deviations of the treatment mean replicates (n=3)

PLB-Mg: poultry litter biochar with 10% of Mg, PMB-Mg: pig manure biochar with 10% of Mg, SSB-Mg: sewage sludge biochar with 10% of Mg.

Scanning electron microscopy (SEM) and Energy Dispersive Spectroscopy (EDS)

SEM-EDS images of the Mg-impregnated P-loaded biochars are shown in Fig 2. The SEM images for PLB-Mg, PMB-Mg, and SSB-Mg show differences in the structure and size of the biochar grains (Fig 2a, d, and g). The EDS spectrum mapping revealed a uniform Mg distribution (Fig 2b, e, and h), which was closely associated with P distribution (Fig 2c, f, and i) and reveal that Mg on the biochar surface is the P binding agent. Although Mg and P are closely linked, the mechanism of P adsorption will be further explored by other techniques along the text.

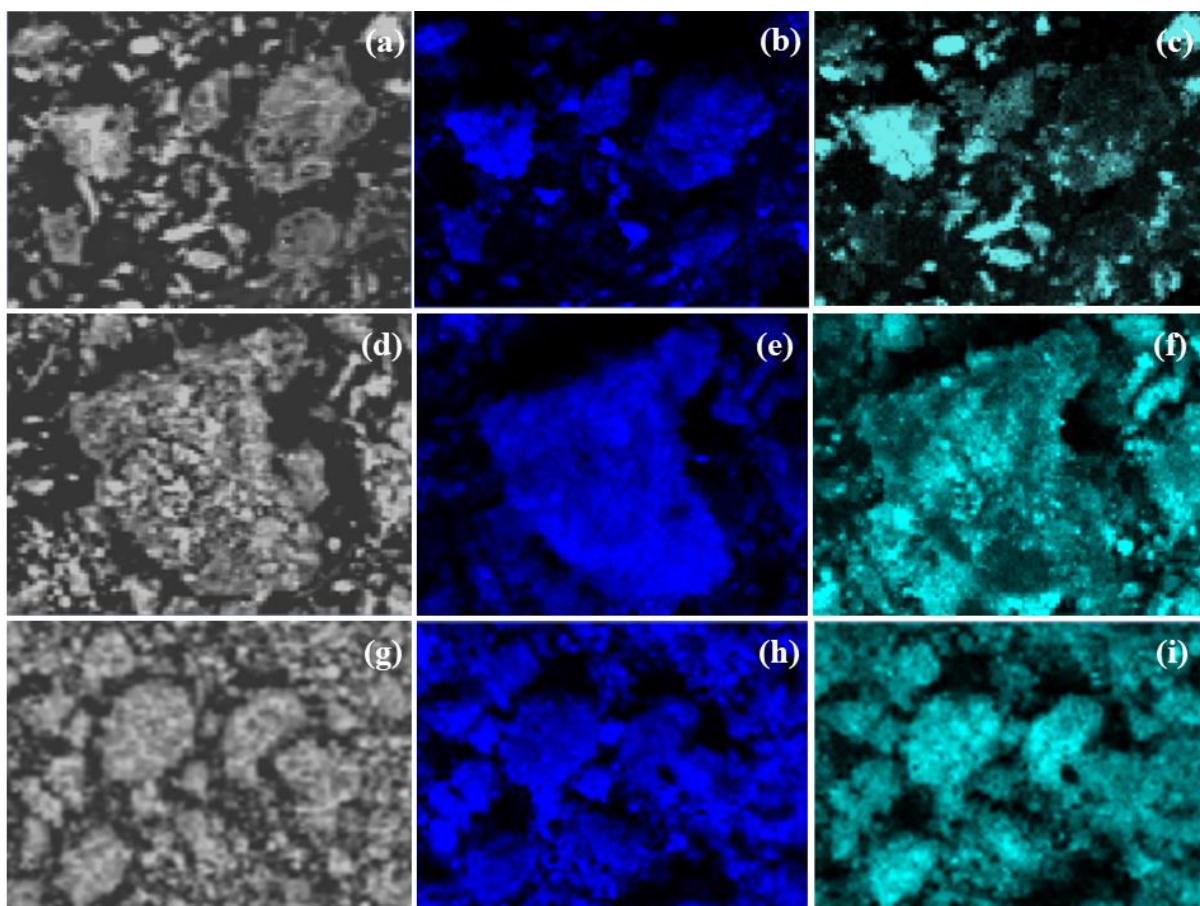


Figure 2. SEM images of biochars (a), (d) and (g) and SEM mapping of Mg (b), (e) and (h) and P (c), (f) and (i) respectively to PLB-Mg-P, PMB-Mg-P, and SSB-Mg-P biochars.

In Fig S1 are shown the peaks of the main elements found on the biochars surface before and after the impregnation and adsorption of P. The high intensity of Mg peaks shows the success of the Mg^{2+} impregnation (Fig S1 and Table S1). PLB showed intense peaks of Cl and K prior to impregnation, which was confirmed by the XRD analysis as Sylvite (KCl) (Fig 4). After Mg impregnation and P adsorption, it was observed a strong peak of Si, probably due to the dissolution of soluble salts (e.g. KCl) and the concentration of insoluble Si compounds in the resulting biochar. PMB showed a greater variety of peaks with prominence of Mg (Fig S1d), which is the result of its element rich composition (Table S1) SSB is mainly composed of Al, Si, and Fe and has a very low C content, which is expected for sewage sludge composition (Li et al. 2018; Agrafioti et al. 2013).

For PLB and PMB, there was an increase in C and O contents with Mg impregnation and P adsorption, while for SSB it was the opposite. The increase in O content suggests that more functional-groups contents are presented on the modified biochars (Cui et al. 2016). Surface oxygen functional groups influence the adsorption of cationic metals in the biochar surface (Uchimiya et al. 2011). It was observed that the higher is the O content on the pristine biochars surface (SSB > PLB > PMB), the lower is the P adsorption, probably due to the negative character that prevent P adsorption even in Mg impregnated materials.

Biomass and biochar composition explain its behavior regarding P adsorption. Thus, the choice of biomass should be made in order to observe the purpose of use, preparation procedures and availability of biomass, in order to obtain a specific biochar for each use (Xiao et al. 2018). In this study, the composition of the biomass influence on the biochar P adsorption capacity and in its fertilizer potential value, as it will be further discussed.

Raman analysis

Raman spectroscopy is an ideal technique for characterization of carbon materials. In the Raman spectra, the area ratio between D-band and G-band (I_D/I_G), and crystallite size (L_a) of pristine biochars and Mg-impregnated biochars after P adsorption are shown in Fig S2. All biochar curves exhibited two relatively broad bands in Raman shifts at 1353-1361 and 1588-1591 cm^{-1} (Fig S2a). The G and D-bands correspond to the in-plane vibrations of the structures connected to sp^2 with structural defects (G-band) and the graphite carbon structures connected to sp^2 (G-band) (Guizani et al. 2017). The D-band represents the amorphous or disordered carbon, while the G-band indicates the presence of C crystallites (Zhang et al., 2015).

The I_D/I_G ratios calculated by the Lorentzian function of each sample were 3.29, 3.16, 3.15, 3.34, 3.33, and 3.02 for PLB, PLB-Mg-P, PMB, PMB-Mg-P, SSB, and SSB-Mg-P, respectively (Fig S2b). The increase of I_D/I_G ratios can indicate the increasing proportion of condensed aromatic ring structures having defects or that graphitic carbon is disordered (Guizani et al. 2017; Chia et al. 2012). However, the area ratios I_D/I_G observed in this study were similar and did not allow us to conclude if there was an increase in amorphous C. This is probably due to the lack of sensitivity of the intensity ratio of the D and G bands as indicator of the degree of organization of the amorphous carbon (Potgieter-Vermaak et al., 2011).

The crystallite sizes (L_a) were: 7.16, 7.72, 7.68, 6.75, 5.54, and 5.90 nm for PLB, PLB-Mg-P, PMB, PMB-Mg-P, SSB, and SSB-Mg-P, respectively (Fig S2c). For the PLB and PMB, there was no significant difference in crystallite size. However, when compared to SSB they presented higher crystallite size. The SSB and SSB-Mg-P presented lower crystallite size, which indicates an increase of amorphous C. The smaller crystallite size (L_a) in the biochars of sewage sludge is due to the presence of higher amounts of Fe, Al, and Si (Table S1). The Raman analysis detects the C=C draw, but in materials rich in these metallic elements the substitution of a C by some of these elements take place, causing a decrease in the crystallite size (Ribeiro-Soares et al., 2013).

Infrared spectroscopy (FTIR)

The FTIR spectra of the biochars before and after impregnation with Mg and P adsorption are shown in Fig 3. For PLB, impregnation with Mg and P adsorption increased the functional groups, while SSB showed a more significant reduction in the number and size of the peaks. This fact may have occurred because SSB characteristic have low C content and high inorganic contents (ash) (Arai and Sparks, 2001).

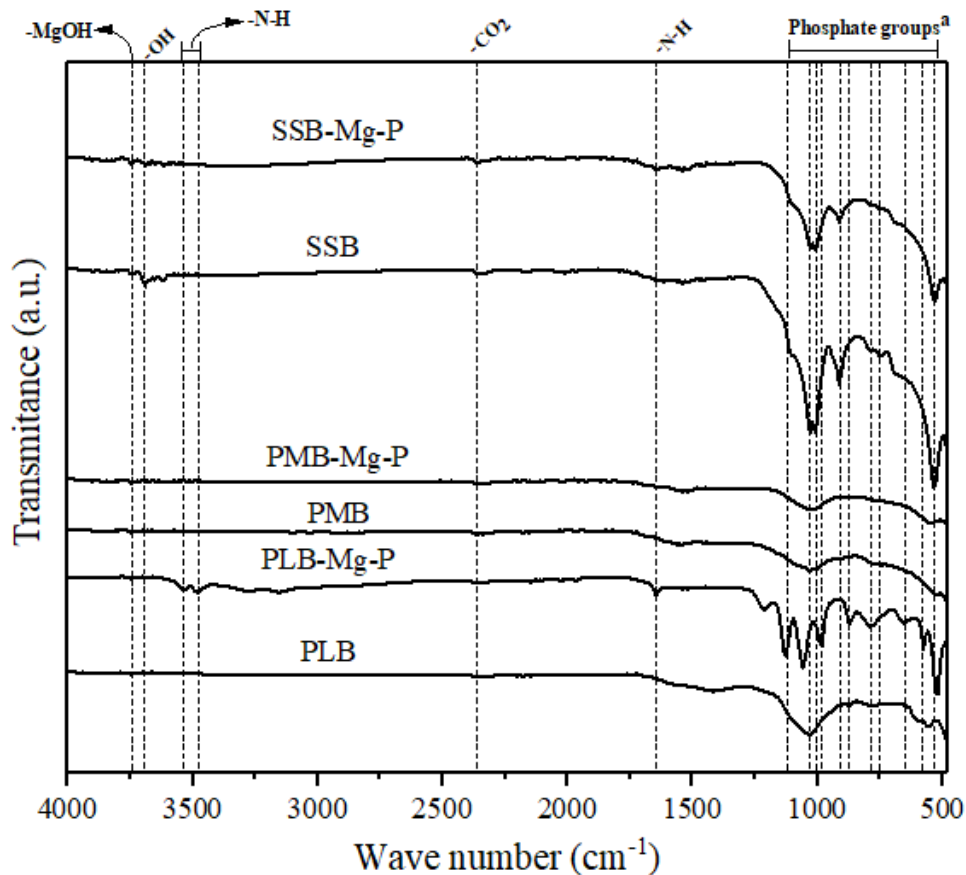


Figure 3. FTIR spectra (4000-500 cm^{-1}) of poultry litter biochar (PLB); pig manure biochar (PMB), sewage sludge biochar (SSB) before and after impregnation with Mg and adsorption with P.

Notes: ^aphosphate groups: O-P-O, P-O, P=O, P-OH, and $\text{CaHPO}_4 \cdot 2\text{H}_2\text{O}$

The discrete band observed at 3743 cm^{-1} was identified as Mg-OH in PMB-Mg-P and SSB (Cui et al. 2016). The characteristic CO_2 band shown in all biochars corresponds to atmospheric CO_2 during the analysis. Hydroxyl bands (-OH) were observed in SSB at 3695 cm^{-1} . Bands related to aromatic amines (N-H) at 3542 and 3480 cm^{-1} in PMB-Mg-P and at 3542 , 3480 , and 1646 cm^{-1} in PLB-Mg-P were observed. Bands at 1548 and 1365 cm^{-1} in PMB and at 1538 cm^{-1} in PMB-Mg-P indicated the presence of secondary amides (Silverstein et al. 1994).

The highest intensities bands were found in the region below 1029 cm^{-1} , indicating the presence of phosphate groups. Bands related to presence of calcium phosphate dibasic dihydrate ($\text{CaHPO}_4 \cdot 2\text{H}_2\text{O}$) was found at 528 cm^{-1} for PMB and SSB-Mg-P and at 871 , 782 , 522 , and 576 cm^{-1} for PLB-Mg-P (Bekiaris et al., 2016). Other phosphorus groups such as O-P-O were observed at 538 cm^{-1} for SSB and at 545 cm^{-1} for PMB-Mg-P, corroborating the results found

by Novais et al. (2018). Bands of P-OH groups were found at higher intensity bands in the region at 1000 cm^{-1} . This group occurred at 1029 cm^{-1} for PMB and PLB, and at 1010 cm^{-1} for SSB-Mg-P (Bekiaris et al., 2016). Bands at 914 cm^{-1} for SSB and SSB-Mg-P, at 1020 cm^{-1} for SSB, and at 985 cm^{-1} for PLB-Mg-P correspond to the of P=O (Gunes et al., 2015).

It was observed the formation of many phosphate functional groups bonded to O (O-P-O, P-O, P=O), which probably occurred due to the increase of O in the biochars after impregnation. Bands of -OH present in SSB may have contributed to the adsorption of P, since they disappear after adsorption (Jiang et al., 2018). The presence of Ca in all biomasses contributed to the formation of $\text{CaHPO}_4 \cdot \text{H}_2\text{O}$ clusters in all biochars. In PLB-Mg-P, it was observed a higher expression of this band (Bekiaris et al., 2016), which is related with its richer Ca composition as compared to the other biomasses (Table 1).

X-ray diffraction

The X-rays diffractograms of biochars before and after Mg impregnation and adsorption with P is shown in Fig 4. In pristine PLB, it was observed the formation of sylvite (KCl) at 28.4° and 40.5° 2θ (Fig 4a). Moreover, many characteristic peaks of calcite (CaCO_3) were observed at 29.4° , 39.4° , 43.2° 47.5° , and 48.5° and a peak of quartz (SiO_2) at 26.7° . In PLB-Mg-P, it was observed an expressive quartz peak at 26.6° , followed by lower peaks at 20.8° , 36.5° , 39.4° , 40.2° , 42.2° , and 45.7° . There was also the formation of diopside ($\text{CaMgSi}_2\text{O}_6$) at 29.3° and 35.6° with the addition of Mg. Phlogopite [$\text{KMg}_3(\text{Si}_3\text{Al})\text{O}_{10}(\text{OH})_2$] was also identified at 8.8° .

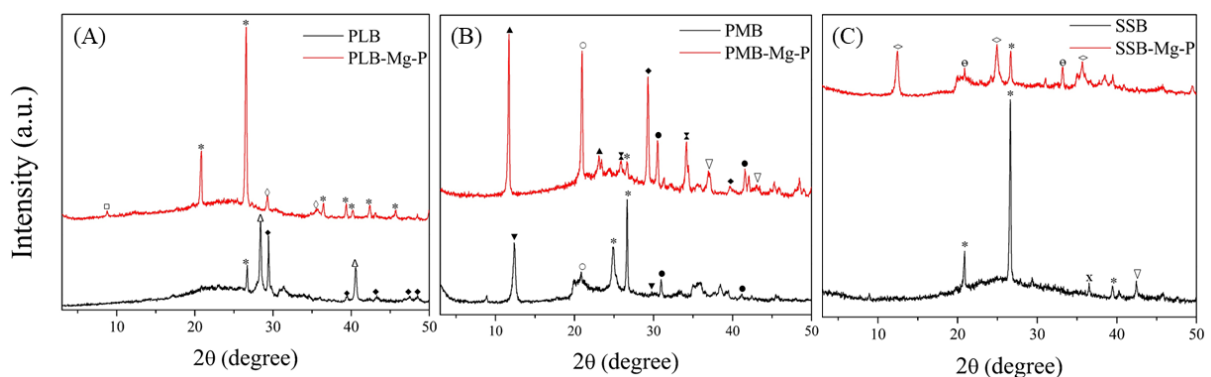


Figure 4. Diffractograms of (a) poultry litter biochar (PLB); (b) pig manure biochar (PMB) and (c) sewage sludge biochar (SSB) before and after impregnation with Mg and adsorption with P. The symbols are for: * Quartz; ◆ Calcite; Δ Sylvite; □ Phlogopite; ◇ Diopside; ● Dolomite;

○ Struvite-K; ▲ Brushite; ▼ Bobierrite; ▽ Periclase; ✕ Akimotoite; ✕ Hercynite; ◐ Foggite; ◇ Berthierine

As for PMB (Fig 5b), peaks at $2\theta = 26.6^\circ$ and 24.8° are related to the presence of quartz (SiO_2), while peaks at 12.3° and 30.1° indicate the formation of bobierrite-like compound (or synthetic bobierrite) $[\text{Mg}_3(\text{PO}_4)_2 \cdot 8\text{H}_2\text{O}]$ (Gong et al. 2017). Peaks at 30.9° and 41° are related to the presence of dolomite-like compound (or synthetic dolomite) $[\text{CaMg}(\text{CO}_3)_2]$, and at 20.8° of struvite-K-like compound $[\text{KMg}(\text{PO}_4)_6 \cdot 6\text{H}_2\text{O}]$. In PMB-Mg-P, increased peaks of struvite-K and dolomite and decreased the peaks of quartz (Fig 4b) were observed. There was also the formation of brushite-like compound ($\text{CaHPO}_4 \cdot 2\text{H}_2\text{O}$) at 11.7° and 23.1° , akimotoide-like compound (MgSiO_3) at 25.9° and 34.2° , periclase-like compound (MgO) at 37.1° and 43.1° , and calcite-like compound at 29.3° and 39.6° (Li et al. 2017).

For SSB, it was observed high peaks of quartz at 20.8° , 26.6° , and 39.4° (Fig 4c). There was also the formation of hercynite ($\text{Fe}^{2+}\text{Al}_2\text{O}_4$) and periclase in less expressive amounts. For SSB-Mg-P, there was a dilution in quartz formation and the formation of berthierine $[(\text{Fe}^{2+}, \text{Fe}^{3+}, \text{Al}) (\text{Si}, \text{Al})_2\text{O}_2(\text{OH})_4]$, at 2θ 12.5° , 25° , and 35.7° , and foggite $[\text{CaAl}(\text{PO}_4) (\text{OH})_2 \cdot 2\text{H}_2\text{O}]$ at 20.94° and 33.2° (Fig 4c).

XRD analysis showed the interaction of Mg^{2+} with P, forming several Mg-P synthetic minerals (e.g. periclase, bobierrite, diopside, struvite-K, akimotoide, and phlogopite). Most of the P-Mg compounds were formed in the biochar of poultry litter and pig manure. For the biochar of sewage sludge, there was greater formation of Fe and Al compounds bound to P due to the higher content of these elements (Table S1). Phosphorus reacts preferentially with trivalent cations such as Al^{3+} and Fe^{3+} and form (hydro)oxides in relation to bivalent cations such as Mg^{2+} , Al^{3+} and Fe^{3+} (hydro)oxides, which are displaced by PO_4^{3-} forming a high energy covalent bond (Rajapaksha et al., 2016). This characteristic explains the low P desorption in SSB-Mg (Fig 1d).

It was also observed the formation of Ca-P compounds such as brushite, dolomite, and calcite, which can be observed with greater intensity in PMB due to the higher Ca content in pig manure biomass (Table S1). Ca^{2+} is a common cation found in the studied biomasses and it is also used in modified biochars for P recovery in aqueous systems (Akgül et al. 2019; Marshall et al. 2017; Jung et al. 2016).

The difference in the formed minerals among samples is mainly due to the difference in biomass composition (Table S1). The minerals found are similar to those found by Xiao et al.

(2018) and Novais et al. (2018). The highest Mg-P mineral diversity occurred in the PMB-Mg-P, which was also the biochar that presented the highest adsorption capacity (Table 2), suggesting that precipitation was also a mechanism involved in the process (Yao et al., 2013)

Adsorption mechanism

The impregnation of biochars with cations such as Mg^{2+} , Ca^{2+} , Fe^{2+} , Fe^{3+} , and Al^{3+} has the function of modifying the surface of the biochar creating new binding sites (Vikrant et al., 2018). The analyzes suggest that the adsorption mechanisms involved in this study were precipitation of P with Mg, Ca, K, Al, Fe cations, ligand exchange reactions on the surface of the biochar and electrostatic attraction.

The high pH of the Mg-impregnated biochars favored the formation of precipitates, including bobierrite, brushite, and struvite-K (Cui et al. 2016). This mechanism was more expressive in the biochar of pig manure (PMB-Mg-P), which presented the greatest variation of Mg-P and Ca-P minerals (Fig 4).

In the biochar of poultry litter (PLB-Mg-P), no clear evidence of precipitation with P was observed, suggesting that the main adsorption mechanism was ligand exchange reaction between the deprotonated O atoms and P. This evidence is supported by the fact that PLB-Mg-P was the material that presented the highest oxygen groups (Table S1) by FTIR analysis and the highest numbers of O-P-O peaks (Fig 3).

As for the sewage sludge biochar, there was formation of Al-P precipitates (Fig 4), which occurred due to the affinity of P to trivalent cations such as Al^{3+} . Akgül et al. (2019) showed that Al^{3+} -impregnated biochar have lower P adsorption capacity as compared with Mg-impregnated biochar. P-OH, P=O, and O-P-O groups were also observed in SSB-Mg-P (Fig 3), suggesting that ligand exchange reactions also took place, most likely as a secondary P adsorption mechanism.

The electrostatic attraction is the mechanism that predominates in modified biochars (Vikrant et al. 2018) since the negatively charged P is attracted by some positive charge on the surface. This mechanism probably occurred in all studied biochars. Vikrant et al. (2018) stated that electrostatic attraction of phosphate to MgO-hydroxylated on the surface, forming binuclear complexes.

Factors such as pH, chemical composition of the biomass, concentration of the cationic elements (mainly Al, Fe, Ca, and Mg), and P concentration of the solution (Akgül et al., 2019a)

will directly affect the formation of functional groups and precipitation of minerals on the biochar surface. This directly interferes in the P adsorption capacity and also its potential reuse as fertilizer that will be discussed below.

P-loaded biochar on maize growth

The potential reuse of biochars after P adsorption as a phosphate fertilizer was evaluated in a pot experiment for the growth and nutrition of maize (Fig 5), and for improving soil fertility (Fig S3). The P-loaded biochars performed equal or greater than triple superphosphate– (TSP) and always greater than to the negative control treatment (without P addition). PLB-Mg-P caused higher dry mass production, while PMB-Mg-P and SSB-Mg-P did not differ to TSP. For plant height, there was no difference among treatments, except for the negative control.

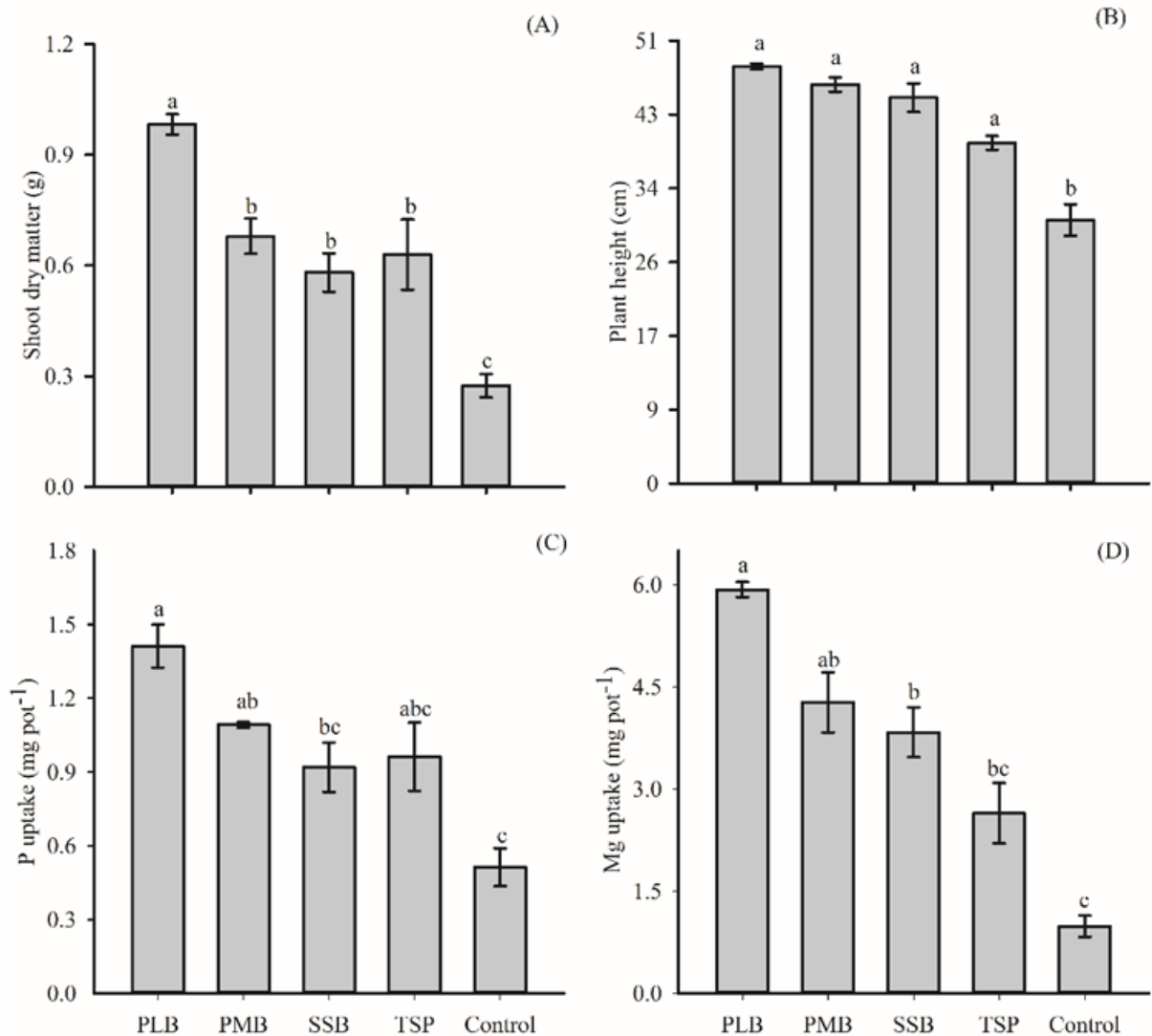


Figure 5. Shoot dry matter (a), plant height (b), P (c) and Mg (d) uptake by maize after 21 days under fertilization with poultry litter biochar (PLB), pig manure biochar (PMB), and sewage sludge biochar (SSB), after impregnation with Mg and adsorption with P, triple superphosphate (TSP), and no fertilizer (control).

Notes: Means followed by the same letter do not differ among themselves, according to the Tukey test ($p < 0.05$). Error bars represent the standard deviations of the treatment mean replicates ($n=4$)

Phosphorus uptake was higher in plants fertilized with PLB-Mg-P (1.41 mg pot^{-1}) when compared with SSB-Mg-P (0.91 mg pot^{-1}) and the negative control (0.51 mg pot^{-1}) (Fig 5c). PMB-Mg-P (1.09 mg pot^{-1}) and SSB-Mg-P did not differ to TSP (0.96 mg pot^{-1}) regarding P uptake. This means that compared to TSP, the plants fertilized with P-loaded biochar samples can uptake equal or higher amounts of P.

Similarly, Mg uptake followed the same trend of P uptake (Fig 5d). Phosphorus and Mg have a synergistic effect, which may have been the case in this study and also observed in other studies (Lustosa Filho et al. 2020; Li et al. 2016). Magnesium acts as an enzymatic activator in almost all phosphorylative enzymes, bridging ATP and/or ADP and the enzyme molecule. The synergistic effect causes the absorption of P to be maximal in the presence of Mg because it activates the ATPase of the membrane responsible for the ionic absorption (Marschner 2012). This might help to explain the better performance of plants fertilized with P-loaded and Mg-impregnated biochars as compared to control pots (positive and negative).

The different P-solubility of the biochar samples also likely played a role in P availability for plant uptake. The composition of the feedstock and consequently the biochar, cause the formation of low water-soluble P minerals, which need a longer contact time for the solubilization by the root system to occur. However, the results of our study show that even in a short-term experiment the P-loaded biochar samples were able to supply P as efficiently as a conventional soluble P source.

The small changes in soil pH are due to the high buffering capacity of this soil and due to the alkaline nature of the biochar fertilizers (Fig S3a). Due to the Mg enrichment in the biochars, there were higher residual levels of Mg^{2+} in the treatments with biochars when compared with the controls (TSP - positive and without P - negative) (Fig S3b). Residual available P showed the same trend either extracted with resin or Mehlich-1 (Fig S3c and S3d), except that resin extract a higher P level as compared to the other biochar treatments, which also correlate better with plant P uptake (Fig S4).

The correlation between the P extractors (Mehlich-1 and resin) and the accumulation of P in plants (Fig S4) showed that resin presented a better correlation ($r = 0.750$) when compared with Mehlich-1 ($r = 0.645$). Resin extract P by exchange reactions and it is not greatly altered by the soil treatments. Therefore, it could be considered a better option to evaluate available P in biochar-treated soils, as observed by Wang et al. (2014). Mehlich-1 is an acid extractor and its extraction capacity is reduced in soils of high buffering capacity (Novais et al. 2015) or treated with alkaline materials such as biochar, which are alkaline in nature and might cause a reduced extraction capacity as observed in this study.

Dai et al. (2016) concluded that biochar can be a viable alternative for recycling P from agricultural residues, compared to the direct application of biomass, being a sustainable source with maximum efficiency and minimum P loss. The combined use of an organic matrix and a mineral source of P may be an effective strategy to decrease the adsorption of P in tropical soils since the organic matrix negatively charged can reduce the adsorption of anions (Jiang et al., 2015).

This behavior indicates that P-loaded biochar is considered an innovative technology to recycle P from wastewaters and have potential for reuse as fertilizers (Fig S5). Further studies are needed to evaluate the P availability of these biochars for a longer period and with other crops and soil types.

Conclusions

The use of poultry litter, pig manure, and sewage sludge biomasses enriched with Mg^{2+} for biochar production and recovery of P from aqueous solution is a promising technology. The highest P adsorption capacity was obtained for the pig manure biochar (PMB-Mg), which reached 68 mg g^{-1} . The main mechanisms of P removal were through precipitation with cations (Mg^{2+} , Ca^{2+} , and Al^{3+}), ligand exchange reactions, and, to a lesser extent, electrostatic attraction on the biochar surface. All Mg-impregnated and P-loaded biochars presented potential to be reused as phosphate fertilizers; their efficiencies were equal or higher to TSP in a short-term plant growth, which improved soil fertility for further cultivations. Cation-modified biochar is a sustainable option to add value to organic residues and recycle P to be reused as an enhanced efficiency fertilizer.

Acknowledgments

This work was financially supported by the National Council for Scientific and Technological Development (CNPq – Grant N° 404076/2016-5). Coordination for the Improvement of Higher Education Personnel (CAPES/PROEX) and Foundation for Research of the State of Minas Gerais (FAPEMIG) also financially supported this work. LCA Melo is a research fellow of the National Council for Scientific and Technological Development (CNPq – Grant N° 308943/2018-0). The authors acknowledge Dr. Carlos Alberto Silva (Federal University of Lavras) for the C elemental analysis. We also acknowledge Dr. Jenaina Ribeiro-Soares (Federal University of Lavras) for the Raman analysis and help with data interpretation. We also thank Dr. Patrícia de Pádua Castro for helping with several data analysis and interpretation.

References

- Agência Nacional de Águas (Brasil). 2017. Atlas esgoto: despoluição de bacias hidrográficas Agência Nacional de Águas, Secretaria Nacional de Saneamento Ambiental. Brasília: ANA, 88p.
- Agrafioti E, Bouras G, Kalderis D, Diamadopoulou E. 2013. Biochar production by sewage sludge pyrolysis. *J Anal Appl Pyrolysis*. 101:72–78. doi: 10.1016/j.jaap.2013.02.010
- Akgül G, Maden B, Diaz E. 2019. Modification of tea biochar with Mg, Fe, Mn and Al salts from aqueous for efficient sorption of PO_4^{3-} and Cd^{2+} from aqueous solutions. *J Water Reuse Desal*. 9:57-66. doi: 10.2166/wrd.2018.018
- Arai Y, Sparks DL. 2001. ATR-FTIR spectroscopic investigation on phosphate adsorption mechanisms at the ferrihydrite-water interface. *J Colloid Interface Sci*. 241:317–326. doi: 10.1006/jcis.2001.7773
- ASTM - American society for testing and material. 2007. Standard Test Method for Chemical Analysis of Wood Charcoal. West Conshohocken, PA: ASTM International, D. 1762 – 84.
- Bekiaris G, Peltre C, Jensen LS, Bruun S. 2016. Using FTIR-photoacoustic spectroscopy for phosphorus speciation analysis of biochars. *Spectrochim Acta A Mol Biomol Spectrosc*. 168:29–36. doi: 10.1016/j.saa.2016.05.049
- Brown, M.B. and Forsythe, A.B. 1974. Robust Tests for the Equality of Variances. *J Am Stat Assoc*, 69, 364-367. doi: 10.2307/2285659
- Cai R, Wang X, Ji X, Peng B, Tan C, Huang X. 2017. Phosphate reclaim from simulated and real eutrophic water by magnetic biochar derived from water hyacinth. *J Environ Manage*. 187:212–219. doi: 10.1016/j.jenvman.2016.11.047
- Chen B, Chen Z, Lv S. 2011. A novel magnetic biochar efficiently sorbs organic pollutants and phosphate. *Bioresour Technol*. 102:716–723. doi: 10.1016/j.biortech.2010.08.067

- Chia CH, Gong B, Joseph SD, Marjo CE, Munroe P, Rich AM. 2012. Imaging of mineral-enriched biochar by FTIR, Raman and SEM-EDX. *Vib Spectrosc.* 62:248–257. doi: 10.1016/j.vibspec.2012.06.006
- Cordell D. 2008. The story of Phosphorus: Missing global governance of a critical resource, Preliminary findings from 2 years of doctoral research. *Pap Prep SENSE Earth Syst Gov.*:1–25. Available from: <http://www.glogov.de/images/doc/Cordell.pdf>.
- Cui X, Dai X, Khan KY, Li T, Yang X, He Z. 2016. Removal of phosphate from aqueous solution using magnesium-alginate/chitosan modified biochar microspheres derived from *Thalia dealbata*. *Bioresour Technol.* 218:1123–1132. doi: 10.1016/j.biortech.2016.07.072
- Dai L, Li H, Tan F, Zhu N, He M, Hu G. 2016. Biochar: a potential route for recycling of phosphorus in agricultural residues. *Glob. Change Biol. Bioenergy.* 8(5):852–858. doi: 10.1111/gcbb.12365
- Dalólio FS, Nogueira J, Cássia A, Oliveira C De, De I, Ferreira F, Christiam R, Oliveira M De, Teixeira F, Teixeira S. 2017. Poultry litter as biomass energy: A review and future perspectives. *Renew Sustain Energy Rev.* 76:941–949. doi: /10.1016/j.rser.2017.03.104
- Domingues RR, Trugilho PF, Silva CA, De Melo ICNA, Melo LCA, Magriotis ZM, Sánchez-Monedero MA. 2017. Properties of biochar derived from wood and high-nutrient biomasses with the aim of agronomic and environmental benefits. *PLoS One.* 12:1–19. doi: 10.1371/journal.pone.0176884
- Enders A, Lehmann J. 2012. Comparison of Wet-Digestion and Dry-Ashing Methods for Total Elemental Analysis of Biochar. *Commun Soil Sci Plant Anal.* 43:1042–1052. doi: 10.1080/00103624.2012.656167
- Ferreira EB, Cavalcanti P, Nogueira DA. 2011. Experimental designs : um pacote R para análise de experimentos. *Revista de Estatística da UFOP.* 1: 1-9.
- Gong YP, Ni ZY, Xiong ZZ, Cheng LH, Xu XH. 2017. Phosphate and ammonium adsorption of the modified biochar based on *Phragmites australis* after phytoremediation. *Environ Sci Pollut Res Int.* 24:8326-8335. doi:10.1007/s11356-017-8499-2
- Guizani C, Haddad K, Limousy L, Jeguirim M. 2017. New insights on the structural evolution of biomass char upon pyrolysis as revealed by the Raman spectroscopy and elemental analysis. *Carbon.* 119:519–521. doi: 10.1016/j.carbon.2017.04.078
- Gunes A, Inal A, Sahin O, Taskin MB, Atakol O, Yilmaz N. 2015. Variations in mineral element concentrations of poultry manure biochar obtained at different pyrolysis temperatures, and their effects on crop growth and mineral nutrition. *Soil Use Manag.* 31:429–437. doi: /10.1111/sum.12205
- Haddad K, Jellali S, Jeguirim M, Ben A, Trabelsi H, Limousy L. 2017. Investigations on phosphorus recovery from aqueous solutions by biochars derived from magnesium-pretreated cypress sawdust. *J Environ Manage.* 216:305-314. doi: 10.1016/j.jenvman.2017.06.020
- Iwaniec DM, Metson GS, Cordell D. 2016. P-FUTURES: towards urban food & water security through collaborative design and impact. *Curr Opin Environ Sustain.* 20:1–7. doi: 10.1016/j.cosust.2016.03.001

- Jeong CY, Dodla SK, Wang JJ. 2016. Fundamental and molecular composition characteristics of biochars produced from sugarcane and rice crop residues and by-products. *Chemosphere*. 142:4–13. doi: 10.1016/j.chemosphere.2015.05.084
- Jiang D, Chu B, Amano Y, Machida M. 2018. Removal and recovery of phosphate from water by Mg-laden biochar: Batch and column studies. *Colloids Surf. A Physicochem. Eng. Asp.* 558:429–437. doi: 10.1016/j.colsurfa.2018.09.016
- Jiang J, Yuan M, Xu R, Bish DL. 2015. Mobilization of phosphate in variable-charge soils amended with biochars derived from crop straws. *Soil Till Res.* 146:139–147. doi: 10.1016/j.still.2014.10.009
- Jung K, Jeong T, Kang H, Ahn K. 2016. Characteristics of biochar derived from marine macroalgae and fabrication of granular biochar by entrapment in calcium-alginate beads for phosphate removal from aqueous solution. *Bioresour Technol.* 211:108–116. doi: 10.1016/j.biortech.2016.03.066
- Jung KW, Hwang MJ, Ahn KH, Ok YS. 2015. Kinetic study on phosphate removal from aqueous solution by biochar derived from peanut shell as renewable adsorptive media. *Int J Environ Sci Technol.* 12:3363–3372. doi: 10.1007/s13762-015-0766-5
- Lehmann, J. (Ed.), Joseph, S. (Ed.). 2015. *Biochar for Environmental Management*. London: Routledge, p. 1-12. doi: 10.4324/9780203762264
- Liang, Y., Cao, X., Zhao, L., Xu, X. and W.H., 2014. Phosphorus Release from Dairy Manure, the Manure-Derived Biochar, and Their Amended Soil: Effects of Phosphorus Nature and Soil Property. *J. Environ. Qual.* 43:1504–1509. doi: 10.2134/jeq2014.01.0021.
- Li H, Shen J, Zhang F, Clairotte M, Drevon JJ, Le Cadre E, Hinsinger P. 2008. Dynamics of phosphorus fractions in the rhizosphere of common bean (*Phaseolus vulgaris* L.) and durum wheat (*Triticum turgidum durum* L.) grown in monocropping and intercropping systems. *Plant Soil.* 312:139–150. doi: 10.1007/s11104-007-9512-1
- Li M, Tang Y, Lu XY, Zhang Z, Cao Y. 2018. Phosphorus speciation in sewage sludge and the sludge-derived biochar by a combination of experimental methods and theoretical simulation. *Water Res.* 140:90–99. doi: /10.1016/j.watres.2018.04.039
- Li R, Wang JJ, Zhou B, Awasthi MK, Ali A, Zhang Z, Lahori AH, Mahar A. 2016. Recovery of phosphate from aqueous solution by magnesium oxide decorated magnetic biochar and its potential as phosphate-based fertilizer substitute. *Bioresour Technol.* 2015: 209-214. doi: 10.1016/j.biortech.2016.02.125
- Li R, Wang JJ, Zhou B, Zhang Z, Liu S, Lei S, Xiao R. 2017. Simultaneous capture removal of phosphate, ammonium and organic substances by MgO impregnated biochar and its potential use in swine wastewater treatment. *J Clean Prod.* 147:96–107, doi:10.1016/j.jclepro.2017.01.069
- Lopes, A.S.; Guilherme, L.R.G. 2016. A career perspective on soil management in the Cerrado Region of Brazil. *Adv Agron.*137:1-72. doi: 10.1016/bs.agron.2015.12.004
- Luo X, Wang X, Bao S, Liu X, Zhang W, Fang T. 2016. Adsorption of phosphate in water using one-step synthesized zirconium-loaded reduced graphene oxide. *Sci Rep* . 6:1–13. doi: 10.1038/srep39108

- Lustosa Filho JF, Penido ES, Castro PP, Silva CA, Melo LCA. 2017. Co-Pyrolysis of Poultry Litter and Phosphate and Magnesium Generates Alternative Slow-Release Fertilizer Suitable for Tropical Soils. *ACS Sustain Chem Eng.* 5:9043–9052. doi: 10.1021/acssuschemeng.7b01935
- Lustosa Filho JF, Carneiro JS da S, Barbosa CF, de Lima KP, Leite A do A, Melo LCA. 2020. Aging of biochar-based fertilizers in soil: Effects on phosphorus pools and availability to *Urochloa brizantha* grass. *Sci Total Environ.* 709:136028. doi: 10.1016/j.scitotenv.2019.136028
- Malavolta E, Vitti GC, Oliveira SA. 1997. *Avaliação do estado nutricional das plantas: princípios e aplicações*. 2nd ed. Piracicaba: Potafos.
- Marschner, P. 2012. *Mineral nutrition of higher plants*. 3^a ed. Austrália: Elsevier, 651p.
- Marshall JA, Morton BJ, Muhlack R, Chittleborough D, Wai C. 2017. Recovery of phosphate from calcium-containing aqueous solution resulting from biochar-induced calcium phosphate precipitation. *J Clean Prod.* 165:27–35. doi: 10.1016/j.jclepro.2017.07.042
- Mehlich, A. 1953. *Determination of P, Ca, Mg, K, Na and NH₄ by North Carolina Soil Testing Laboratories*. Raleigh, University of North Carolina.
- Meroufel B, Benali O, Benyahia M, Benmoussa Y, Zenasni MA. 2013. Adsorptive removal of anionic dye from aqueous solutions by Algerian kaolin: Characteristics, isotherm, kinetic and thermodynamic studies. *J Mater Environ Sci.* 4:482–491. doi: 10.5829/idosi.ijee.2015.06.02.11
- Novais SV, Mattiello EM, Vergutz L, Carrijo L, Melo A, Freitas ÍF De, Novais RF. 2015. Loss of Extraction Capacity of Mehlich-1 and Monocalcium Phosphate as a Variable of Remaining P and its Relationship to Critical Levels of Soil Phosphorus and Sulfur. *Rev. Bras. Ciênc. Solo*:1079–1087. doi: 10.1590/01000683rbc20140551
- Novais SV, Zenero MDO, Tronto J, Conz RF, Cerri CEP. 2018. Poultry manure and sugarcane straw biochars modified with MgCl₂ for phosphorus adsorption. *J Environ Manage.* 214:36–44. doi: 10.1016/j.jenvman.2018.02.088
- Novais, R. F.; Neves, J. C. L.; Barros, N. F. 1991. Ensaio em ambiente controlado. In *Métodos de pesquisa em fertilidade do solo*; Oliveira, A. J., Garrido, W. E., Araújo, J. D., Lourenço, S., Eds.; Embrapa-SEA: Brasília, 189–253
- Pinto LP, Cabral AC, Schneider LT, Frigo KD de A, Frigo JP, Frigo EP. 2014. Levantamento de dados sobre os dejetos suínos e suas características. *Rev Bras Energias Renov.* 3:179–187. doi: 10.5380/rber.v3i3.38467
- Potgieter-Vermaak S, Maledi N, Wagner N, Van Heerden JHP, Van Grieken R, Potgieter JH. 2011. Raman spectroscopy for the analysis of coal: a review. *J Raman Spectrosc.* 42:123–129. doi: 10.1002/jrs.2636
- R Core Team. R: 2017. A language and environment for statistical computing; (accessed: 2019 Jan 23). <http://www.r-project.org>.
- Raij B van, Quaggio, JA. & da Silva, NM. 1986. Extraction of phosphorus, potassium, calcium, and magnesium from soils by an ion-exchange resin procedure, *Commun Soil Sci Plant Anal*, 17:547-566. doi: 10.1080/00103628609367733

- Rajapaksha AU, Chen SS, Tsang DCW, Zhang M, Vithanage M, Mandal S, Gao B, Bolan NS, Sik Y. 2016. Engineered / designer biochar for contaminant removal / immobilization from soil and water : Potential and implication of biochar modification. *Chemosphere*. 148:276–291. doi: 10.1016/j.chemosphere.2016.01.043
- Ribeiro-Soares J, Caçado LG, Falcão NPS, Martins Ferreira EH, Achete CA, Jorio A. 2013. The use of Raman spectroscopy to characterize the carbon materials found in Amazonian anthrosoils. *J Raman Spectrosc*. 44:283–289. doi: doi.org/10.1002/jrs.4191
- Roy ED, Richards PD, Martinelli LA, Coletta L Della, Lins SRM, Vazquez FF, Willig E, Spera SA, VanWey LK, Porder S. 2016. The phosphorus cost of agricultural intensification in the tropics. *Nat Plants*. 2:16043. doi: 10.1038/nplants.2016.43
- Saadat S, Raei E, Talebbeydokhti N. 2018. Enhanced removal of phosphate from aqueous solutions using a modified sludge derived biochar: Comparative study of various modifying cations and RSM based optimization of pyrolysis parameters. *J Environ Manage*. 225:75–83. doi: 10.1016/j.jenvman.2018.07.037
- Shapiro, S.S. and Wilk, M.B. 1965. An analyze of variance test for normality: complete samples. *Biometrika*. 52:591-611.doi: 10.2307/2333709
- Shepherd JG, Sohi SP, Heal K V. 2016. Optimising the recovery and re-use of phosphorus from wastewater effluent for sustainable fertiliser development. *Water Res*. 94:155–165. doi: 10.1016/j.watres.2016.02.038
- Silverstein, R. M., Bassler, G. C., Morrill, T. C., 1994. Identificação Espectrométrica de Compostos Orgânicos, E. Guanabara Koogan. *Rio de Janeiro*.
- Singh B, Dolk MM, Shen Q, Camps-Arbestain M. 2017. Biochar pH, electrical conductivity and liming potencial. Singh B, Camps-Arbestain M, Lehmann J editors. *Biochar: a guide to analytical methods*. Australia: CSIRO Publishing, p. 23-38.
- Takaya CA, Fletcher LA, Singh S, Anyikude KU, Ross AB. 2016. Phosphate and ammonium sorption capacity of biochar and hydrochar from different wastes. *Chemosphere*. 145:518–527. doi: 10.1016/j.chemosphere.2015.11.052
- Tan X, Liu Y, Zeng G, Wang X, Hu X, Gu Y, Yang Z. 2015. Application of biochar for the removal of pollutants from aqueous solutions. *Chemosphere* 125:70–85. doi: 10.1016/j.chemosphere.2014.12.058
- Trazzi PA, Leahy JJ, Hayes MHB, Kwapinski W. 2016. Adsorption and desorption of phosphate on biochars. *J Environ Chem Eng*. 4:37–46. doi: 10.1016/j.jece.2015.11.005
- Tsai W, Liu S, Chen H, Chang Y, Tsai Y. 2012. Textural and chemical properties of swine-manure-derived biochar pertinent to its potential use as a soil amendment. *Chemosphere*. 89:198–203. doi: 10.1016/j.chemosphere.2012.05.085
- Uchimiya M, Chang SC, Klasson KT. 2011. Screening biochars for heavy metal retention in soil: Role of oxygen functional groups. *J Hazard Mater*. 190:432–441. doi: 10.1016/j.jhazmat.2011.03.063
- Ucker FE, Almeida R de A, Kemerich PD da C. 2012. Removal of nitrogen and phosphorus from wastewater in a constructed wetland system using vetiver grass. *Rev Ambient Água*. 7:87–98. doi: 10.4136/1980-993X

- Vikrant K, Kim KH, Ok YS, Tsang DCW, Tsang YF, Giri BS, Singh RS. 2018. Engineered/designer biochar for the removal of phosphate in water and wastewater. *Sci Total Environ.* 616–617:1242–1260. doi: 10.1016/j.scitotenv.2017.10.193
- Wang T, Wang T, Camps-arbestain M, Hedley M. 2014. The fate of phosphorus of ash-rich biochars in a soil-plant system. *Plant Soil* 375: 61–74. doi: 10.1007/s11104-013-1938-z
- Wang Z, Shen D, Shen F, Li T. 2016. Phosphate adsorption on lanthanum loaded biochar. *Chemosphere.* 150:1–7. doi: /10.1016/j.Chemosphere.2016.02.004
- Withers PJA, Rodrigues M, Soltangheisi A, Carvalho TS De. 2018. Transitions to sustainable management of phosphorus in Brazilian agriculture. *Sci Rep.* 8: 2537. doi: 10.1038/s41598-018-20887-z
- Xiao X, Chen B, Chen Z, Zhu L, Schnoor JL. 2018. Insight into Multiple and Multilevel Structures of Biochars and Their Potential Environmental Applications: A Critical Review. *Environ Sci Technol.* 52:5027–5047. doi: 10.1021/acs.est.7b06487
- Yao Y, Gao B, Chen J, Zhang M, Inyang M, Li Y, Alva A, Yang L. 2013. Engineered carbon (biochar) prepared by direct pyrolysis of Mg-accumulated tomato tissues: Characterization and phosphate removal potential. *Bioresour Technol.* 138:8–13. doi: 10.1016/j.biortech.2013.03.057
- Yin Q, Wang R, Zhao Z. 2018. Application of Mg e Al-modi fi ed biochar for simultaneous removal of ammonium , nitrate , and phosphate from eutrophic water. *J Clean Prod .* 176:230–240. doi: 10.1016/j.jclepro.2017.12.117
- Yuan Liang, Xinde Cao, Ling Zhao, Xiaoyun Xu and WH. 2014. Phosphorus Release from Dairy Manure, the Manure-Derived Biochar, and Their Amended Soil: Effects of Phosphorus Nature and Soil Property. *J Environ Qual.* 43:1504–1509. doi: 10.2134/jeq2014.01.0021
- Zeng Z, Zhang S-D, Li T-Q, Zhao F-L, He Z-L, Zhao H-P, Yang X-E, Wang H-L, Zhao J, Tariq Rafiq M. 2013. Sorption of ammonium and phosphate from aqueous solution by biochar derived from phytoremediation plants. *J Zhejiang Univ-Sci B.* 14:1152–1161. doi: 10.1631/jzus.B1300102
- Zhang, J., Lü, F., Zhang, H., Shao, L., Chen, D., & He, P. 2015. Multiscale visualization of the structural and characteristic changes of sewage sludge biochar oriented towards potential agronomic and environmental implication. *Scientific reports.* 5:9406. doi:10.1038/srep09406
- Zhu D, Chen Y, Yang H, Wang S, Wang X, Zhang S, Chen H. 2020. Synthesis and characterization of magnesium oxide nanoparticle-containing biochar composites for efficient phosphorus removal from aqueous solution. *Chemosphere.* .125847. doi: 10.1016/j.chemosphere.2020.125847

Appendix A. Supplementary Information

PHOSPHORUS RECOVER USING MAGNESIUM-ENRICHED BIOCHAR AND ITS POTENTIAL USE AS FERTILIZER

RAMAN SPECTRUM AND DATA ANALYSIS

Raman analysis was performed with a LabRAM HR Evolution spectrometer. The backscattering configuration was used with a 50x objective lens in an Olympus BX41 microscope. The samples were excited by a 532 nm green laser and the power at the sample was kept lower than 5 mW to avoid sample heating and degradation. Each spectrum was collected point-by-point in a backscattering configuration from 100 to 3200 cm^{-1} with acquisition time of 10 s and with 10 accumulations. The Raman measurements were performed at three different points on each sample.

For statistical analysis, the procedure for the baseline exclusion used to all spectra was the exclusion of a linear baseline between 800 and 2000 cm^{-1} according to the procedure described by Ribeiro-Soares et al. (2013). The data were analyzed by determining the area ratio between the D and G bands (I_D/I_G), and also the relation of the G band full width at half maximum (Γ_G) with the estimated crystallite size of these carbonaceous materials. The fitting procedure was performed by using two Lorentzian peaks. The crystallite size was estimated by equation 1 (Ribeiro-Soares et al., 2013).

$$L_a(\text{nm}) = \frac{496}{(\Gamma_G - 15)} \quad (1)$$

where L_a is the estimated crystallite size and Γ_G is the full-width at half maximum.

ADSORPTION ISOTHERMS

Langmuir and Freundlich isotherm models were used to simulate the adsorption isotherm experimental data, which are expressed as equations (2) and (3):

Langmuir model:

$$Q_e(\text{mg g}^{-1}) = \frac{q_m \cdot K_L}{1 + K_L \cdot C_e} \quad \text{Eq. (2)}$$

Freundlich model:

$$Q_e(\text{mg g}^{-1}) = K_F \cdot C_e^{\frac{1}{n}} \quad \text{Eq. (3)}$$

where Q_e is the amount of adsorbate adsorbed at the equilibrium (mg g^{-1}), K_L is the Langmuir equilibrium constant (L mg^{-1}), K_F is the Freundlich equilibrium constant (mg g^{-1}), q_m is the maximum adsorption capacity of the adsorbate (mg g^{-1}), C_e is the adsorbate concentration at the equilibrium solution (mg L^{-1}), and n is the Freundlich nonlinearity constant.

SOIL CHARACTERIZATION AND FERTILIZER INFORMATION

The Oxisol was characterized by a very low level of available P (0.41 mg kg^{-1} , Mehlich-1 soil test) (Mehlich 1953), high clay content (640 g kg^{-1}) (Bouyoucos 1951), and pH_{water} of 4.8; Ca^{2+} and Mg^{2+} concentrations were 0.24 and $0.10 \text{ cmol}_c \text{ kg}^{-1}$ (KCl 1 mol L^{-1} extractor), respectively (Chapman 1965) and soil organic carbon was 11.8 g kg^{-1} (Walkley and Black 1934). In order to evaluate the P-loaded biochars as fertilizers, 200 g of soil was placed into clean and sterilized plastic pots and mixed with $\text{CaCO}_3 + \text{MgCO}_3$ at a Ca/Mg molar ratio of 3:1, aiming to increase the soil base saturation to 70%. Soil was wetted to 80% of field capacity and incubated for 30 days to correct soil acidity. In sequence, soil material was air-dried, homogenized, and fertilized with the following nutrients: N, K, S, Zn, Mn, Fe, Cu, B, and Mo, which were applied at the rates of 100, 100, 40, 4.0, 3.66, 1.55, 1.33, 0.81, and 0.15 mg kg^{-1} , respectively, to ensure a proper fertility condition for optimum plant growth in pots (Novais et al. 1991).

Table S1. EDX elemental content before and after impregnation with Mg and adsorption with P.

Element	PLB	PLB-Mg-P	PMB	PMB-Mg-P	SSB	SSB-Mg-P
%						
C	9.54	25.38	10.3	13.8	1.73	0.74
O	24.2	30.15	11.5	26.6	28.6	26.2
Na	1.90	30.15	-	-	0.23	-
Mg	2.48	9.24	1.28	20.4	0.60	7.00
Al	0.45	0.30	9.27	2.19	25.8	19.0
Si	3.34	20.1	10.2	2.28	21.2	14.3
P	3.58	3.18	8.05	9.02	0.89	8.53
S	1.02	0.29	0.78	-	2.45	0.03
Cl	18.6	7.50	-	10.6	-	2.53
K	26.6	0.28	6.87	0.54	0.57	1.11
Ca	8.31	3.59	14.1	8.19	1.72	5.64
Fe	-	-	20.4	6.46	15.2	14.3
Ti	-	-	3.84	-	1.03	0.62
Mn	-	-	0.71	-	-	-
Cu	-	-	1.06	-	-	-
Zn	-	-	1.73	-	-	-

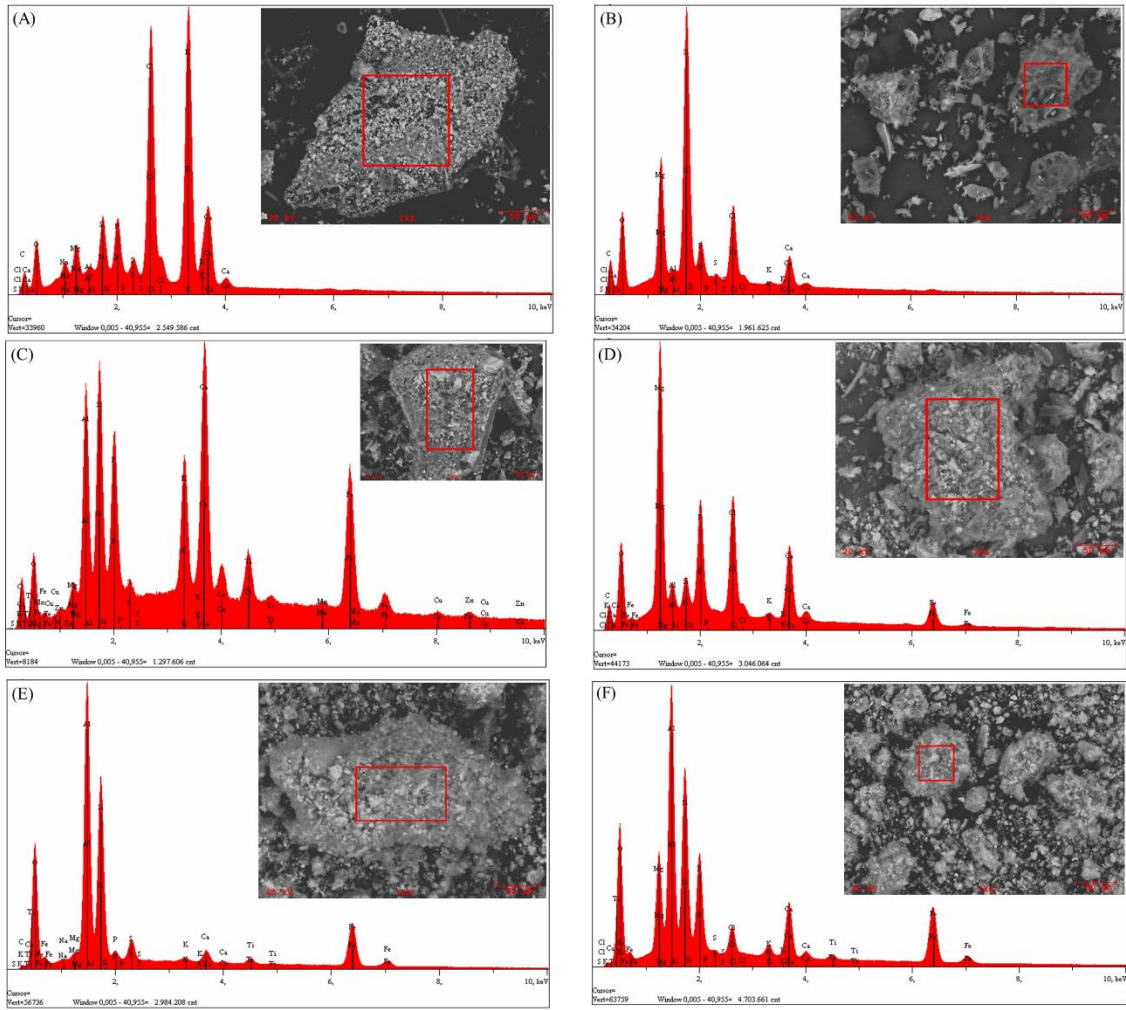


Figure S1. SEM-EDX of poultry litter biochar (A-B); pig manure biochar (C-D) and sewage sludge biochar (E-F) before and after impregnation with Mg and adsorption with P.

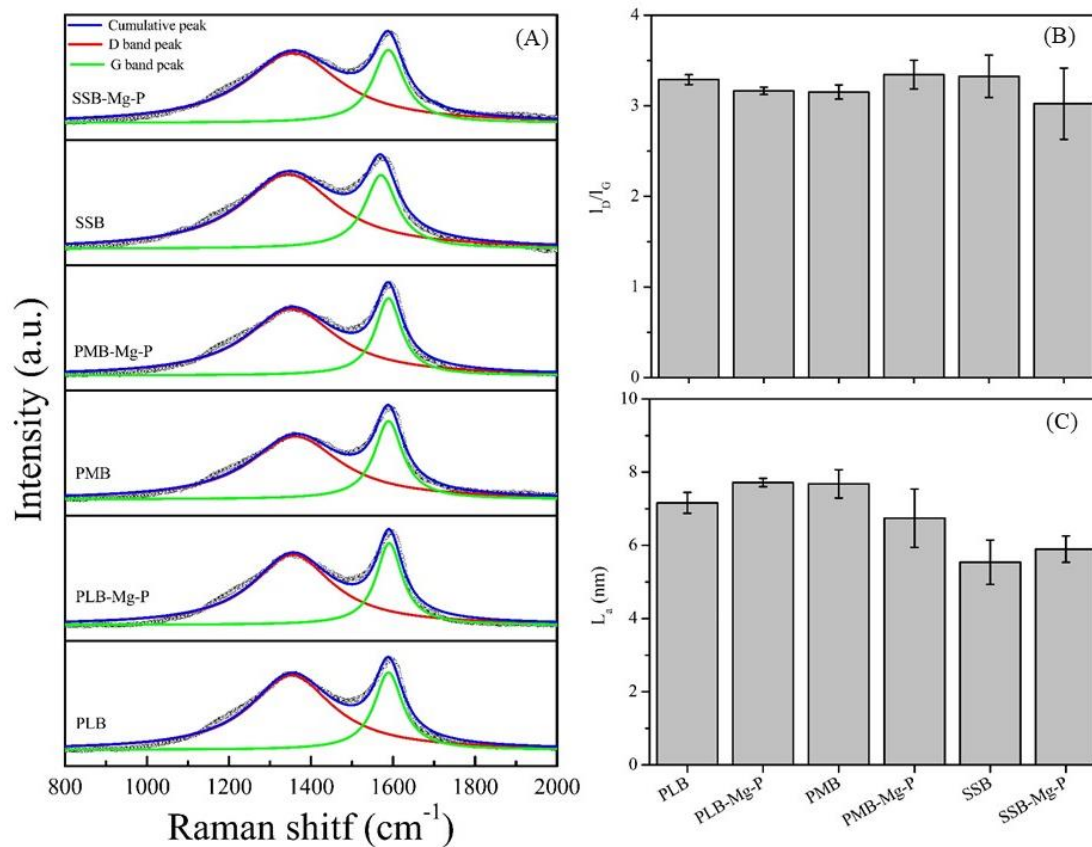


Fig S2. Raman spectra of biochars from poultry litter (PLB); pig manure (PMB) and sewage sludge (SSB) before and after impregnation with Mg and adsorption with P (A), calculated integrated area ratio of the D and G bands (I_D/I_G) (B), and estimated crystallite size (L_a) of carbonaceous materials (C).

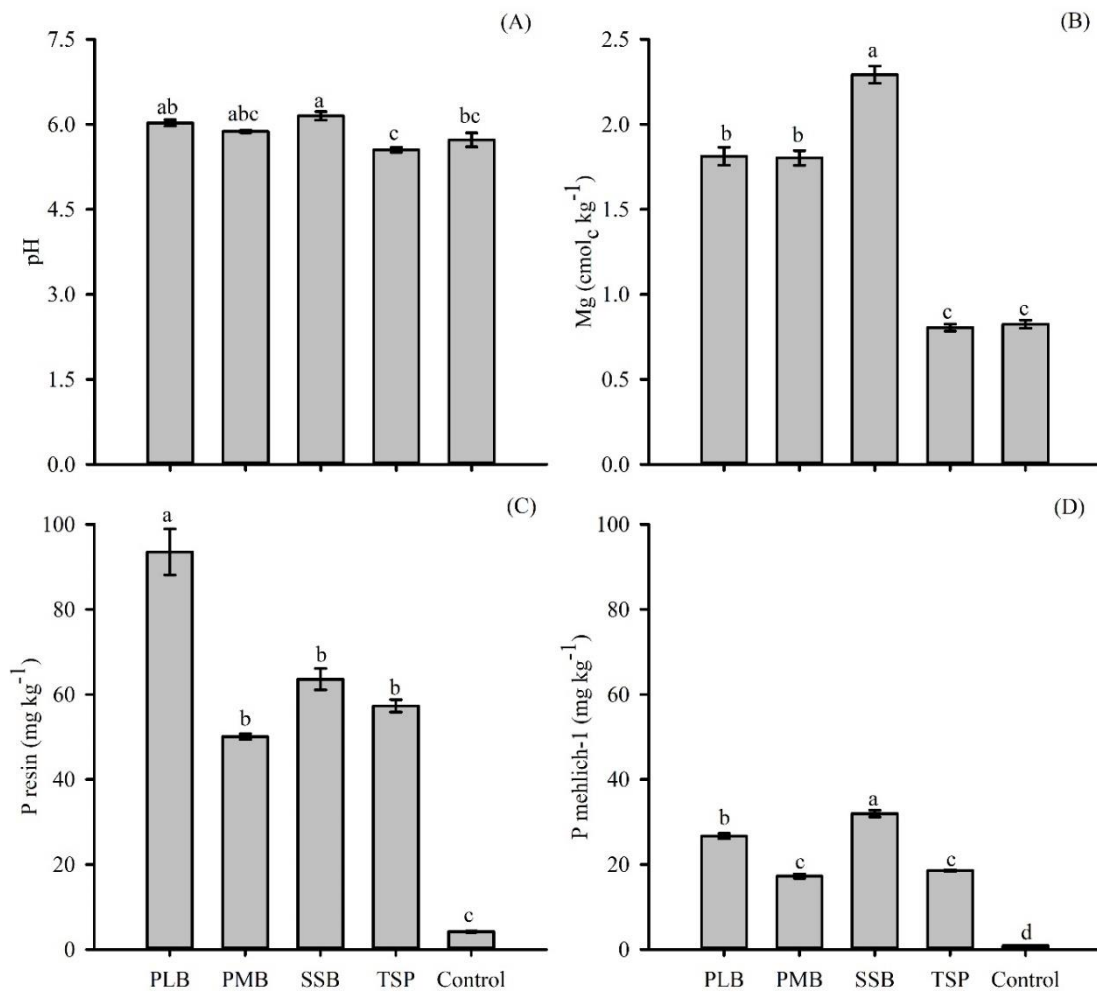


Fig S3. pH value of soil (A), Mg (B), P resin (C) and P Mehlich-1 (D) after maize growth under poultry litter biochar (PLB), pig manure biochar (PMB), sewage sludge biochar (SSB), after impregnation with Mg and adsorption with P, triple superphosphate (TSP) and no fertilizer (control).

Notes: Means followed by the same letter do not differ among themselves, according to the Tukey test ($p < 0.05$). Error bars represent the standard deviations of the treatment mean replicates ($n=4$)

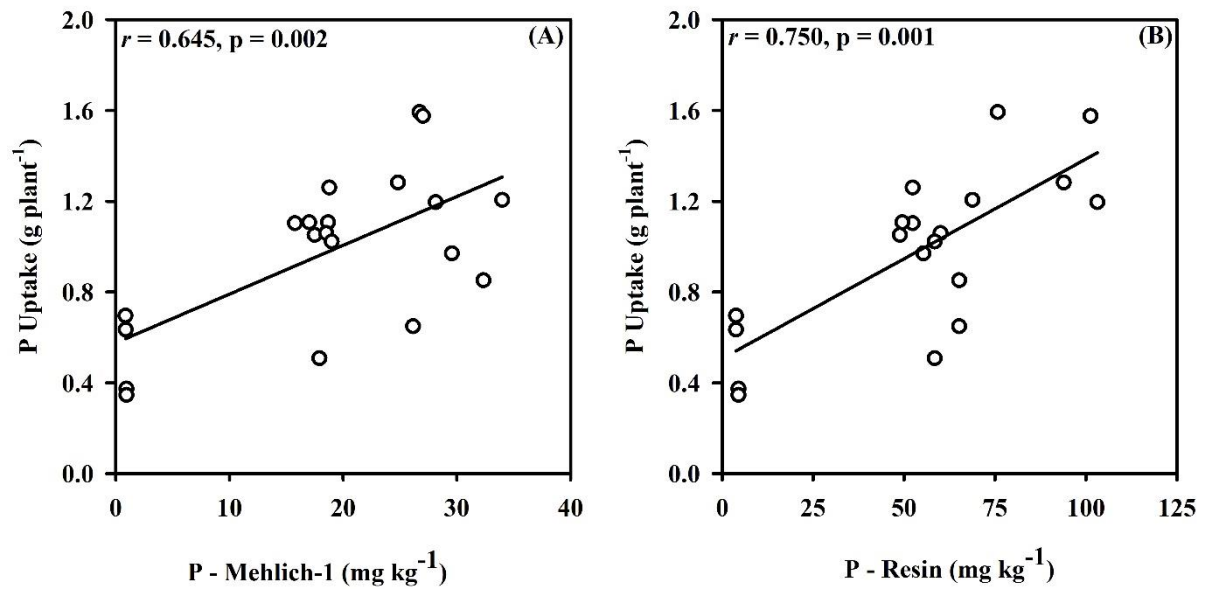


Figure S4. Correlation of Pearson (r) between P uptake and soil available P-Mehlich-1 (A) and P-Resin (B).



Figure S5. Growth of maize fertilized with P adsorbed biochar

References

- Bouyoucos, G.H. 1951. A Recalibration of the Hydrometer for Making Mechanical Analysis of Soils. *Agronomy J.* 43:434-438. doi: 10.2134/agronj1951.00021962004300090005x
- Chapman, H. D. 1965. Cation-exchange capacity In: Black, C.A., Ed., *Methods of Soil Analysis*, American Society of Agronomy, Madison, 891-901. doi:10.2134/agronmonogr9.2.2ed.c8
- Mehlich, A. 1953. Determination of P, Ca, Mg, K, Na and NH₄ by North Carolina Soil Testing Laboratories. Raleigh, North Carolina State University.
- Ribeiro-Soares J, Cançado LG, Falcão NPS, Martins Ferreira EH, Achete CA, Jorio A. 2013. The use of Raman spectroscopy to characterize the carbon materials found in Amazonian anthrosoils. *J Raman Spectrosc.* 44:283–289. doi: doi.org/10.1002/jrs.4191
- Walkley. A.; Black. I. A. 1934. An examination of the Degtjareff method for determining soil organic matter and a proposed modification of the chromic acid titration method. *Soil Science.* 37:29-38. doi: 10.1097/00010694-193401000-00003

CHAPTER 2

Production of engineered-biochar under different pyrolysis condition for phosphorus removal from aqueous solution

Chapter prepared following the guidelines of the Journal of Cleaner Production (to be submitted)

Production of engineered-biochar under different pyrolysis conditions for phosphorus removal from aqueous solution

Bárbara Olinda Nardis^a, José Romão Franca^b, Jefferson Santana da Silva Carneiro^a, Jenaina Ribeiro Soares^b, Luiz Roberto Guimarães Guilherme^a, Leônidas Carrijo Azevedo Melo^{a*}

^aSoil Science Department, Federal University of Lavras, 37200-900 Lavras, Minas Gerais, Brazil

^bPhysics Department, Federal University of Lavras, 37200-900 Lavras, Minas Gerais, Brazil

*Corresponding author

Leônidas Carrijo Azevedo Melo

E-mail: leonidas.melo@ufla.br

Abstract

Phosphorus (P) recycling from wastewater using biochar is an alternative to build a sustainable P circular economy. Due to negative surface charge of biochar, cation impregnation is needed to enhance its P removal capacity. However, the efficiency of different cations under different pyrolysis environment is still not completely understood. We aimed at studying the P adsorption and release capacity of biochar enriched with aluminum (Al^{3+}), iron (Fe^{3+}), and magnesium (Mg^{2+}) prepared under different pyrolysis conditions (Air-limited and N_2 -flow). Biochar samples were produced from pig manure (PMB) impregnated, separately, with 20% of AlCl_3 , MgCl_2 , and FeCl_3 solution on either in an air-limited adapted muffle furnace or in a furnace under N_2 -flow. The synthesized materials were characterization by pH value, electrical conductivity, total nutrient, moisture, ash, specific surface area (S_{BET}), pore volume, FTIR, XRD, and SEM-EDX. Phosphorus adsorption was studied by kinetics models and adsorption isotherms, and desorption was also assessed. The biochar impregnated with Mg^{2+} and produced in the muffle furnace, obtained the maximum P adsorption (231 mg g^{-1} , SIPS isotherm), with 100% of this adsorbed P being released in acidic solution (Mehlich-1 and Citric acid 2%). The pyrolysis conditions had small or no influence on the biochar characteristics that govern P

adsorption, such as chemical functional groups, surface area, quantity and size of pores and formation of synthetic minerals. Therefore, it is possible to produce biochar in a simpler way, without using a carrier gas when it comes to P adsorption studies. The main mechanisms of P removal were through precipitation with cations, surface complexation, protonation process, ligand exchange reactions and electrostatic attraction on the biochar surface. In conclusion, Mg-impregnated biochar is a sustainable option to add value to organic residues and to recycle P to be reused as enhanced efficiency fertilizer.

Keywords: recycling, metals, activation; impregnation

Highlights

- Biochars of pig manure were produced under N₂-flow (PMB-N₂) and air-limited pyrolysis (PMB-M).
- Biochars impregnated with Al, Fe and Mg were produced under different pyrolysis conditions.
- Biochar impregnated with Mg and produced in the furnace muffle showed maximum removal rate (231 mg g⁻¹).
- The pyrolysis conditions had small influence on the phosphate adsorption.

1. Introduction

Phosphorus (P) is an essential nutrient for plants and a finite resource. Most phosphate fertilizers used in the agriculture come from phosphate rocks, which are concentrated in a few countries such as Morocco, Russia, China, and USA, increasing the pressure for improving the use efficiency and recycling of this nutrient. Moreover, due to the population increase there is a higher demand of phosphate fertilizers in order to meet the increased demand for food and fibers (Schröder et al., 2011).

Currently, there is a great effort towards improving P management with techniques aimed at recycling and recovering P from wastes and wastewaters (Nesme and Withers, 2016), and, in this context, biochar is a promising adsorbent material for this purpose (Xiang et al. 2020). Biochar is the solid product of biomass pyrolysis in the absence or low availability of oxygen (Lehmann and Joseph, 2009). The interest in biochar has been growing in recent years due to several environmental applications such as retention of organic (e.g. pesticides) and inorganic contaminants (e.g. heavy metals), and also in carbon sequestration (Rodriguez-Narvaez et al. 2019). The applications of biochar depend on its properties, such as functional groups, surface area and porosity, which depend on its conditions of preparation and production (De Gisi et al. 2016). Recent studies with biochar have focused on the optimization of production processes to reduce environmental costs, reduce energy consumption, and enhance its applicability (Luo et al. 2015; Chen et al. 2020).

Most researchers report the biochar production by using N₂ flow as a carrier gas, which is intended to remove gases formed during pyrolysis and thereby obtaining a "cleaner" biochar, which might influence characteristics such as porosity, surface area and chemical functional groups (Zhu et al. 2018). Muffle furnaces adapted to prevent air-flow is also a common method used to produce biochar (Gonzaga et al., 2017; Thines et al. 2017; Tan et al. 2018). Bekiaris et al. (2016), for instance, produced biochar in different temperatures in a muffle furnace using two crucibles by placing one upside down on the top of the other, where the biomass was compacted inside, creating a filled cavity. This way, there is no entry of oxygen (O₂) and allows gases to be released during pyrolysis. This condition is considered more rudimentary, since it does not require any equipment adapted for N₂ flow. The absence of a carrier gas can cause the gases produced on the surface of the biochar to overlap, which can accumulate in the pores and thereby reduce the porosity and specific surface area (Buss et al. 2016).

Biochar surface is usually dominated by negative charges due to the high pH value and the presence of oxygenated groups, which leads to a low P recovery capacity from aqueous solutions (Zeng et al. 2013; Takaya et al. 2016; Shepherd et al. 2017). To overcome this low recovery, an alternative is the impregnation of raw material with cations for subsequent pyrolysis. Cations additions creates cationic bridges and substantially increase the P adsorption capacity from wastewater (Li et al. 2016; Nardis et al. 2020). The most used cations for the treatment of biochar aiming to recover phosphate are magnesium (Mg^{2+}), iron (Fe^{2+}), and aluminum (Al^{3+}) (Zhang et al. 2012; Cui et al. 2016; Jung & Ahn, 2016; Li et al. 2016; Cai et al. 2017; Wan et al. 2017; Novais et al. 2018; Yang et al. 2018).

There are several studies on biochar impregnated with metals for P adsorption, but few researchers compared biochar impregnated with different cations and especially, produced under different atmospheres - muffle furnace (low O_2) and a furnace under N_2 (without O_2). We hypothesized that biochar produced under N_2 flow will increase the porosity and consequently will increase the P adsorption capacity when compared with that prepared in muffle furnace. Also, impregnation with cations modifies the properties of the biochar and increase the adsorption of P under the influence of different atmospheres.

Therefore, the objective of this work was to evaluate the effect of biomass impregnation with different cations (Mg^{2+} , Fe^{3+} and Al^{3+}) and pyrolysis conditions to prepare biochar (furnace with N_2 flow and muffle furnace) on their physicochemical properties and their consequent influence on P adsorption capacity.

2. Material and methods

2.1 Biomass preparation

Pig manure was collected in a farm near Lavras, Minas Gerais state, Brazil ($21^{\circ}13'34''$ S and $44^{\circ}58'31''$ W). The feedstock was oven dried at $50^{\circ}C$ until constant weight, ground in a mill equipped with a 10-mesh sieve (<0.25 mm) and stored in plastic recipients. The amounts of macro and micronutrients in the biomass were determined using ICP-OES, after nitric-perchloric digestion. The nitrogen was determined by Kjeldahl method after sulfuric acid (Malavolta et al. 1997). Later, the material was impregnated with magnesium chloride ($MgCl_2 \cdot 6H_2O$), (Synth, 98%) iron chloride ($FeCl_3 \cdot 6H_2O$) (Vetec, 98%) and aluminum chloride

($\text{AlCl}_3 \cdot 6\text{H}_2\text{O}$) (Merk, 97%) with prepared solutions aiming to reach 20% of Mg, Fe and Al in the biochar, according to Li et al. (2016) with modifications. For this, 50 g of pig manure was mixed with 150 mL of each solution (MgCl_2 , FeCl_3 and AlCl_3), by shaking for 24 h at 120 oscillations per minute in a shaker (TE 240/1 Tecnal) and then oven dried at 80 °C to constant weight.

2.2 Biochar production

The biochar samples were produced under two different atmospheres. Firstly, pig manure without and with Mg^{2+} , Fe^{3+} and Al^{3+} impregnation were tightly accommodated in porcelain crucibles, which were overlapped to prevent O_2 flow and allow pyrolysis in a muffle furnace (Bekiaris et al. 2016). The same materials were pyrolyzed in a horizontal furnace EDG/FT-HI series under N_2 atmosphere (200 mL min^{-1}). In both furnaces, the materials were subjected to a heating rate of $\sim 10 \text{ }^\circ\text{C min}^{-1}$ up to reach 500 °C, with 2 h of holding time (Lustosa Filho et al. 2017). After pyrolysis, the samples were slowly cooled to room temperature inside the furnaces, ground in a porcelain mortar, and sieved to $<0.25 \text{ mm}$. The pig manure biochar samples are herein identified with a code comprising the feedstock (PMB), the pyrolysis conditions (M – muffle furnace or N_2 – horizontal furnace under N_2 flow), and the impregnated cation (Mg, Fe, Al). Therefore, the produced materials were as follows: PMB-M, PMB- N_2 , PMB-M-Mg, PMB- N_2 -Mg, PMB-M-Al, PMB- N_2 -Al, PMB-M-Fe and PMB- N_2 -Fe.

2.3 Biochar characterization

The values of electrical conductivity (EC) and pH were determined, in triplicate, according to Singh et al. (2017). The ash contents were evaluated by the standard method ASTM D1762-84 (ASTM, 2007). Total amounts of Al, Ca, Fe, Mg, and P were determined according to Enders and Lehmann (2012). The C amount was determined in an elemental analyzer (model Vario TOC cube, Elementar, Germany). The specific surface area (S_{BET}) and pore volumes were determined by N_2 adsorption/desorption analysis at 77 K using a Micromeritics ASAP 2420. The point of zero charge (pH_{PZC}) of the adsorbent was determined by the pH drift method, as described by Bayazit and Kerkez (2014).

Microscopic features and morphology were characterized using a field emission gun scanning electron microscopy (SEM) (LEO EVO 40 XVP - Carl Zeiss) equipped with an energy-dispersive X-ray (EDX) spectroscopy (Brunker - Quantax EDX) to measure the percent

of elements on the surface of the materials. Fourier transform infrared (FTIR) spectroscopy was recorded using a Digilab Excalibur spectrometer with a spectral range 4000–400 cm^{-1} with 32 scans and 4 cm^{-1} resolutions. X-ray diffraction (XRD) analysis was also carried out to identify any crystallographic structure in the samples using a $\text{CuK}\alpha$ ($\lambda = 0.1540 \text{ nm}$) radiation, operated at 40 kV and 40 mA, with Ni filter (Bruker D8 Advance Davinci). XRD patterns were identified on a program MATCH 3.8.3.151.

FTIR and XRD analyzes were performed on biochar samples without and with Mg^{2+} , Fe^{3+} and Al^{3+} impregnation and analyses with SEM-EDX were also measured after P adsorption.

2.4 Batch adsorption experiments

Batch adsorption study was performed as described by Li et al. (2016) with modifications. Briefly, 500 mg of biochar samples were placed in 50 mL polypropylene tubes and 20 mL of phosphate solution (KH_2PO_4) was added (i.e. 25.0 g L^{-1} of adsorbent dose) with different P concentrations (0, 10, 20, 50, 100, 200, 300, 400 and 500 mg L^{-1} for PMB-Fe; 0, 10, 20, 50, 100, 200, 300, 400, 500, 800, 1000, 2000, 3000 and 4000 mg L^{-1} for PMB-Al; 0, 10, 20, 50, 100, 200, 300, 400, 500, 800, 1000, 2000, 3000, 4000, 5000, 8000 and 10000 mg L^{-1} for PMB-Mg), which were prepared using 0.01 mol L^{-1} $\text{Ca}(\text{NO}_3)_2$ as background solution. The mixture was stirred for 24 h at 120 oscillations per minute at room temperature. After this period, the extracts were filtered in membranes ($<0.45 \mu\text{m}$, Millex HP). To evaluate adsorption kinetics, 60 mg of each biochar were mixed with 30 mL of a solution containing 50 mg L^{-1} of P, and the mixture was stirred and filtered at predetermined regular time intervals (0, 10, 20, 30, 60, 120, 240, 480, 960, and 1440 min) (Cui et al. 2016). All experiments were performed in triplicate using deionized water (Milli-Q) and blank samples were included in each batch to check any cross contamination. The P concentration at equilibrium solutions was measured by ICP-OES. All reagents were of analytical grade and used without further purification.

For the desorption study (extraction) 200 mg of biochar were added in 40 mL of KH_2PO_4 solution containing 500 mg L^{-1} of P. After adsorption, the P-loaded adsorbent was separated from the solution through centrifugation (4340 g-force) and the P concentration was determined in the supernatant to calculate the amount of adsorbed P. Then, three solutions were tested for P extraction, i.e. 10 mL of deionized water, 2% citric acid or Mehlich-1 solution (0.025 mol L^{-1} de H_2SO_4 + 0.05 mol L^{-1} de HCl). These solutions were added separately to the

tubes, which were shaken for another 4 h. After, the supernatant was filtered in blue band filter (Unifil C42, blue band of slow filtering) and P was measured by ICP-OES. The amount of desorbed P was calculated by dividing the desorbed amount by the adsorbed amount.

2.5 Isotherm and kinetics models

The adsorption capacity (Q_e) of the different biochar materials was calculated by mass balance as expressed by equation (1):

$$Q_e (mg g^{-1}) = \frac{V(C_i - C_e)}{m} \quad (1)$$

where V is the volume of solution (L), C_i and C_e are the initial and equilibrium P concentrations ($mg L^{-1}$), respectively, and m is the biochar (adsorbent) mass (g).

Langmuir, Freundlich and SIPS (Langmuir-Freundlich) isotherm models were used to fit the experimental data, using the Origin 8.0 software, which are expressed as equations (2), (3) and (4):

Langmuir model:

$$Q_e (mg g^{-1}) = \frac{q_m \cdot K_L}{1 + K_L \cdot C_e} \quad (2)$$

Freundlich model:

$$Q_e (mg g^{-1}) = K_F \cdot C_e^{\frac{1}{n}} \quad (3)$$

SIPS model:

$$Q_e (mg g^{-1}) = q_m \frac{k C_e^{n_s}}{1 + k C_e^{n_s}} \quad (4)$$

where Q_e is the amount of adsorbate adsorbed at the equilibrium ($mg g^{-1}$), K_L is the Langmuir equilibrium constant ($L mg^{-1}$), K_F is the Freundlich equilibrium constant ($mg g^{-1}$), q_m is the maximum adsorption capacity of the adsorbate ($mg g^{-1}$), C_e is the adsorbate concentration at

the equilibrium solution (mg L^{-1}), n is the Freundlich nonlinearity constant and K_s and n_s are the SIPS constants.

For kinetics study, pseudo first-order, pseudo second-order and intra-particle diffusion (Weber-Morris, 1963) models were used for assessing the reaction order of P adsorption onto biochar samples, which are expressed as equations (5), (6) and (7):

$$Q_t = qe(1 - e^{-k_1 t}) \quad (5)$$

$$Q_t = \frac{q_e^2 k_2 t}{1 + q_e k_2 t} \quad (6)$$

$$Q_t = K_i t^{\frac{1}{2}} + C \quad (7)$$

In which Q_t is the amount of P adsorbed (mg g^{-1}) at time t , q_e is the amount of P adsorbed (mg g^{-1}) at equilibrium time, k_1 (h^{-1}), k_2 ($\text{g mg}^{-1} \text{h}^{-1}$), and K_i ($\text{g mg}^{-1} \text{h}^{-0.5}$) are constants of the pseudo first-order, pseudo second-order and intra-particle diffusion models, respectively (Simonin, 2016). The C is constant related to diffusion layer thickness (mg g^{-1}).

2.6 Statistical analysis

To check for differences between pyrolysis conditions the data of chemical properties and P desorption were analyzed by normality using the Shapiro Wilk test (Shapiro and Wilk, 1965), and homoscedasticity was verified using the variance equation test (or the Levene test) (Brown and Forsythe, 1974). Also, data were subjected to analysis of T-student (significant ($p < 0.05$) using software R 3.4.1. (R Core Team, 2017).

3. Results and discussion

3.1 Effect of cation impregnation and pyrolysis conditions on biochar physicochemical properties

The chemical characteristics of biochar produced under different pyrolysis conditions and impregnated with different cations are presented in Table 1. The pH values ranged from

1.6 to 9.8, with Fe-impregnated biochar being the most acidic and non-impregnated biochar had the highest pH values. The pH value was not affected by the biochar pyrolysis conditions. The higher pH value of pristine biochar (PMB) and biochar impregnated with Mg (PMB-Mg) is due to the release of alkaline groups during pyrolysis, since these are rich mainly in Ca and Mg (Mukherjee and Lal, 2016) (Table 1). The relatively lower pH value of the biochar impregnated with Al may be related to the lower release of alkaline groups, and the higher formation of acid groups during pyrolysis (Yin et al. 2018). PMB-Fe biochar have acid characteristics probably due to the source used ($\text{FeCl}_3 \cdot 6\text{H}_2\text{O}$), which upon contact with water is hydrolyzed and generates an acid reaction, producing HCl (equation 8) which has a pH value of 1.5-2.0 (Lussiez and Beckstead, 1997).



The impregnation and pyrolysis conditions of biochar influenced the yield of the biochar, which was lower in the biochar without impregnation (Table 1). There was less yield in biochar samples produced in the muffle furnace, except for PMB-Al. The presence of O_2 (muffle), even at low concentrations, may have accelerated the biomass carbonization by drastic combustion, increasing aromaticity and decreasing yield compared to the use of N_2 (Luo et al. 2015).

Table 1. Chemical properties of the pristine and cation-impregnated biochar produced in muffle furnace (M) or under N₂ flow (N₂).

Properties	Biochar							
	PMB-M	PMB-N ₂	PMB-M-Mg	PMB-N ₂ -Mg	PMB-M-Al	PMB-N ₂ -Al	PMB-M-Fe	PMB-N ₂ -Fe
Yield (%)	30* ± 0.9	40* ± 0.2	39* ± 0.3	55* ± 0.6	68* ± 0.6	39* ± 0.0	55* ± 0.3	59* ± 0.3
pH (Water)	9.77 ^{ns} ± 0.01	9.68 ^{ns} ± 0.03	9.25 ^{ns} ± 0.01	9.25 ^{ns} ± 0.01	5.23* ± 0.06	5.64* ± 0.05	1.66* ± 0.01	1.70* ± 0.01
CE (mS cm ⁻¹)	0.76* ± 0.0	0.06* ± 0.0	4.79* ± 0.03	4.54* ± 0.01	1.76* ± 0.03	2.17* ± 0.02	4.24* ± 0.01	5.01* ± 0.02
C (%)	57.9 ^{ns} ± 2.80	44.8 ^{ns} ± 0.70	25.5 ^{ns} ± 0.05	26.9 ^{ns} ± 0.25	24.9* ± 0.20	23.4* ± 0.20	18.5 ^{ns} ± 0.05	18.8 ^{ns} ± 0.25
Ash (%)	39.2* ± 0.9	36.4* ± 0.1	47.9 ^{ns} ± 0.5	44.2 ^{ns} ± 0.8	47.5* ± 0.3	45.4* ± 0.1	47.8 ^{ns} ± 0.1	47.0 ^{ns} ± 0.3
Ca (g kg ⁻¹)	65.7* ± 0.5	95.8* ± 0.7	22.0* ± 0.3	14.4* ± 0.1	32.2 ^{ns} ± 0.3	32.0 ^{ns} ± 0.1	32.7 ^{ns} ± 0.3	32.9 ^{ns} ± 0.3
Mg (g kg ⁻¹)	4.70 ^{ns} ± 0.04	4.83 ^{ns} ± 0.05	169* ± 2	149* ± 5	2.02 ^{ns} ± 0.02	2.31 ^{ns} ± 0.11	2.07* ± 0.01	2.44* ± 0.01
Fe (g kg ⁻¹)	3.99 ^{ns} ± 0.08	5.89 ^{ns} ± 0.48	0.63 ^{ns} ± 0.19	0.44 ^{ns} ± 0.09	5.57* ± 0.14	3.82* ± 0.12	115 ^{ns} ± 2	113 ^{ns} ± 3
Al (g kg ⁻¹)	3.77 ^{ns} ± 0.21	4.81 ^{ns} ± 0.44	0.69 ^{ns} ± 0.09	0.52 ^{ns} ± 0.09	168 ^{ns} ± 2	171 ^{ns} ± 1	0.48 ^{ns} ± 0.06	0.42 ^{ns} ± 0.03

Notes: ns - not significant. * Significant at 5% probability ($p < 0.05$) by the T-student test. The test compares pyrolysis conditions (M-muffle and N₂- with N₂ flow), inside each impregnated cation. Values are average ± standard error (n=3).

There was a large variation on the C content (18.5% to 57.9%) among the biochar materials, and this was affected by both cation impregnation type and pyrolysis conditions (Table 1). The pristine biochar had the highest C content, and the Fe-impregnated biochar the lowest. The lower C content can be attributed to the increase in the metals Al, Fe, and Mg in the biochar, which act as activators causing an increase in the release of volatile carbonic gases produced during a pyrolysis (Yin et al. 2018; Zhang et al. 2012). Among the pyrolysis conditions, the biochar produced in the muffle furnace showed lower C content in PMB-Mg and PMB-Fe compared to biochar prepared under N₂ flow, while PMB and PMB-Al had lower C content under N₂ flow.

The largest specific surface area (Fig. 1) was found in the PMB-N₂-Mg (33.78 m² g⁻¹), followed by PMB-M-Mg (23.76 m² g⁻¹), which was 3-4 times larger than other biochar samples. The relatively low specific surface area found may be due to the fact that there was no chemical activation process such as acid washing after pyrolysis for pore cleaning and biochar functionalization (Penido et al. 2019).

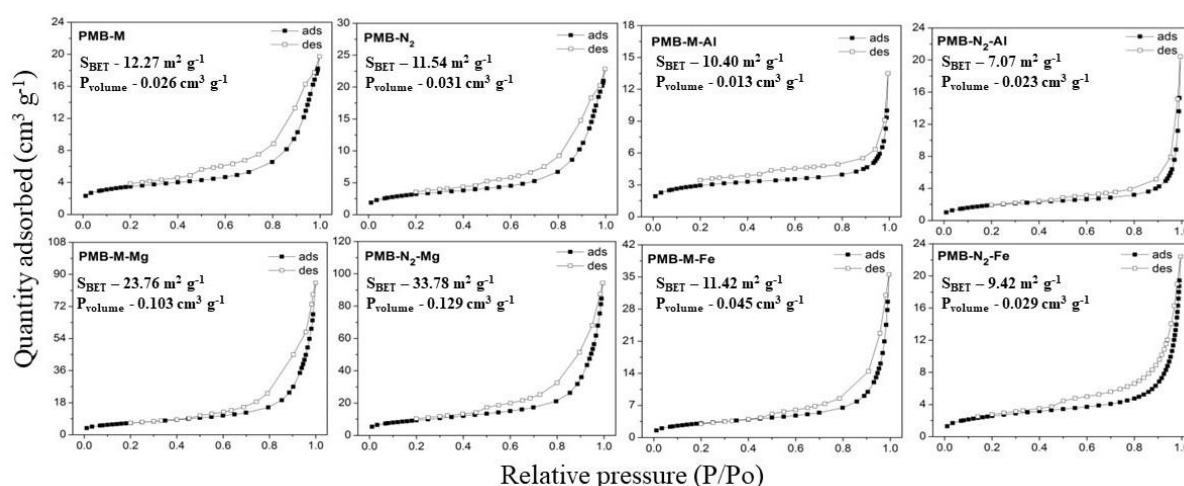


Fig. 1. Nitrogen isotherms of biochar samples, BET surface areas (S_{BET}) and the total pore volume (P_{volume}). Notes: The specific surface area (S_{BET}) was calculated based on BET method. P_{volume} was the total pore volume of pores less than 333.89 nm in diameter at $P/P_0 = 0.995$ in single-point desorption.

The S_{BET} found in the biochar impregnated with Mg was similar to that found for sugarcane harvest residue biochar (27.22 m² g⁻¹) impregnated with 20% Mg (Li et al. 2016). For biochar impregnated with Al, the surface area was up to forty times lower than that obtained in a poplar chip biochar impregnated with 20% Al (418 m² g⁻¹) (Yin et al., 2018). The biochar impregnated with Fe also had lower surface area values than those reported in the literature for biochar of forestry wood waste impregnated with 26% Fe (223 m² g⁻¹) (Sun et al. 2019). In general, biochars from ash-rich residues (e.g. manures and sludges) tend to have a much lower

surface area than those produced from wood biomass (Hassan et al., 2020). The different types of raw material respond heterogeneously to the different pyrolysis conditions due to variations in the composition such as quantity of minerals, lignin, cellulose and hemicellulose (Clemente et al., 2018).

The difference in values found in S_{BET} , P_{volume} (Fig. 1) and pore distribution (Fig. 2) is different from the values related in the literature due to differences in the feedstock used, production process, metal level in the impregnation, source of mineral salt, pH of the reaction, feedstock nutrient content, type of pyrolysis oven, pyrolysis atmosphere, among other factors (Luo et al. 2015; Rawal et al. 2016).

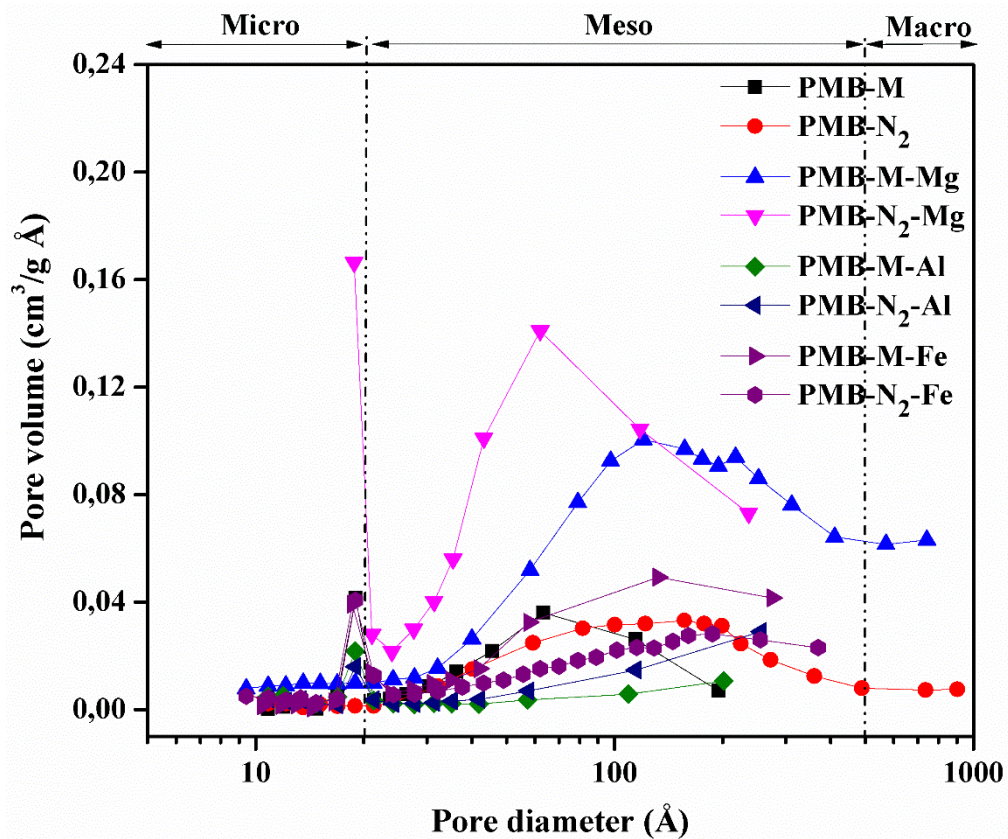


Fig. 2. Pore size distribution of biochar samples using $dV/d\log(r)$ vs r plots.

Magnesium impregnation did not substantially increase the area (Fig.1) but had a major contribution to the increase in total pore volume (P_{volume}) (Fig. 2). Such fact was not observed when biochars were impregnated with Al and Fe. The pore distribution shows that in all biochar samples there is a predominance of mesopores of size between 20 and 500 Å (IUPAC, 2014). However, the treatment with Mg developed a greater amount of mesopores.

The greater pore volume in the PMB-Mg biochar may have been caused by the effect of Mg on the decomposition of the biomass altering the path of the decomposition. $MgCl_2$ alters

the cellulose pyrolysis reaction pathways present in the biomass, causing an improvement in the crosslinking of hydroxyl groups releasing water during heating. This process results in a more crosslinked cellulose and consequently producing a more porous biochar (Liu et al. 2015). During the pyrolysis, the MgCl_2 is converted to MgO and crystals formed on the surface of the biochar can promote the blockage of the smaller pores, resulting in a biochar with a greater amount of mesopores (Fig. 2) (Zhu et al. 2020).

The low S_{BET} with consequent low P_{volume} value in the biochar samples impregnated with Al and Fe may have been caused by the collapse of the pore system in the presence of metals, which, unlike Mg, did not interact with cellulose (Akgül et al. 2019; Batista et al. 2018).

3.2 Phosphorus adsorption studies using cation-modified biochar

3.2.1 Batch adsorption experiments

The P adsorption isotherms are shown in Fig. 3 and the fit parameters for Langmuir, Freundlich, and SIPS are shown in Table 2. The highest adsorption capacity was obtained for PMB-M-Mg, followed by the sequence $\text{PMB-N}_2\text{-Mg} > \text{PMB-M-Al} > \text{PMB-N}_2\text{-Al} > \text{PMB-N}_2\text{-Fe} > \text{PMB-M-Fe}$. The maximum adsorption capacity estimated by the Langmuir model was 324 mg g^{-1} for PMB-M-Mg, and 226 mg g^{-1} for PMB-N₂-Mg, which is much higher than when the biochar was impregnated with Al (39.6 mg g^{-1} for PMB-M-Al and 23.4 mg g^{-1} for PMB-N₂-Al). The pyrolysis conditions influenced the adsorption capacity, and the biochar produced in the muffle promoted greater adsorption of P. According to Chacón et al. (2020) the use of an inert gas in the production of the biochar is important, however, the presence of oxygen (muffle furnace) increases the biochar's ability to accept electrons, consequently increasing the adsorption of anions such as phosphate.

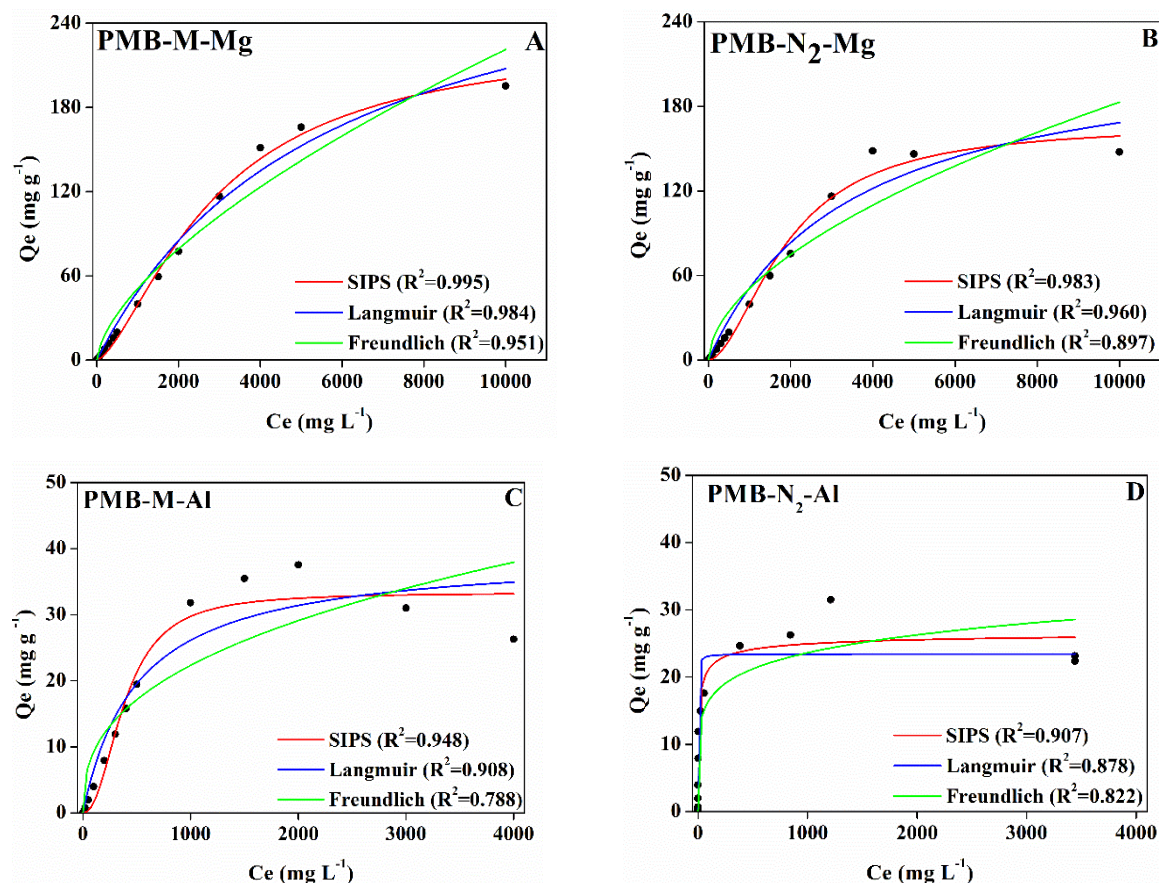


Fig. 3. Adsorption isotherms of biochar samples impregnated with different cations and prepared in muffle furnace (M) or under N₂ flow (N₂).

Fe-impregnated biochar showed the lowest P adsorption and did not fit Langmuir, Freundlich and SIPS models (Fig. S1). This low adsorption capacity may be due to the pH value of the biochar PMB-M-Fe and PMB-N₂-Fe (~1.7) being higher than their pH_{PZC} (1.0) causing a predominance of negative charges and thus an electrostatic repulsion that inhibit P adsorption on the biochar surface (Fig. S3). The impregnation with Fe promotes an increase in the dominant mineral phase in the biochar in the form of oxide (Fig. S5), in addition to increasing the functional groups (discussed in later sections), which increases the biochar's ability to donate electrons (Chacón et al. 2020). This feature decreases the biochar's ability to adsorb P, in addition to the low S_{BET} and the porosity of this biochar (Fig. 1).

The Langmuir model proposes that adsorption occurs homogeneously on the entire surface of the adsorbent, and supposedly the P affinity is equally distributed over the biochar surface, whereas the adsorption constant (K_F) of the Freundlich model suggest that the adsorption occurs differently on the surface of the biochar (Table 2). The values of $1/n$

(Freundlich Isotherms) in all biochar samples were lower than 1, and this index describes the distribution of the active sites and consequently to the adsorption capacity (Table 2). Low $1/n$ values (< 1) indicate that the adsorption intensity is favorable (Ahmad et al. 2017).

Table 2. Langmuir, Freundlich, and SIPS isotherm parameters for P adsorption on Mg and Al impregnated biochar.

Biochar	Isotherm models									
	Langmuir			Freundlich			SIPS			
	q_m	K_L	R^2	K_F	$1/n$	R^2	q_m	K_S	n_s	R^2
PMB-M-Mg	324.17	17.78	0.98	0.62	0.63	0.95	231.27	0.68	1.49	0.99
PMB-N ₂ -Mg	226.29	29.13	0.96	1.08	0.55	0.89	167.21	0.13	1.79	0.98
PMB-M-Al	39.35	0.001	0.90	1.59	0.38	0.78	33.33	1.72	2.22	0.94
PMB-N ₂ -Al	23.44	0.73	0.87	8.13	0.15	0.82	27.16	0.26	0.49	0.90

SIPS model showed the best fit to the adsorption data, according to the determination coefficients (R^2) (Table 2). This model is generally the best to explain heterogeneous adsorption systems (Foo and Hameed, 2010), because it is a combination of the Langmuir and Freundlich models, which indicate that adsorption is controlled by different mechanisms that is generally the case for biochar (Fang et al. 2020; Penido et al. 2019), due to the heterogeneity of the material as confirmed by SEM-EDX (Fig. 9) and XRD (Fig. 10) analyzes.

In the SIPS, isotherm the value of n_s represents the heterogeneity degree of the adsorption sites. The closer to zero the more heterogeneous are the sites (Ayawei et al. 2017). The PMB-N₂-Al showed the lowest n_s value, while the PMB-M-Al showed the highest n_s value. This difference in the n_s values indicates that the pyrolysis furnaces modify the biomass differently, and for the biochar samples impregnated with Mg this difference was smaller. The SIPS model reduces the limitation of increased adsorbate concentration associated with the Freundlich model, which in high adsorbate concentration predicts that the dominant model is the monolayer adsorption indicated by the Langmuir model (Foo and Hameed, 2010). In view of this fact, one can infer that the biochar samples impregnated with Mg have more homogeneous sites when compared with the Al-impregnated biochar.

3.2.2 Point of zero charge (pH_{PZC}) and pH from P adsorption

The pH value of the aqueous solution can affect the phosphate speciation, consequently altering the adsorption. Fig. 4 shows the initial (pH_i) and final (pH_f) pH values of the solution containing phosphate in contact with the biochar samples.

The point of zero charge (pH_{PZC}) is a pH value in which the charge density on the surface of the biochar is neutral (Kosmulski, 2011). The pH_{PZC} values for pristine biochar are 7.4 for PMB-M and 8.0 for PMB-N₂. The values for the modified biochar are 10.4 for the PMB-M-Mg and 10.6 for the PMB-N₂-Mg. While for PMB-M-Al and PMB-N₂-Al is 6.2 and for PMB-M-Fe and PMB-N₂-Fe is 1.0. The biochar samples that showed the highest pH_{PZC} values were due to the predominance of dominant basic groups on the biochar surface. These basic groups promote a greater presence of positive charges on the surface of the biochar. The surface is supposed to be positively charged when the pH value $< pH_{PZC}$ and negatively charged when the pH value $> pH_{PZC}$. Since the predominant charge on the biochar surface is a factor that coordinates adsorption, the predominance of positive charges favors the adsorption of anions such as phosphate (Oh et al. 2012).

In samples of biochar impregnated with Mg and Al (Fig. 4), the values of the phosphate solution are below the pH_{PZC} value. Therefore, the surface of the modified biochar was positively charged and the electrostatic attraction between the biochar and negatively adsorbate (PO_4^{3-}) is favored. The difference in pH of adsorption and pH_{PZC} is greater in PMB-Mg, resulting in a more protonated biochar and, consequently, a greater amount of positive charges and, therefore, greater adsorption of P (Zhu et al., 2020).

The biochar samples impregnated with Mg showed higher P adsorption values (Fig. 3), which is partially explained by the reactions that take place on the surface of Mg-impregnated biochar. As reported by Zhu et al. (2020), when the pH increases from 5 to 12, the phosphate is deprotonated ($H_3PO_4 - H_2PO_4^- - HPO_4^{2-} - PO_4^{3-}$). At pH values between 5 and 10, $H_2PO_4^-$, and HPO_4^{2-} species are more strongly adsorbed by $MgOH^+$ by electrostatic attraction. The H^+ protons resulting from the deprotonation of phosphate in aqueous solution are consumed by the MgO contained on the surface of the biochar, as shown in reaction (9) below:



This reaction promotes an increase in the pH value of the medium and below the pH_{PZC} keeping the biochar surface constantly positively charged and consequently adsorbing larger amounts of P (Yao et al. 2011).

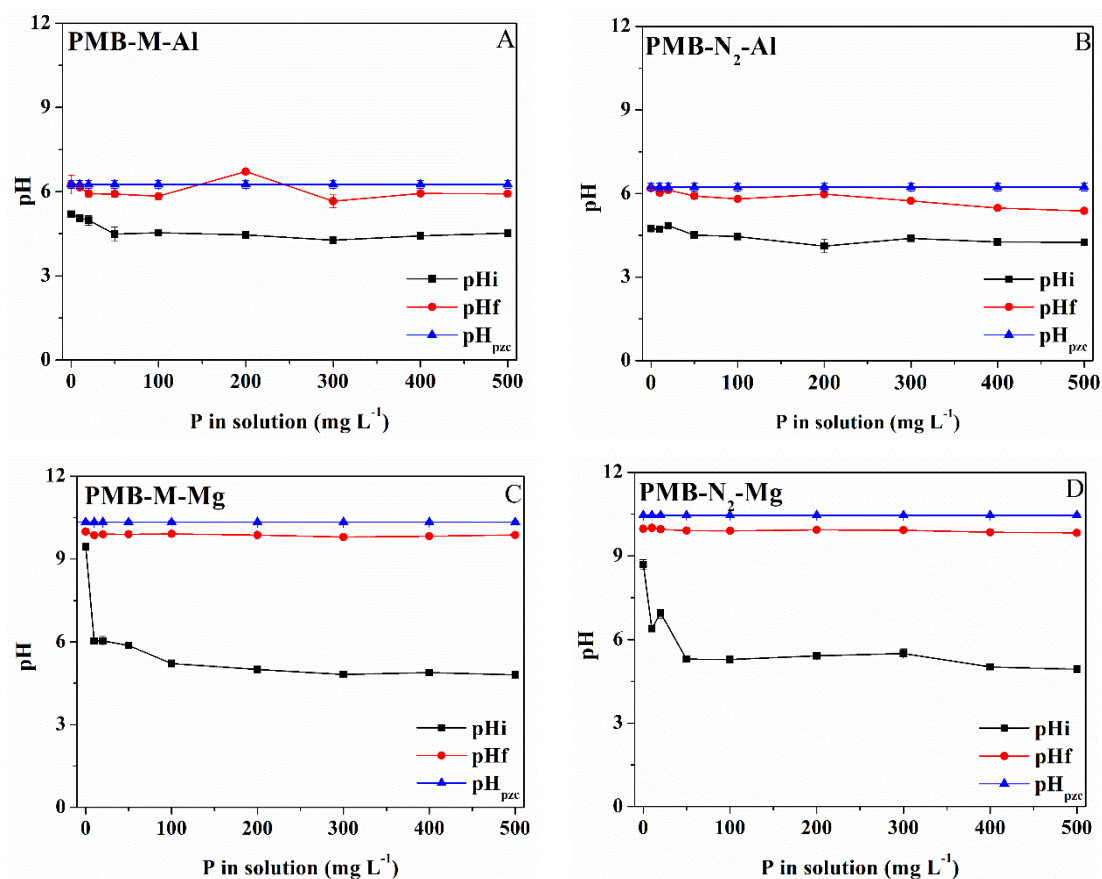


Fig. 4. Initial pH (pHi), final pH (pHf) from P adsorption and pH_{PZC} values in samples biochar modified.

In the PMB-Al it is observed that the difference in the pH value of the solution and the pH_{PZC} is smaller when compared with the PMB-Mg. This smaller difference indicates that less intensity of positive charges is created, thus occurring less electrostatic attraction, consequently less P adsorption.

In biochar samples impregnated with Fe, the pH value of the solution containing phosphate is greater than the pH_{PZC} value (Fig. S3), making the biochar surface negatively charged, thus causing electrostatic repulsion between the surface charges and the phosphate contained in the solution. As shown previously, the biochar samples impregnated with Fe adsorbed small amounts of P (Fig. S1). The low pH_{PZC} value of the biochar impregnated with Fe may be due the amount of Fe impregnated as well as the source used (FeCl₃), which when in contact with water generates an acid reaction as shown previously (eq. 8). Due to the presence of oxyhydroxides formed during the production of the biochar, the charges generated are pH-dependent charges, that in contact with water cause a hydroxylation on the surface and thus depending on the pH of the solution create of positive or negative surface charge (Kosmulski,

2011). In general, oxyhydroxides have a greater positive charge with a reduction in pH, generated by an increase in the capacity of anion retention. However, as shown by Lawrinenko et al. (2017), in acid pH values, Fe oxides behave in the opposite way having a low capacity of anion retention.

3.2.3 Desorption experiment

The P desorption (extraction) was evaluated in deionized water, 2% citric acid and Mehlich-1 solution (Fig. 5). Fe-impregnated biochar was not included due to its low and erratic adsorption profile, as discussed previously. Water-soluble P represents the readily available fraction for plant absorption, but also is the fraction that is readily leached in sandy soils or fixed in clayey and oxide-rich soils. Mehlich-1 and citric acid available P represent the fractions that are potentially available to plants through rhizosphere solubilization.

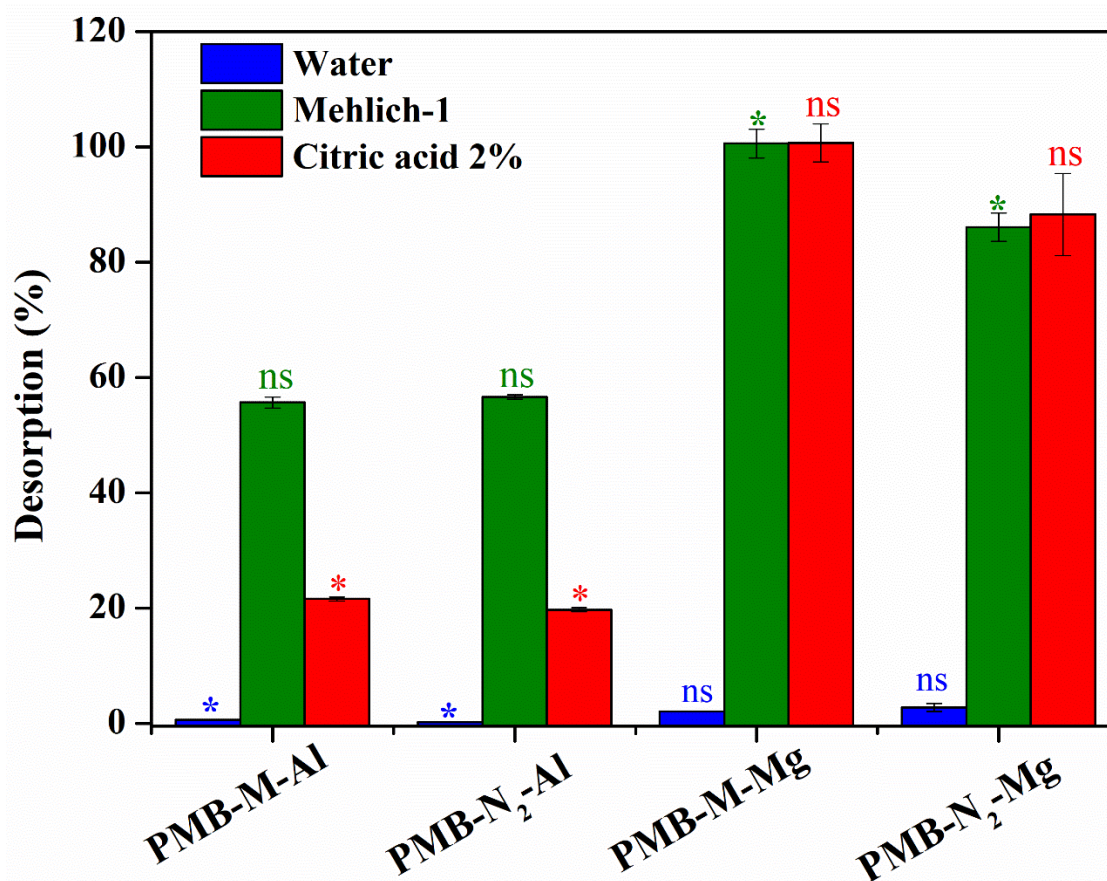


Fig. 5. Phosphorus desorption (%) using different extractants (water, Mehlich-1 and citric). Notes: ns - not significant ($p > 0.05$). * Significant at 5% probability by the T-student test ($p < 0.05$). The test compares the pyrolysis conditions (M-muffle and N₂- with N₂ flow), inside each cation-impregnated biochar. Average of 3 replicates.

The desorbed P fraction was higher in the Mg-impregnated biochar when compared with Al-impregnated biochar, regardless of the extractant (Fig. 5). Generally, lower desorption values indicate a strong interaction between adsorbent and adsorbate. The lower percentage of P desorption of biochar samples impregnated with Al is due to the high binding energy of P with the formed Al oxides and hydroxides (Fig. 10B), which is favored in medium with acid pH value (Biederman and Harpole, 2013). When comparing the extractors studied, the lower extraction capacity of citric acid ($C_6H_8O_7$) when compared with the Mehlich-1 solution was due to the lower acidifying power, being considered a low molecular mass acid that, when dissociated, forms organic carboxylic acids $-COOH$ that reacts and releases H^+ protons. However, the number of protons released by citric acid is lower than those released by the Mehlich-1 solution. Citric acid is efficient in solubilizing Ca and Mg phosphate compounds, but it has low solubilization capacity of Al and Fe phosphates (Wei et al. 2010).

In the biochar samples impregnated with Mg, the greater release of P is due to the lower binding energy of P-Mg, where there is a greater presence of P in the form of pyrophosphates and Ca and Mg orthophosphates, such as $CaHPO_4$ and $Mg_3(PO_4)_2 \cdot 8H_2O$ (Li et al. 2019). Although the Mehlich-1 solution is a combination of strong acids ($0.0125 \text{ mol L}^{-1} H_2SO_4 + 0.05 \text{ mol L}^{-1} HCl$), they are added at low concentrations. This combination of acids simulates the solubilization of P by the roots, which promote hydrolysis reactions of P species formed in PMB-Mg to reuse phosphate, thus extracting higher levels of P (McBeath et al. 2007).

As for the pyrolysis conditions, PMB-M-Al showed slightly higher P values soluble in water and in citric acid, whereas for PMB-N₂-Al the highest value was obtained for Mehlich-1. As for the Mg-impregnated biochar, there was a significant difference only for the extraction with Mehlich-1. PMB-M-Mg showed higher levels of Mehlich-1 and citric acid soluble P, while PMB-N₂-Mg showed greater P solubility in water.

3.2.4 Kinetics study

In all biochar samples the P adsorption was fast in the first 4 h becoming slower until reaching after this time (Fig. 6). In all models studied, it is possible to observe that the pyrolysis conditions did not influence on the amount of P adsorbed and the equilibrium time. The pseudo-first order and pseudo-second order were used to simulate the adsorption kinetics. The pseudo-second order model showed the best fit (R^2) in all biochar samples. The sorption parameters of the biochar that showed adjustment are shown in Table 3. The biochar impregnated with Fe

(PMB-M-Fe and PMB-N₂-Fe) did not show a trend of P adsorption (Fig. S2), consequently it did not fit the studied models.

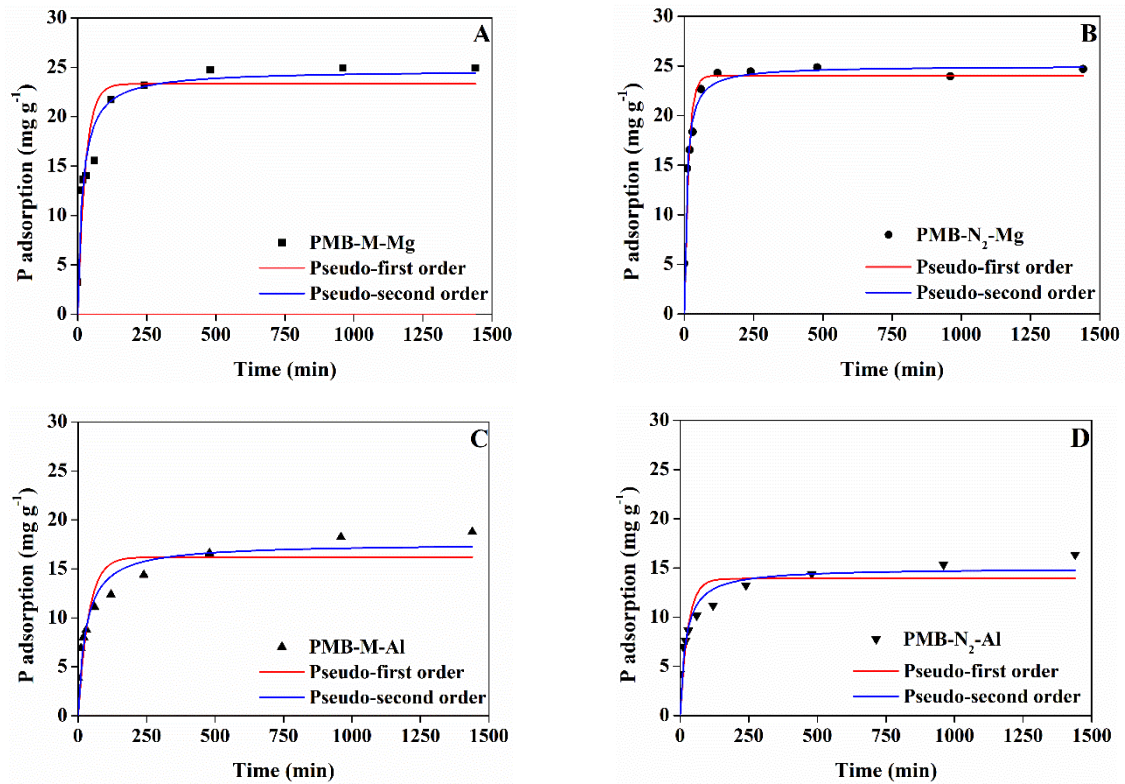


Fig. 6. Kinetics of phosphate adsorption on modified biochar data fitting for pseudo-first order and pseudo-second order.

The pseudo-second order model suggests that the chemisorption process is the predominant mechanism in comparison to the physical adsorption suggested by the pseudo-first order model (Tran et al. 2017). As previously shown, electrostatic attraction is a mechanism involved in the adsorption of P on the surface of the modified biochar.

Table 3- Kinetic parameters of phosphate adsorption onto selected biochar samples obtained from different models.

Biochar	Pseudo-first order			Pseudo-second order		
	$q_e(1)$	K_1	R^2	$q_e(2)$	K_2	R^2
PMB-M-Mg	23.318	0.036	0.829	24.716	0.002	0.913
PMB-N ₂ -Mg	24.024	0.024	0.880	25.006	0.004	0.913
PMB-M-Al	16.209	0.026	0.736	17.608	0.002	0.850
PMB-N ₂ -Al	13.920	0.035	0.634	14.992	0.003	0.766

Porous adsorbents tend to present adsorption in multiple linear regions following the Weber-Morris model or intra-particle diffusion model (Tran et al., 2017). This model is used to describe how adsorbate is diffused into the pores of adsorbent particles. In Fig. 7 is shown that

at zero contact time, P adsorption is low, but fast in all biochar samples. Subsequently, there is an increase in the adsorption rate (green line), which can be attributed to the greater number of binding sites for phosphate and by the abundance of ions. The biochar samples impregnated with Mg (Fig. 7A and 7B) showed a faster adsorption in this phase when compared with the biochar impregnated with Al (Fig. 7C and 7D).

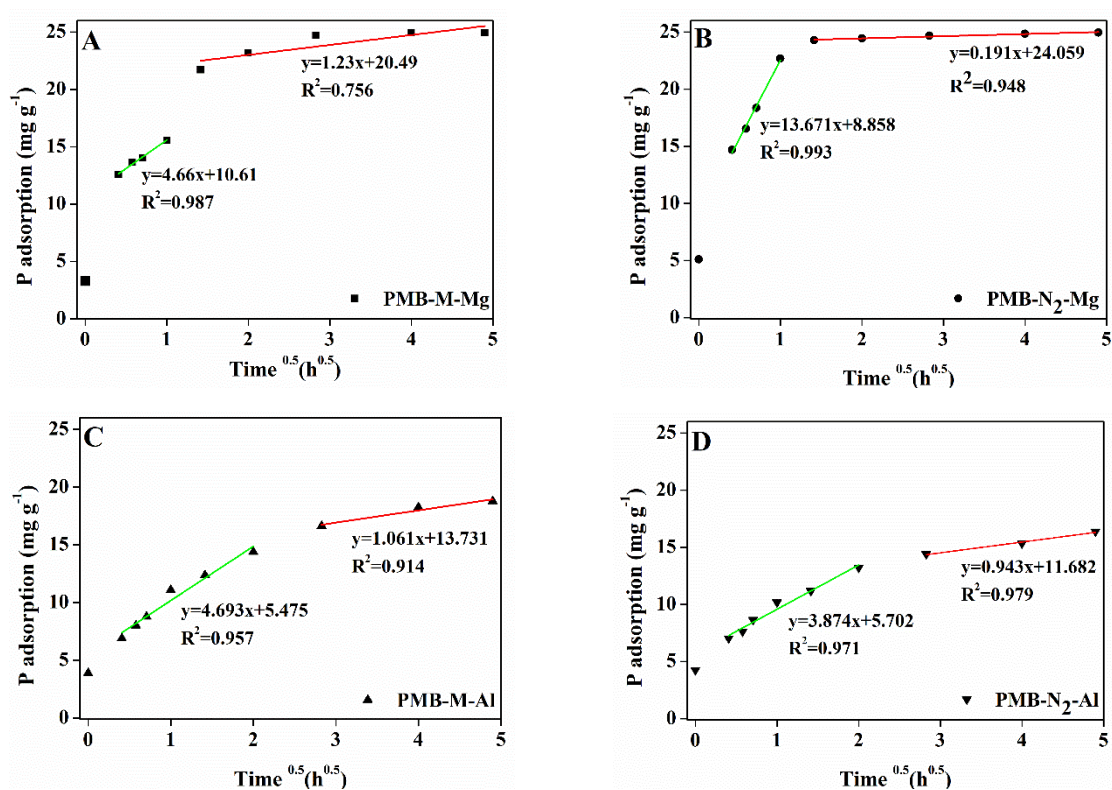


Fig. 7. Kinetics of phosphate adsorption on modified biochar data fitting for Weber-Morris model (Intra-particle diffusion).

The third stage of adsorption is characterized by the red line and shows reduced adsorption. This step is the intra-particle phase in which the phosphate molecules are transported into the pores along the surface. In the biochar impregnated with Mg this step was reached more quickly than in the biochar impregnated with Al, however the amount of P adsorbed is lower in the latter than in the former. The lower P adsorption in the biochar impregnated with Al may be due to the smaller volume of pores it presents (Fig. 2) and also due to the lower amount of mesopores, which can make it difficult to approach P in the smaller pores (Zhu et al. 2020).

3.3 Characterization of P-loaded biochar

3.3.1 FTIR

FTIR analysis is an important analysis to identify functional groups responsible for ion adsorption (Bekiaris et al. 2016). There was no significant difference in the formation of functional groups when comparing the pyrolysis conditions of biochar production (Fig. 8). The functional groups found in biochars and their respective vibrational modes are shown in table 4. There is a greater abundance of functional groups in the biochar impregnated with Mg, followed by Al and Fe, compared to the pristine biochar. This result indicates that impregnation is an efficient method for generating functional groups in biochar (Wang et al. 2015).

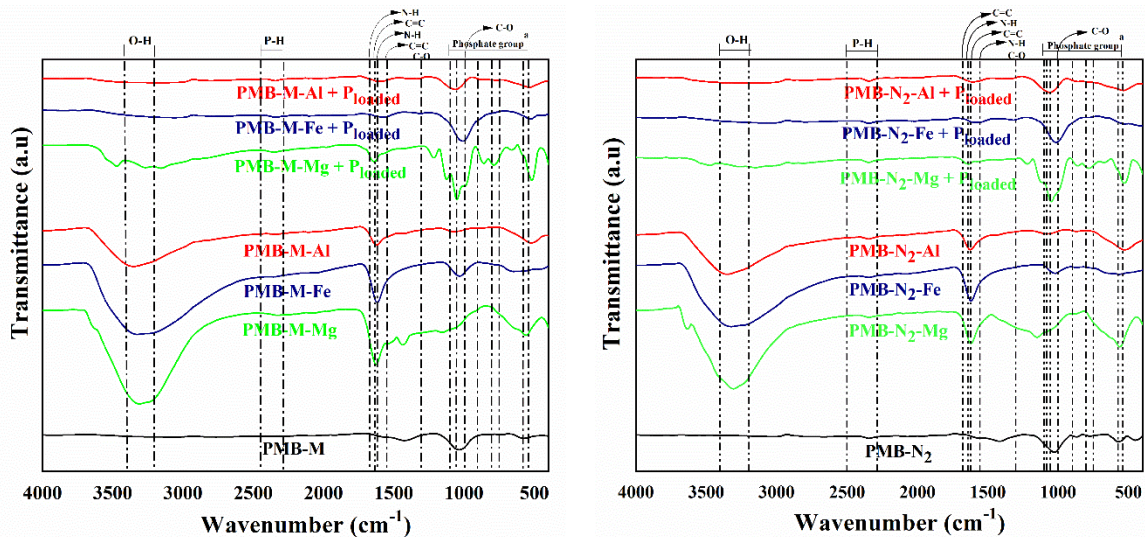


Fig. 8. FTIR spectra (4000-500 cm^{-1}) of pristine biochars, impregnated with Al, Fe, and Mg, and adsorption with P. Notes: ^aPhosphorus group: **P-H₂** angular deformation, **P-H**, **P-O-C** and **PO₄³⁻** (inorganic) complex band.

O-H groups of alcohols and associated phenols were observed by hydrogen bonding (3400 - 3200 cm^{-1}). The bands in 1640 and 1550 cm^{-1} were assigned to groups of primary and secondary amines. C-O bonds (1300-1000 cm^{-1}) and sharp C=C bands (1680-1620 cm^{-1}) were found. The P adsorption promoted an increase in phosphate groups, mainly in biochar impregnated with Mg that might help to explain its higher P adsorption capacity. Bands of P-H (2450-2280 cm^{-1}), angular deformation of PH₂ (1100-1080 cm^{-1}) were found and P-O-C connections between 800-750 cm^{-1} . A complex band of PO₄³⁻ (inorganic) was observed at bands between 1100-1000 and 580-540 cm^{-1} .

Table 4 - Functional groups, wavenumbers and vibrational mode of infrared bands from biochars.

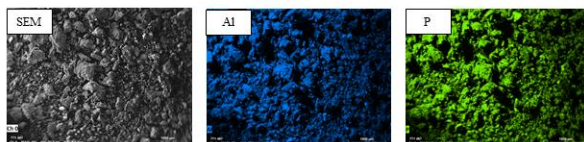
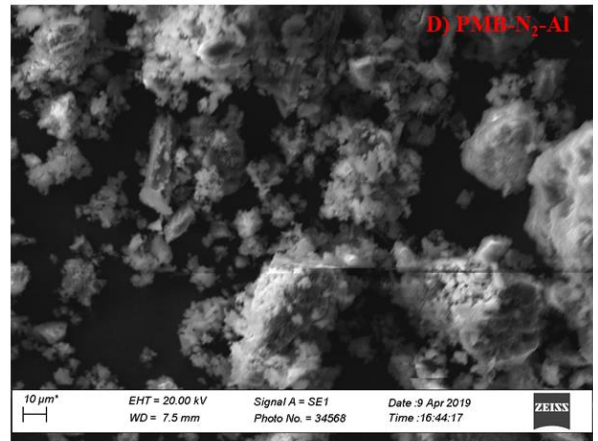
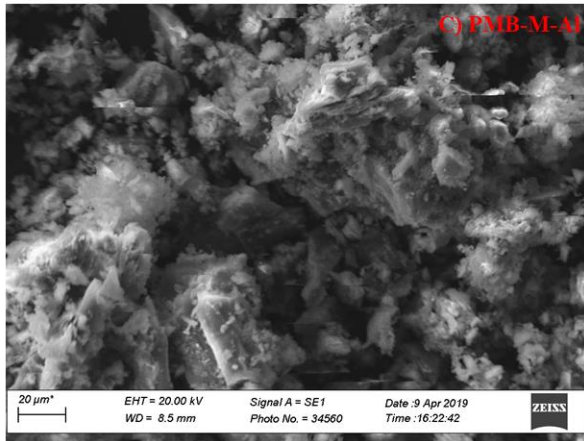
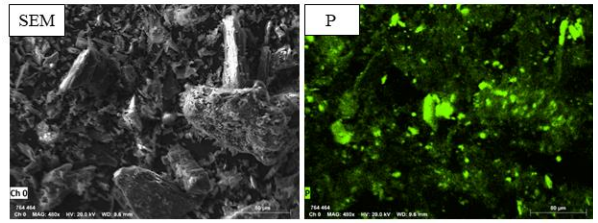
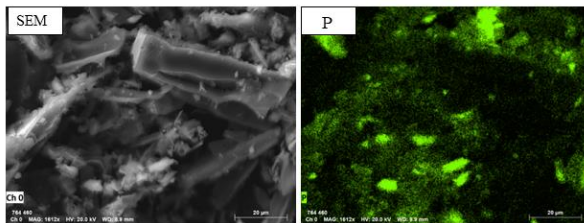
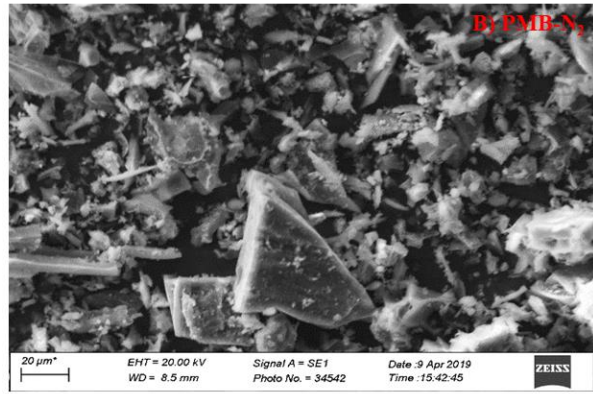
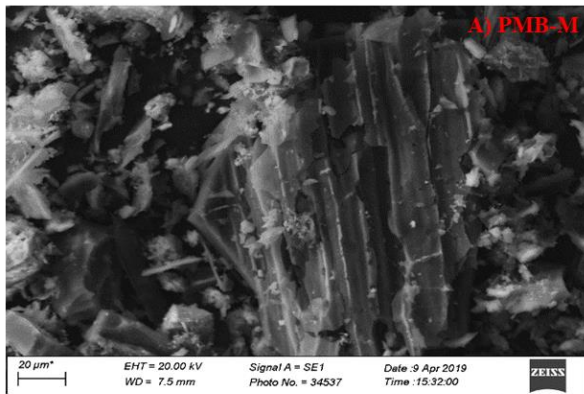
Functional group	Group frequency wavenumber (cm ⁻¹)	Assignment*
O-H	3400 – 3200	Alcohols and phenols associated with hydrogen bonding
N-H	1640-1550	Primary and secondary amines
C-O	1300 – 1000	Carbonyl group
C=C	1680 – 1620	Alkenyl
P-H	2450 – 2280	Phosphonic derivatives
PH ₂	1100 -1080	Angular deformations
P=O	1050 – 900	Organic phosphates
P-O-C	800 – 750	Aromatic phosphates
PO ₄ ³⁻	1100 – 1000 and 580 – 540	complex band (inorganic)

*Interpretation of the bands - Bekiaris et al. (2016); Silverstein et al., (2014); Coates (2004); Colthup and Grasselli (1992).

The increase in functional groups, mainly compounds containing O and H, indicate that there was an increase in these elements, mainly forming compounds of P-O and P-H. This result confirms that possibly ligand exchange and hydrogen bonding are mechanisms of P adsorption on the surface of modified biochar (Inyang and Dickenson, 2015).

3.3.2 SEM-EDX

SEM-EDX analysis of P-loaded biochar samples are shown in Fig. 9. SEM analysis shows that the pyrolysis conditions did not alter the morphology of the biochar. The impregnation with cations made the biochar more flocculated when compared with the non-impregnated biochar, which have a flatter surface (Fig. 9A and B).



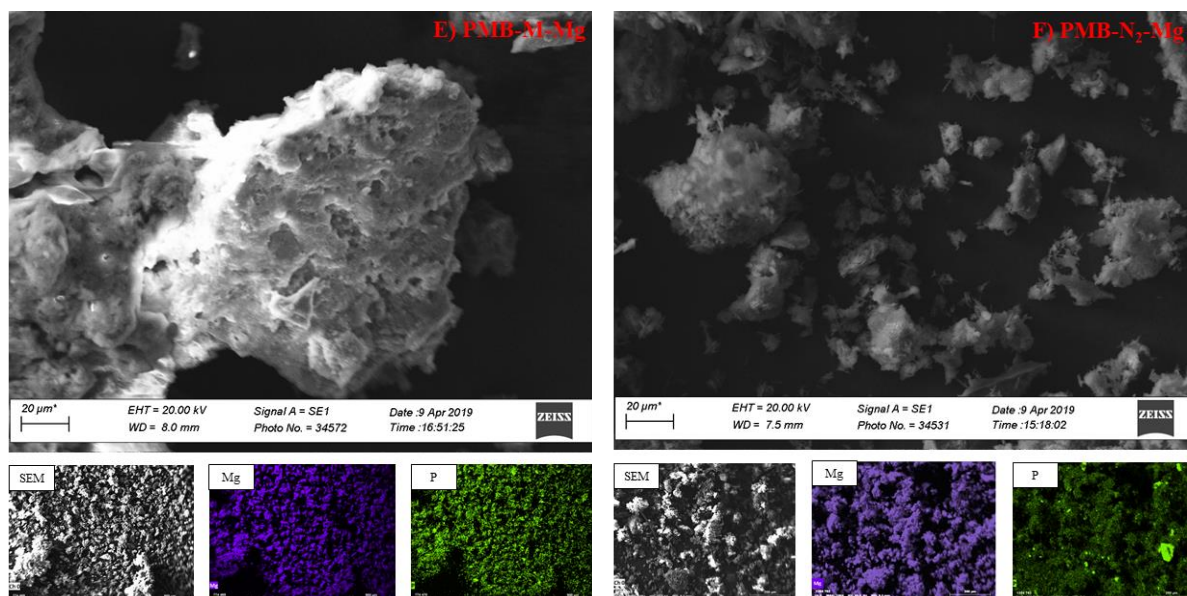


Fig. 9. SEM micrographs) and EDX elemental maps of modified biochars.

The EDX analysis indicates that P is evenly distributed on surface of the pristine biochar. For the impregnated biochar, Al, Fe, and Mg are well distributed over the entire surface and P seem to overlap the cations as sorption sites.

3.3.3 XRD

Several peaks of crystalline materials (synthetic minerals) were clearly observed in the X-ray diffraction (XRD) spectra in all studied biochar samples (Fig. 10). The pristine biochar (Fig. 10A) showed mainly quartz (SiO_2) and calcite like-compound (CaCO_3). There was also the formation of Ca-P compounds, such as monetite (CaHPO_4), hydroxyapatite [$\text{Ca}_5(\text{PO}_4)_3(\text{OH})$] and brushite [$\text{CaHPO}_4 \cdot 2(\text{H}_2\text{O})$]. Calcium is the element at the highest concentration in the feedstock and consequently in the pristine biochar (Table S1).

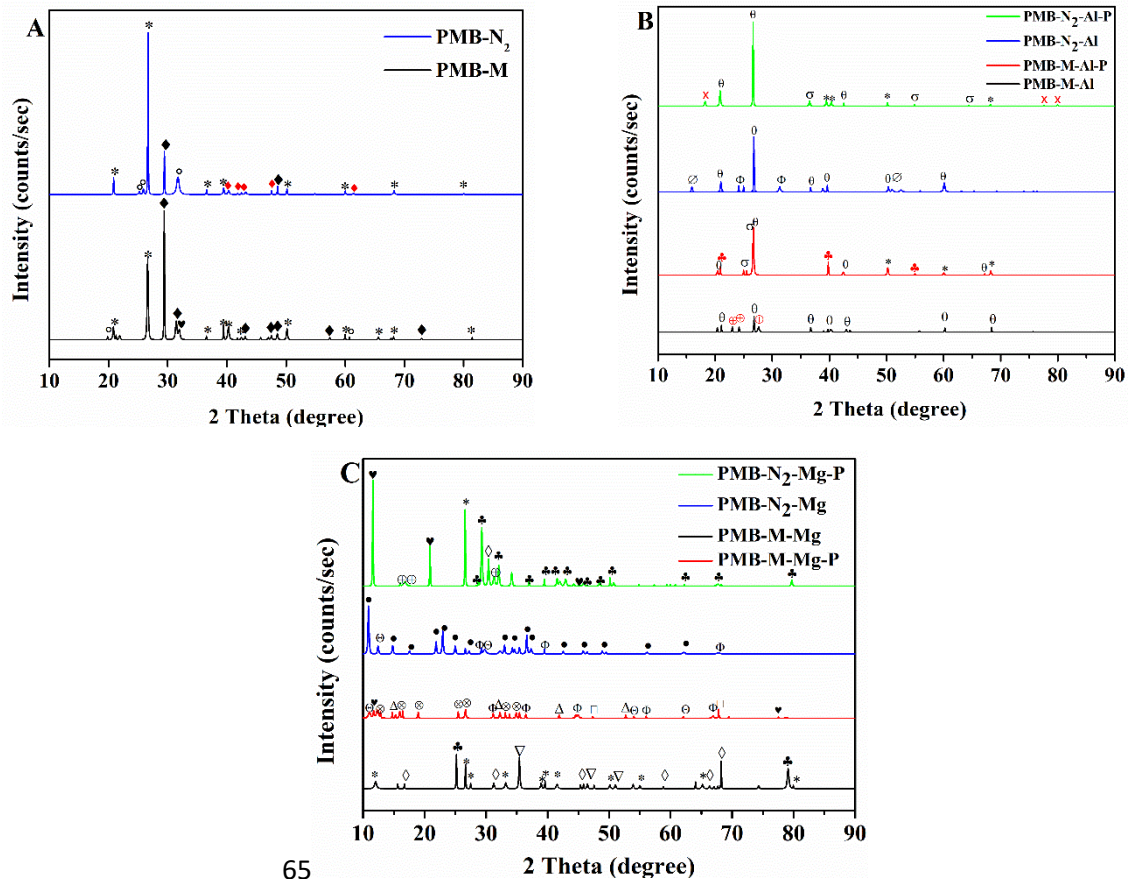


Fig. 10. XRD patterns of different biochars.

Notes: ϕ Akermanite; \emptyset Andalusite; σ Augelite; θ Berlinite; \circ Bobierite; \heartsuit Brushite; \blacklozenge Calcite; \blacklozenge Cattiite; \oplus Chloroaluminite; ∇ Chloromagnesite; \diamond Dolomite; \spadesuit $\text{FeCl}_2 \cdot 2\text{H}_2\text{O}$; ∞ Fe_3O_4 ; \times Gibbsite; \circ Hydroxyapatite; \triangle Iron phosphate; \triangle Iron phosphate dihydrate; \bullet Korshunorvskite; \bullet Kovdorskite; ∇ Magnesiowuestite; \bullet Magnetite; \blacklozenge Monetite; \clubsuit Newberyite; $*$ Quartz; π Strengite; \clubsuit Variscite; $\#$ Wollastonite.

The main crystalline phases formed in the Al-impregnated biochar (Fig. 10B) were berlinite (AlPO_4) and chloroaluminite (AlCl_3O_6) in PMB-M-Al and berlinite, andalusite [$\text{Al}_2(\text{SiO}_4)\text{O}$] and akermanite ($\text{Ca}_2\text{MgSi}_2\text{O}_7$) in the PMB- N_2 -Al. After P adsorption in the PMB-M-Al there was the formation of augelite [$\text{Al}_2(\text{PO}_4)(\text{OH})_3$], berlinite (AlPO_4) and variscite [$\text{AlPO}_4 \cdot 2(\text{H}_2\text{O})$]. Quartz peaks were also observed in this P-loaded biochar while it was not observed in the PMB-M-Al, which might have occurred because Si became more concentrated when in contact with the aqueous solution of the adsorption process due to its low water solubility. In the P-loaded PMB- N_2 -Al was also identified augelite [$\text{Al}_2(\text{PO}_4)(\text{OH})_3$], berlinite (AlPO_4), gibbsite $\text{Al}(\text{OH})_3$ and quartz peaks.

For the PMB-M-Fe biochar (Fig. S5) the identified minerals were composed of Ca, Fe, P and Si, such as brushite [$\text{CaHPO}_4 \cdot 2(\text{H}_2\text{O})$], dolomite [$\text{CaMg}(\text{CO}_3)_2$], wollastonite (CaSiO_3),

$\text{FeCl}_2 \cdot 2\text{H}_2\text{O}$ and Fe_3O_4 . In the PMB- N_2 -Fe there was the formation of $\text{FeCl}_2 \cdot 2\text{H}_2\text{O}$, dolomite and hydroxyapatite. And after P adsorption (PMB-M-Fe-P) it was observed the formation of very intense brushite and strengite peaks [$\text{Fe}^{3+}\text{PO}_4 \cdot 2(\text{H}_2\text{O})$]. As previously presented, this biochar showed the lowest P adsorption (Fig. S1) and through XRD is shown that P bound in greater quantity to Ca (brushite) when compared with Fe (strengite). The biochar produced under N_2 flow (PMB- N_2 -Fe-P) the minerals formed were iron phosphate (FePO_4); iron phosphate dihydrate ($\text{FePO}_4 \cdot 2\text{H}_2\text{O}$), magnesiowuestite ($\text{Fe}_{0.4}\text{Mg}_{0.6}\text{O}$), magnetite (Fe_3O_4) and hydroxyapatite.

The highest amounts of peaks were identified in the biochar impregnated with Mg (Fig. 10C). The main peaks observed contained Ca and Mg in the PMB-M-Mg as dolomite, newberyite [$\text{Mg}(\text{PO}_3)\text{OH} \cdot 3(\text{H}_2\text{O})$], chloromagnesite (MgCl_2) and quartz peaks. The P-loaded Mg-impregnated biochar showed mainly peaks of akermanite ($\text{Ca}_2\text{MgSi}_2\text{O}_7$), bobierrite [$\text{Mg}_3(\text{PO}_4)_2 \cdot 8(\text{H}_2\text{O})$], kovdorskite [$\text{Mg}_2\text{PO}_4(\text{OH}) \cdot 3\text{H}_2\text{O}$], newberyite, dolomite and hydroxyapatite. In the biochar produced under N_2 atmosphere (PMB- N_2 -Mg), most of the identified ones were peaks containing Mg in the form of korshunovskite [$\text{Mg}_2\text{Cl}(\text{OH})_3 \cdot 4(\text{H}_2\text{O})$], bobierrite and akermanite. After P adsorption (PMB- N_2 -Mg-P) there was the formation of P peaks linked to Mg such as newberyite and cattite [$\text{Mg}_3(\text{PO}_4)_2 \cdot 22(\text{H}_2\text{O})$], with the formation of brushite, dolomite and quartz.

3.4 Adsorption mechanisms

The main mechanisms of phosphate adsorption by modified biochar are protonation processes, surface complexes, physical adsorption in the pores, electrostatic attraction and precipitation (Li et al. 2016).

The kinetics study indicated that in the Mg-impregnated biochar (PMB-Mg), chemical adsorption first occurred, in which, electrostatic attraction probably occurred by the positive charges created by MgOH^+ , attracting the phosphate charges available in the solution. The formation of MgOH^+ from the MgO compounds that consume the H^+ released in the solution keeps the pH of the solution always lower than the pH_{PZC} value of the biochar, so it remains protonated, increasing the affinity with phosphate anions (Zhu et al., 2020). Concurrent with this process, FTIR analysis (Fig. 8) showed that part of the P was complexed on the surface by the functional groups contained in the biochar. One possibility is that the O-H clusters present

in the impregnated biochar ($3400\text{-}3200\text{ cm}^{-1}$) that disappeared after adsorption, it may also have bound to Mg and formed MgOH^+ groups.

As the contact time of the phosphate solution increases the biochar P moves into the larger pores and successively into the smaller pores as the layer to be diffused is broken (Wu et al. 2009), the physical adsorption mechanisms then start taking action, as indicated by the pseudo-first order and intra-particle diffusion models (Fig. 6 and 7). For the biochar impregnated with Al, the kinetic results indicate that intra-particle diffusion and chemical adsorption were mechanisms involved. The FTIR analysis shows that few phosphate groups were formed by surface complexes.

Another mechanism involved in P adsorption is precipitation, identified in the XRD analysis (Fig. 10). For the biochar impregnated with Mg (PMB-Mg) the main minerals formed were newberyite [$\text{Mg}(\text{PO}_3)\text{OH}\cdot 3(\text{H}_2\text{O})$] and also precipitation with the Ca present in the biomass (Table S1), in the form of brushite [$\text{CaHPO}_4\cdot 2(\text{H}_2\text{O})$]. For biochar impregnated with Al (PMB-Al), the formation of augelite [$\text{Al}_2(\text{PO}_4)(\text{OH})_3$] and berlinite (AlPO_4) was observed.

The biochar samples that have a higher external surface (S_{BET}) and also a greater volume of pores (P_{volume}), have a greater number of active sites and therefore have a high adsorption capacity and also a faster adsorption rate (Zhu et al. 2020). This characteristic also contributed to biochar impregnated with Mg adsorbed higher concentrations of P.

3.5 Agronomic and Environmental Implications

Phosphorus recovery from waste is a worldwide concern and studies on this topic should be encouraged. Adsorption is an effective technology, with high selectivity and easy operation (Loganathan et al. 2014), and the use of modified biochar as a P adsorbent is an excellent alternative. However, large-scale production of modified biochar still needs to be improved, to reduce costs and make the process more sustainable.

Mg was the best cation to be used in the impregnation for recovery of P, as it adsorbs the largest amounts and releases more recovered P. In addition, the use of N_2 as carrier gas does not promote significant changes in biochar that directly influence the adsorption and desorption of P. Therefore, it is possible to produce modified biochar in a simpler way but obtaining an efficient material in the recovery of P from wastewater.

In humid tropical soils, P is the most limiting element for agricultural production, because these soils have an intense relationship of P with mineralogical constituents. The P

adsorption can be as high as 1,000 times the P applied in a single fertilization (Roy et al. 2016). This adsorption occurs due to the predominance of Fe and Al hydroxides that have high affinity with P, leading to the formation of inner sphere surface complexes. This fraction is called non-labile P, where the phosphate is linked to hydroxyl by one, two or three covalent bonds (Novais et al. 2007). Precipitation of P with ionic forms of Fe and Al may also occur in acidic soils and with Ca in basic soils, which form low solubility compounds such as hydroxyapatite or carbonate-apatite (Fink et al. 2016).

For this reason, the implementation of new technologies to P recycle from waste is urgent in Brazil, aiming its use in agriculture. In addition, there are several organic residues that have significant amounts of P in organic and inorganic forms (Withers et al. 2018). Animal production, in particular, has had an impact on the environment by producing a considerable number of residues, which needs to be treated properly and is also rich in nutrients and organic matter. In the specific case of Pig manure, due to the confinement of animals, intensive use of water is required for hygiene, generating a considerable volume of wastewater that is rich in nutrients, especially P (Rosa et al. 2017). Also, the large-scale manure production can be a useful biomass to be used as a basis for biochar production, as demonstrated in this study.

4. Conclusions

Maximum adsorption was obtained in biochars impregnated with Mg, with the biochar produced in muffle (PMB-M-Mg) being the most efficient, removing 231 mg g^{-1} , while the one produced under N_2 atmosphere (PMB- N_2 -Mg) reached a value of 167 mg g^{-1} . The pyrolysis conditions (muffle – low O_2 or furnace under N_2) had no significant influence on the characteristics that govern adsorption, such as functional group, surface area, quantity and size of pores, and the formation of crystalline compounds (synthetic minerals). Thus, it is possible to produce biochar in a simpler way, without using a carrier gas, and thereby making the biochar production process sustainable and economical.

Acknowledgements

This work was financially supported by the National Council for Scientific and Technological Development (CNPq – Grant N° 404076/2016-5). Coordination for the

Improvement of Higher Education Personnel (CAPES/PROEX) and Foundation for Research of the State of Minas Gerais (FAPEMIG) also financially supported this work. LCA Melo is a research fellow of the National Council for Scientific and Technological Development (CNPq – Grant N° 308943/2018-0). The authors would like to thank the Laboratory of Electron Microscopy and analysis of Ultrastructural Federal University of Lavras, and Finep, Fapemig, CNPq e Capes for supplying the equipment and technical support for experiments involving electron microscopy. We also acknowledge the CETENE (Northeast Strategic Technologies Center) for technical support and availability of infrastructure. The authors acknowledge Dr. Carlos Alberto Silva (Federal University of Lavras) for the C elemental analysis. We also thank the Dr. Evanise Silva Penido for helping with several data analysis and interpretation.

References

- Ahmad, Munir, Ahmad, Mahtab, Usman, A.R.A., Al-faraj, A.S., Ok, S., Hussain, Q., Abduljabbar, A., Al-wabel, M.I., 2017. An Efficient Phosphorus Scavenging from Aqueous Solution using Magnesiothermally Modified Bio- Calcite 3330. <https://doi.org/10.1080/09593330.2017.1335349>
- Akgül, G., Maden, T.B., Diaz, E., Jiménez, E.M., 2019. Modification of tea biochar with Mg, Fe, Mn and Al salts for efficient sorption of PO₃-4 and Cd²⁺ from aqueous solutions. *J. Water Reuse Desalin.* 9, 57–66. <https://doi.org/10.2166/wrd.2018.018>
- Ayawei, N., Ebelegi, A.N., Wankasi, D., 2017. Modelling and Interpretation of Adsorption Isotherms. *J. Chem.* 2017. <https://doi.org/10.1155/2017/3039817>
- Batista, E., Shultz, J., Matos, T.T.S., Fornari, M.R., Ferreira, T.M., Szpoganicz, B., de Freitas, R.A., Mangrich, A.M., 2018. Effect of surface and porosity of biochar on water holding capacity aiming indirectly at preservation of the Amazon biome 1–9. <https://doi.org/10.1038/s41598-018-28794-z>
- Bayazit, Ş.S., Kerkez, Ö., 2014. Hexavalent chromium adsorption on superparamagnetic multi-wall carbon nanotubes and activated carbon composites. *Chem. Eng. Res. Des.* 92, 2725–2733. <https://doi.org/10.1016/j.cherd.2014.02.007>
- Bekiaris, G., Peltre, C., Jensen, L.S., Bruun, S., 2016. Using FTIR-photoacoustic spectroscopy for phosphorus speciation analysis of biochars. *Spectrochim. Acta - Part A Mol. Biomol. Spectrosc.* 168, 29–36. <https://doi.org/10.1016/j.saa.2016.05.049>
- Biederman, L.A., Stanley Harpole, W., 2013. Biochar and its effects on plant productivity and nutrient cycling: A meta-analysis. *GCB Bioenergy* 5, 202–214. <https://doi.org/10.1111/gcbb.12037>
- Buss, W., Graham, M.C., MacKinnon, G., Mašek, O., 2016. Strategies for producing biochars with minimum PAH contamination. *J. Anal. Appl. Pyrolysis* 119, 24–30. <https://doi.org/10.1016/j.jaap.2016.04.001>

- Cai, R., Wang, X., Ji, X., Peng, B., Tan, C., Huang, X., 2017. Phosphate reclaim from simulated and real eutrophic water by magnetic biochar derived from water hyacinth. *J. Environ. Manage.* 187, 212–219. <https://doi.org/10.1016/j.jenvman.2016.11.047>
- Chacón, F.J., Sánchez-monedero, M.A., Lezama, L., Cayuela, M.L., 2020. Enhancing biochar redox properties through feedstock selection, metal preloading and post-pyrolysis treatments. *Chem. Eng. J.* 395, 125100. <https://doi.org/10.1016/j.cej.2020.125100>
- Chen, W., Ding, S., Lin, Z., Peng, Y., Ni, J., 2020a. Science of the Total Environment Different effects of N₂-flow and air-limited pyrolysis on bamboo-derived biochars' nitrogen and phosphorus release and sorption characteristics 711, 1–10.
- Chen, W., Ding, Shuya, Lin, Zerui, Peng, Yuanzhen, Ni, Jinzhi, Ding, S, Lin, Z, Peng, Y, Ni, J, 2020b. Different effects of N₂-flow and air-limited pyrolysis on bamboo-derived biochars' nitrogen and phosphorus release and sorption characteristics. *Sci. Total Environ.* 711, 134828. <https://doi.org/10.1016/j.scitotenv.2019.134828>
- Clemente, J.S., Beauchemin, S., Thibault, Y., Mackinnon, T., Smith, D., 2018. Differentiating Inorganics in Biochars Produced at Commercial Scale Using Principal Component Analysis. *ACS omega* 3, 6931–6944. <https://doi.org/10.1021/acsomega.8b00523>
- Coates, J., 2004. Encyclopedia of Analytical Chemistry -Interpretation of Infrared Spectra, A Practical Approach. *Encycl. Anal. Chem.* 1–23.
- Colthup, N.B., Grasselli, J.G., 1992. The Handbook of infrared and Raman characteristic frequencies of organic molecules, Choice Reviews Online. <https://doi.org/10.5860/choice.29-5702>
- Cui, X., Dai, X., Khan, K.Y., Li, T., Yang, X., He, Z., 2016. Removal of phosphate from aqueous solution using magnesium-alginate/chitosan modified biochar microspheres derived from *Thalia dealbata*. *Bioresour. Technol.* 218, 1123–1132. <https://doi.org/10.1016/j.biortech.2016.07.072>
- De Gisi, S., Lofrano, G., Grassi, M., Notarnicola, M., 2016. Characteristics and adsorption capacities of low-cost sorbents for wastewater treatment: A review. *Sustain. Mater. Technol.* 9, 10–40. <https://doi.org/10.1016/j.susmat.2016.06.002>
- Enders, A., Lehmann, J., 2012. Comparison of Wet-Digestion and Dry-Ashing Methods for Total Elemental Analysis of Biochar. *Commun. Soil Sci. Plant Anal.* 43, 1042–1052. <https://doi.org/10.1080/00103624.2012.656167>
- Fang, L., Li, J. shan, Donatello, S., Cheeseman, C.R., Poon, C.S., Tsang, D.C.W., 2020. Use of Mg/Ca modified biochars to take up phosphorus from acid-extract of incinerated sewage sludge ash (ISSA) for fertilizer application. *J. Clean. Prod.* 244, 118853. <https://doi.org/10.1016/j.jclepro.2019.118853>
- Fink, J.R., Inda, A.V., Tiecher, T., Barrón, V., 2016. Iron oxides and organic matter on soil phosphorus availability - Review. *Cienc. e Agrotecnologia* 40, 369–379. <https://doi.org/10.1590/1413-70542016404023016>
- Foo, K.Y., Hameed, B.H., 2010. Insights into the modeling of adsorption isotherm systems. *Chem. Eng. J.* 156, 2–10. <https://doi.org/10.1016/j.cej.2009.09.013>
- Gonzaga, M.I.S., Mackowiak, C.L., Comerford, N.B., Moline, E.F. da V., Shirley, J.P.,

- Guimaraes, D.V., 2017. Soil & Tillage Research Pyrolysis methods impact biosolids-derived biochar composition , maize growth and nutrition. *Soil Tillage Res.* 165, 59–65. <https://doi.org/10.1016/j.still.2016.07.009>
- Hassan, M., Liu, Y., Naidu, R., Parikh, S.J., Du, J., Qi, F., Willett, I.R., 2020. Influences of feedstock sources and pyrolysis temperature on the properties of biochar and functionality as adsorbents: A meta-analysis. *Sci. Total Environ.* 744, 1–15. <https://doi.org/https://doi.org/10.1016/j.scitotenv.2020>
- Inyang, M., Dickenson, E., 2015. The potential role of biochar in the removal of organic and microbial contaminants from potable and reuse water: A review. *Chemosphere* 134, 232–240. <https://doi.org/10.1016/j.chemosphere.2015.03.072>
- IUPAC, 2014. Compendium of Chemical Terminology 1670. <https://doi.org/10.1351/goldbook>
- Jung, K.W., Ahn, K.H., Technology, B., Jung, K.W., Ahn, K.H., 2016. Fabrication of porosity-enhanced MgO/biochar for removal of phosphate from aqueous solution: Application of a novel combined electrochemical modification method. *Bioresour. Technol.* 200, 1029–1032. <https://doi.org/10.1016/j.biortech.2015.10.008>
- Kosmulski, M., 2011. Journal of Colloid and Interface Science The pH-dependent surface charging and points of zero charge V . Update. *J. Colloid Interface Sci.* 353, 1–15. <https://doi.org/10.1016/j.jcis.2010.08.023>
- Lawrinenko, M., Jing, D., Banik, C., Laird, D.A., 2017. Aluminum and iron biomass pretreatment impacts on biochar anion exchange capacity Aluminum and iron biomass pretreatment impacts on biochar anion exchange capacity. <https://doi.org/10.1016/j.carbon.2017.03.056>
- Lehmann, J., Joseph, S., 2009. Biochar for environmental management : An introduction. *Biochar Environ. Manag. - Sci. Technol.* 1, 1–12. <https://doi.org/10.1016/j.forpol.2009.07.001>
- Li, F., Liang, X., Niyungeko, C., Sun, T., 2019. Effects of biochar amendments on soil phosphorus transformation in agricultural soils, 1st ed, *Advances in Agronomy*. Elsevier Inc. <https://doi.org/10.1016/bs.agron.2019.07.002>
- Li, R., Wang, J.J., Zhou, B., Awasthi, M.K., Ali, A., Zhang, Z., Lahori, A.H., Mahar, A., 2016. Recovery of phosphate from aqueous solution by magnesium oxide decorated magnetic biochar and its potential as phosphate-based fertilizer substitute. *Bioresour. Technol.* 215, 209–214. <https://doi.org/10.1016/j.biortech.2016.02.125>
- Liu, D., Yu, Y., Long, Y., Wu, H., 2015. ScienceDirect Effect of MgCl₂ loading on the evolution of reaction intermediates during cellulose fast pyrolysis at 325 ° C. *Proc. Combust. Inst.* 35, 2381–2388. <https://doi.org/10.1016/j.proci.2014.05.026>
- Loganathan, P., Vigneswaran, S., Kandasamy, J., Bolan, N.S., 2014. Removal and Recovery of Phosphate From Water Using Sorption. *Crit. Rev. Environ. Sci. Technol.* 44, 847–907. <https://doi.org/10.1080/10643389.2012.74131>
- Luo, L., Xu, C., Chen, Z., Zhang, S., 2015. Properties of biomass-derived biochars: Combined effects of operating conditions and biomass types. *Bioresour. Technol.* 192, 83–89.

- <https://doi.org/10.1016/j.biortech.2015.05.054>
- Lussiez, G., & Beckstead, L., 1997. Hydrolysis of ferric chloride in solution. <https://doi.org/10.2172/426965>.
- Lustosa Filho, J.F., Penido, E.S., Castro, P.P., Silva, C.A., Melo, L.C.A., 2017. Co-Pyrolysis of Poultry Litter and Phosphate and Magnesium Generates Alternative Slow-Release Fertilizer Suitable for Tropical Soils. *ACS Sustain. Chem. Eng.* 5, 9043–9052. <https://doi.org/10.1021/acssuschemeng.7b01935>
- Malavolta, E., Vitti, G.C., Oliveira, S.A., 1997. Avaliação do estado nutricional das plantas: princípios e aplicações, 2nd ed. Potafos, Piracicaba.
- Mcbeath, T.M., Lombi, E., McLaughlin, M.J., 2007. Pyrophosphate and orthophosphate addition to soils : sorption , cation concentrations , and dissolved organic carbon 237–245. <https://doi.org/10.1071/SR07014>
- Mukherjee, A., Lal, R., 2016. Biochar and Soil Characteristics. *Encycl. Soil Sci.* Third Ed. 184–188. <https://doi.org/10.1081/E-ESS3-120053997>
- Nardis, B.O., Santana Da Silva Carneiro, J., Souza, I.M.G. De, Barros, R.G. De, Azevedo Melo, L.C., 2020. Phosphorus recovery using magnesium-enriched biochar and its potential use as fertilizer. *Arch. Agron. Soil Sci.* 1–17. <https://doi.org/10.1080/03650340.2020.1771699>
- Nesme, T., Withers, P.J.A., 2016. Sustainable strategies towards a phosphorus circular economy. *Nutr. Cycl. Agroecosystems* 104, 259–264. <https://doi.org/10.1007/s10705-016-9774-1>
- Novais, R., Alvarez, V.V., De Barros, N.F., Fontes, R.L., Cantarutti, R., Neves, J.C.L., 2007. Fertilidade do solo, 1ª edição. ed. SBCS, Viçosa- Mg.
- Novais, S.V., Zenero, M.D.O., Tronto, J., Conz, R.F., Cerri, C.E.P., 2018. Poultry manure and sugarcane straw biochars modified with MgCl₂ for phosphorus adsorption. *J. Environ. Manage.* 214, 36–44. <https://doi.org/10.1016/j.jenvman.2018.02.088>
- Oh, T.K., Choi, B., Shinogi, Y., Chikushi, J., 2012. Effect of pH conditions on actual and apparent fluoride adsorption by biochar in aqueous phase. *Water. Air. Soil Pollut.* 223, 3729–3738. <https://doi.org/10.1007/s11270-012-1144-2>
- Penido, E.S., Melo, L.C.A., Guilherme, L.R.G., Bianchi, M.L., 2019. Cadmium binding mechanisms and adsorption capacity by novel phosphorus/magnesium-engineered biochars. *Sci. Total Environ.* 671, 1134–1143. <https://doi.org/10.1016/j.scitotenv.2019.03.437>
- Rawal, A., Joseph, S.D., Hook, J.M., Chia, C.H., Munroe, P.R., Donne, S., Lin, Y., Phelan, D., Mitchell, D.R.G., Pace, B., Horvat, J., Webber, J.B.W., 2016. Mineral – Biochar Composites: Molecular Structure and Porosity. <https://doi.org/10.1021/acs.est.6b00685>
- Rodriguez-narvaez, O.M., Peralta-hernandez, J.M., Goonetilleke, A., Bandala, E.R., 2019. Journal of Industrial and Engineering Chemistry Biochar-supported nanomaterials for environmental applications. *J. Ind. Eng. Chem.* 78, 21–33. <https://doi.org/10.1016/j.jiec.2019.06.008>

- Rosa, D.M., Sampaio, S.C., Pereira, P.A.M., Mauli, M.M., Dos Reis, R.R., 2017. Swine wastewater: Impacts on soil, plant, and leachate. *Eng. Agric.* 37, 928–939. <https://doi.org/10.1590/1809-4430-Eng.Agric.v37n5p928-939/2017>
- Roy, E.D., Richards, P.D., Martinelli, L.A., Coletta, L. Della, Lins, S.R.M., Vazquez, F.F., Willig, E., Spera, S.A., VanWey, L.K., Porder, S., 2016. The phosphorus cost of agricultural intensification in the tropics. *Nat. Plants* 2, 16043. <https://doi.org/10.1038/nplants.2016.43>
- Schröder, J.J., Smit, A.L., Cordell, D., Rosemarin, A., 2011. Improved phosphorus use efficiency in agriculture : A key requirement for its sustainable use. *Chemosphere* 84, 822–831. <https://doi.org/10.1016/j.chemosphere.2011.01.065>
- Shepherd, J.G., Joseph, S., Sohi, S.P., Heal, K. V, 2017. Biochar and enhanced phosphate capture: Mapping mechanisms to functional properties. *Chemosphere* 179, 57–74. <https://doi.org/10.1016/j.chemosphere.2017.02.123>
- SILVERSTEIN, R.M., WEBSTER, F.X., KIEMLE, D.J., BRYCE, D.L., 2014. *Spectrometric Identification of Organic Compounds*, 8th ed.
- Simonin, J.P., 2016. On the comparison of pseudo-first order and pseudo-second order rate laws in the modeling of adsorption kinetics. *Chem. Eng. J.* 300, 254–263. <https://doi.org/10.1016/j.cej.2016.04.079>
- Singh, B., Camps-Arbestain, M., Lehmann, J., CSIRO (Australia), 2017. *Biochar: A Guide to Analytical Methods*, Csiro publishing.
- Sun, Y., Yu, I.K.M., Tsang, D.C.W., Cao, X., Lin, D., Wang, L., Graham, N.J.D., Alessi, D.S., Komárek, M., Ok, Y.S., Feng, Y., Li, X.D., 2019. Multifunctional iron-biochar composites for the removal of potentially toxic elements, inherent cations, and heterochloride from hydraulic fracturing wastewater. *Environ. Int.* 124, 521–532. <https://doi.org/10.1016/j.envint.2019.01.047>
- Takaya, C.A., Fletcher, L.A., Singh, S., Okwuosa, U.C., Ross, A.B., 2016. Recovery of phosphate with chemically modified biochars. *J. Environ. Chem. Eng.* 4, 1156–1165. <https://doi.org/10.1016/j.jece.2016.01.011>
- Tan, G., Liu, Y., Xiao, D., 2018. Influence of different pyrolysis methods on the sorption property of rice straw biochar. *Sep. Sci. Technol.* 00, 1–10. <https://doi.org/10.1080/01496395.2018.1553981>
- Thines, K.R., Abdullah, E.C., Mubarak, N.M., Ruthiraan, M., 2017. Biomass and Bioenergy In-situ polymerization of magnetic biochar e polypyrrole composite : A novel application in supercapacitor 98, 95–111.
- Tran, H.N., You, S., Hosseini-bandegharai, A., Chao, H., 2017. Mistakes and inconsistencies regarding adsorption of contaminants from aqueous solutions: A critical review. *Water Res.* <https://doi.org/10.1016/j.watres.2017.04.014>
- Wan, S., Wang, S., Li, Y., Gao, B., 2017. *Journal of Industrial and Engineering Chemistry* Functionalizing biochar with Mg – Al and Mg – Fe layered double hydroxides for removal of phosphate from aqueous solutions. *J. Ind. Eng. Chem.* 47, 246–253. <https://doi.org/10.1016/j.jiec.2016.11.039>

- Wang, Z., Guo, H., Shen, F., Yang, G., Zhang, Y., Zeng, Y., Wang, L., Xiao, H., Deng, S., 2015. Biochar produced from oak sawdust by Lanthanum (La)-involved pyrolysis for adsorption of ammonium (NH₄⁺), nitrate (NO₃⁻), and phosphate (PO₄³⁻). *Chemosphere* 119, 646–653. <https://doi.org/10.1016/j.chemosphere.2014.07.084>
- Wei, L., Chen, C., Xu, Z., 2010. Citric acid enhances the mobilization of organic phosphorus in subtropical and tropical forest soils. *Biol. Fertil. Soils* 46, 765–769. <https://doi.org/10.1007/s00374-010-0464-x>
- Withers, P.J.A., Rodrigues, M., Soltangheisi, A., Carvalho, T.S. De, 2018. Transitions to sustainable management of phosphorus in Brazilian agriculture. *Sci. Rep.* 8, 1–13. <https://doi.org/10.1038/s41598-018-20887-z>
- Wu, F.C., Tseng, R.L., Juang, R.S., 2009. Initial behavior of intraparticle diffusion model used in the description of adsorption kinetics. *Chem. Eng. J.* 153, 1–8. <https://doi.org/10.1016/j.cej.2009.04.042>
- Xiang, W., Zhang, X., Chen, J., Zou, W., He, F., Hu, X., Tsang, D.C.W., Sik, Y., Gao, B., 2020. *Chemosphere* Biochar technology in wastewater treatment : A critical review 252.
- Yang, Q., Wang, X., Luo, W., Sun, J., Xu, Q., Chen, F., Zhao, J., Wang, S., Yao, F., Wang, D., Li, X., Zeng, G., 2018. Effectiveness and mechanisms of phosphate adsorption on iron-modified biochars derived from waste activated sludge. *Bioresour. Technol.* 247, 537–544. <https://doi.org/10.1016/j.biortech.2017.09.136>
- Yao, Y., Gao, B., Inyang, M., Zimmerman, A.R., Cao, X., Pullammanappallil, P., Yang, L., 2011. Removal of phosphate from aqueous solution by biochar derived from anaerobically digested sugar beet tailings. *J. Hazard. Mater.* 190, 501–507. <https://doi.org/10.1016/j.jhazmat.2011.03.083>
- Yin, Q., Ren, H., Wang, R., Zhao, Z., 2018. Evaluation of nitrate and phosphate adsorption on Al-modified biochar: Influence of Al content. *Sci. Total Environ.* 631–632, 895–903. <https://doi.org/10.1016/j.scitotenv.2018.03.091>
- Zeng, Z., Zhang, S.-D., Li, T.-Q., Zhao, F.-L., He, Z.-L., Zhao, H.-P., Yang, X.-E., Wang, H.-L., Zhao, J., Tariq Rafiq, M., 2013. Sorption of ammonium and phosphate from aqueous solution by biochar derived from phytoremediation plants. *J Zhejiang Univ-Sci B (Biomed Biotechnol)* 14, 1152–1161. <https://doi.org/10.1631/jzus.B1300102>
- Zhang, M., Gao, B., Yao, Y., Xue, Y., Inyang, M., 2012. Synthesis of porous MgO-biochar nanocomposites for removal of phosphate and nitrate from aqueous solutions. *Chem. Eng. J.* 210, 26–32. <https://doi.org/10.1016/j.cej.2012.08.052>
- Zhu, D., Chen, Y., Yang, H., Wang, S., Wang, X., Zhang, S., Chen, H., 2020a. Synthesis and characterization of magnesium oxide nanoparticle-containing biochar composites for efficient phosphorus removal from aqueous solution. *Chemosphere* 247, 125847. <https://doi.org/10.1016/j.chemosphere.2020.125847>
- Zhu, D., Chen, Y., Yang, H., Wang, S., Wang, X., Zhang, S., Chen, H., 2020b. *Chemosphere* Synthesis and characterization of magnesium oxide nanoparticle- containing biochar composites for efficient phosphorus removal from aqueous solution. *Chemosphere* 247, 125847. <https://doi.org/10.1016/j.chemosphere.2020.125847>

Zhu, X., Li, C., Li, J., Xie, B., Lü, J., Li, Y., 2018. Thermal treatment of biochar in the air/nitrogen atmosphere for developed mesoporosity and enhanced adsorption to tetracycline. *Bioresour. Technol.* 263, 475–482.
<https://doi.org/10.1016/j.biortech.2018.05.041>

Supplementary Information

Production of engineered-biochar under different pyrolysis conditions for phosphorus removal from aqueous solution

Bárbara Olinda Nardis^a, José Romão Franca^b, Jefferson Santana da Silva Carneiro^a, Jenaina Ribeiro Soares^b, Luiz Roberto Guimarães Guilherme^a, Leônidas Carrijo Azevedo Melo^{a*}

^aSoil Science Department, Federal University of Lavras, 37200-900 Lavras, Minas Gerais, Brazil

^bPhysics Department, Federal University of Lavras, 37200-900 Lavras, Minas Gerais, Brazil

*Corresponding author

Leônidas Carrijo Azevedo Melo

E-mail: leonidas.melo@ufla.br

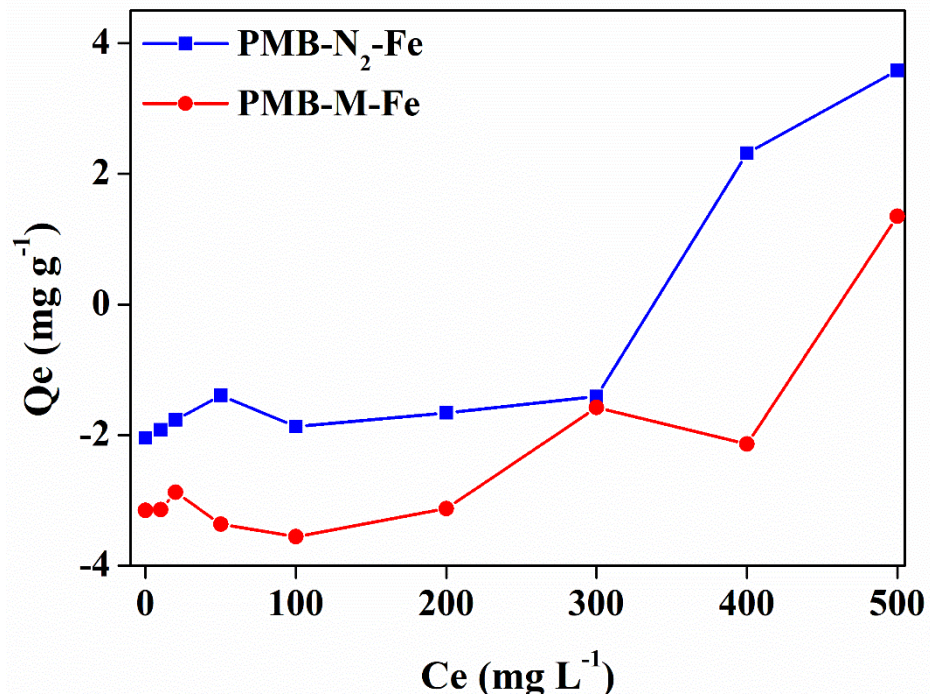


Figure S1. Adsorption isotherms of biochar samples impregnated with Fe and either prepared in muffle furnace (M) or under N₂ flow (N₂).

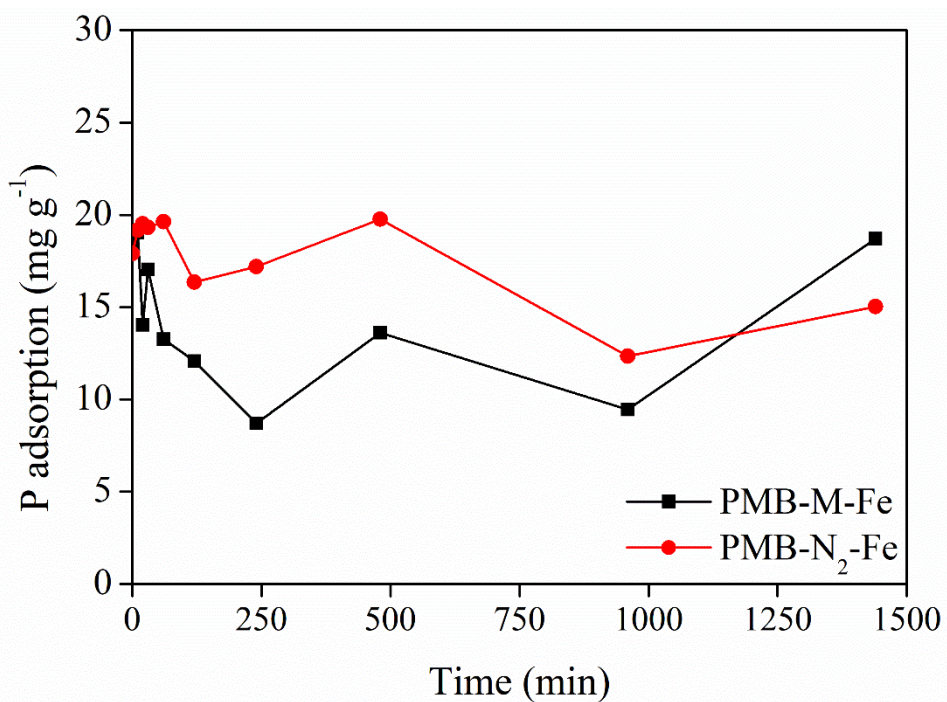


Figure S2. Effect of contact time on P retention onto impregnated Fe biochars using a biochar dose of 4 g L⁻¹ and solution of 50 mg L⁻¹ of P.

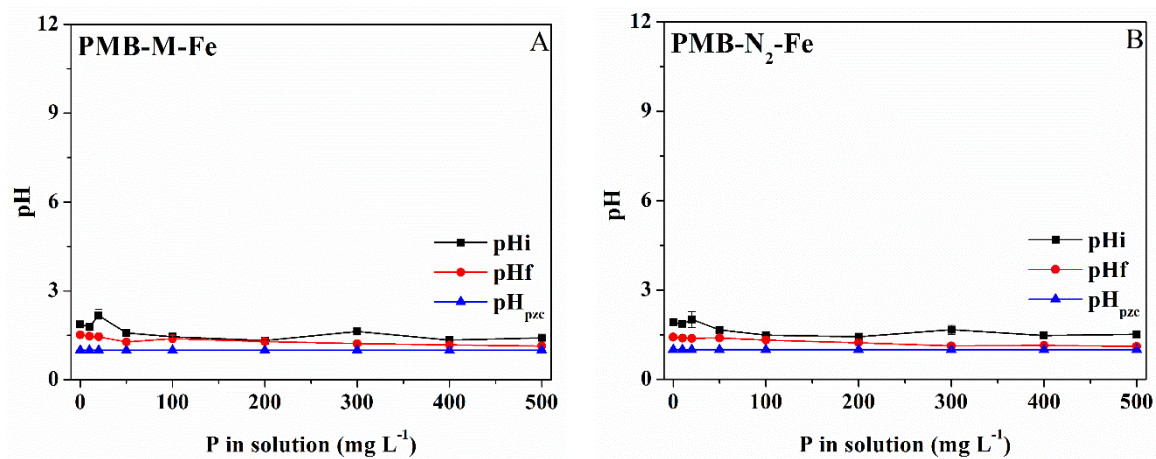


Figure S3. pH initial (pHi), pH final (pHf) from P adsorption and pH_{PZC} values in samples biochar impregnated with Fe.

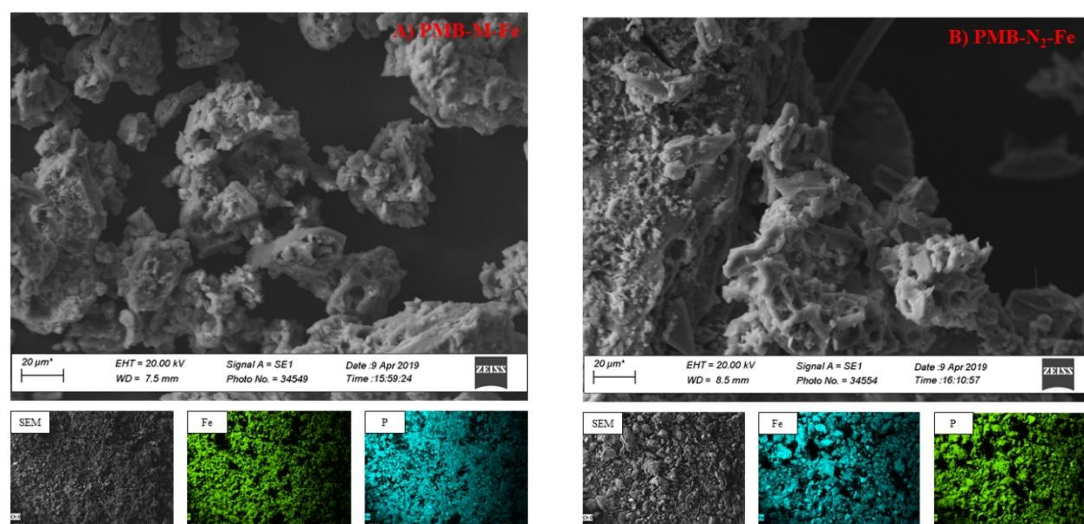


Figure S4. SEM micrographs and EDX elemental maps of modified biochars.

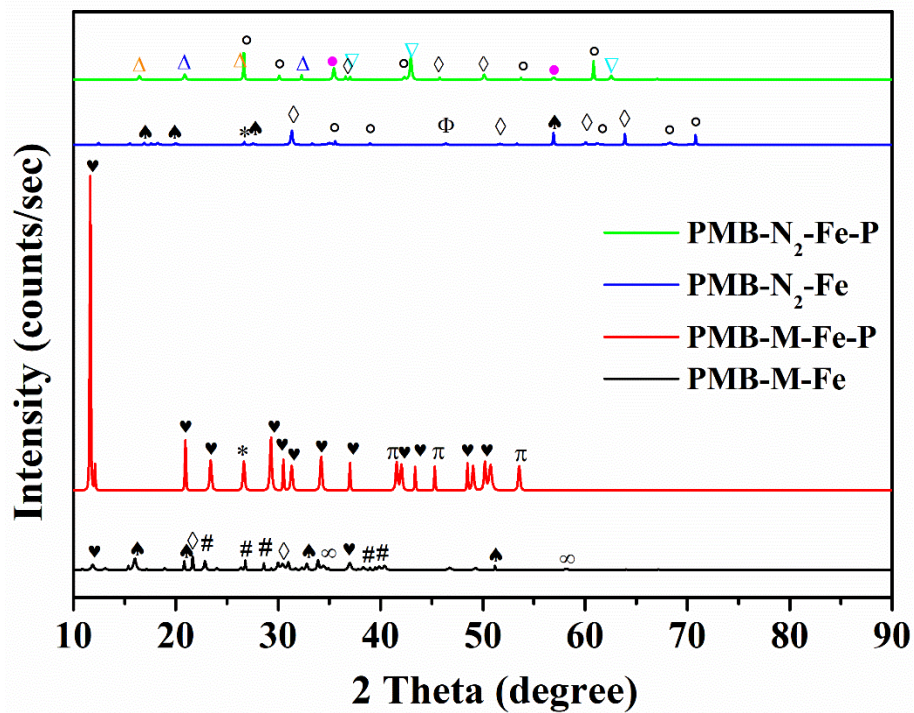


Figure S5. XRD patterns of different biochars.

Notes: ϕ Akermanite; \emptyset Andalusite; \otimes Antigorite-T; σ Augelite; θ Berlinite; \circ Bobierite; \heartsuit Brushite; \blacklozenge Calcite; \oplus Cattiite; $\opl�$ Chloroaluminite; ∇ Chloromagnesite; \times Diopside; \diamond Dolomite; \blacklozenge $\text{FeCl}_2 \cdot 2\text{H}_2\text{O}$; ∞ Fe_3O_4 ; \bullet Korshunovskite; \triangle Magnesioferrite; ∇ Magnesiowuestite; \blacklozenge Magnetite; \triangle MgCl_2 ; \clubsuit Newberyite; \square Periclase; $*$ Quartz; π Strengite; \clubsuit Variscite; $\#$ Wollastonite.

Table S1 – Nutrient content of pig manure

N	P	K	Ca	Mg	S
g/kg					
15.7±0.4	11.6±0.5	6.9±0.1	39.3±1.6	2.40±0.06	2.50±0.04
B	Cu	Fe	Mn	Zn	
mg/kg					
15.6±0.6	217±1	3184±265	212±30	447±13	

CHAPTER 3

Phosphorus removal from aqueous solution using cation-modified biochars: speciation using P K-edge XANES spectroscopy

*Chapter prepared according to the guidelines of the Journal of Cleaner Production (to be
submitted)*

Phosphorus removal from aqueous solution using cation-modified biochars and its speciation using P K-edge XANES spectroscopy

Bárbara Olinda Nardis^a, Cristiane Francisca Barbosa^a, Evanise Silva Penido^b, Dean Hesterberg^c, Luis Carlos Colucho Hurtarte^d, Luiz Roberto Guimarães Guilherme^a, Leônidas Carrijo Azevedo Melo^{a*}

^aDepartment of Soil Science, Federal University of Lavras, 37200-900 Lavras, Minas Gerais, Brazil

^bDepartment of Chemistry, Federal University of Lavras, 37200-900 Lavras, Minas Gerais, Brazil

^cDepartment of Crop and Soil Sciences, North Carolina State University, 27695-7619, Raleigh, NC, United States

^dLehrstuhl für Bodenkunde, Research Department Ecology and Ecosystem Management, Technische Universität München, Emil-Ramann-Straße 2, 85354 Freising, Germany

*Corresponding author

Leônidas Carrijo Azevedo Melo E-mail: leonidas.melo@ufla.br

Abstract

The recycling of phosphorus (P) from organic waste and wastewater is essential for environmental sustainability. The use of biochar impregnated with magnesium (Mg^{2+}), aluminum (Al^{3+}) and iron (Fe^{3+}) is an alternative to increase the capacity of P removal by biochar from wastewater. We aimed at studying the P removal of biochar enriched with cations prepared under different pyrolysis conditions (air-limited and N_2 -flow) and to evaluate the P speciation adsorbed on cation-modified biochar, using the X-ray absorption spectroscopy (XAS). Biochar samples were produced from pig manure (PMB) impregnated, separately, with 20% of $AlCl_3$, $MgCl_2$ and $FeCl_3$ solutions either in an air-limited adapted muffle furnace and in a furnace under N_2 -flow. Phosphorus removal was studied in these cation-modified biochars. Then, speciation analyses after P adsorption (P-enriched biochars) were carried out by P K-edge X-ray Absorption Near Edge Structure (XANES) spectroscopy to identify the P species in non-modified and cation-modified biochars. XANES results showed that in non-modified biochar (PMB-M and PMB- N_2), P-Ca compounds (mainly hydroxyapatite) prevailed. In the biochars impregnated with Al, there was a predominance of P-Al compounds most being found as P sorbed on gibbsite-like compound $[Al(OH)_3]$. In biochars impregnated with Fe, P-Fe compounds (ferrihydrite and $FePO_4$) were identified. For the biochars impregnated with Mg, species of P-Mg and P-Ca were identified. Although Mg is in greater quantity in the Ca:Mg ratio, there was a predominance of the P-Ca species because of due to these compounds [e.g. octacalcium phosphate (OctaCaP)] were preferentially crystallized in comparison to P-Mg. The pyrolysis conditions mainly influenced the temperature in the biomass core, which resulted in a differentiated degradation of lignocellulose, affecting the mineral and organic content. In conclusion, Mg-impregnated biochar is a sustainable option to add value to organic residues and to recycle P to be reused as enhanced efficiency fertilizer.

Keywords – sustainability; phosphate recycling; P species; synchrotron.

1. Introduction

Phosphorus (P) is an essential element for living organisms and a major element limiting crop growth in Brazil, but P sources are finite and scarce. Less than half of the P applied as a plant nutrient is assimilated by human and animal consumers of food crops, and most P is eliminated via excrement (Liu and Chen, 2008). If human and animal wastes are not correctly treated for land application, mobilized P (and nitrogen - N) in the wastes can reach surface waters and result in eutrophication (Ngatia and Taylor, 2019). Swine wastewaters produced in confined feeding operations are particularly problematic because of the large volumes produced from intensive water usage in these systems. These wastewaters contain suspended organic solids that are rich in N, P, and K (potassium) (Bradford et al., 2008). There is an urgent need to recover these nutrients, especially P, from these wastewaters to recycle these essential nutrients and avoid pollution.

The recovery of P from wastewater and other complex environmental matrices by adsorption in biochar has been highlighted in recent research (Cui et al., 2016; Riddle et al., 2019; Zhu et al., 2020). Because the surfaces of the biochars are predominantly composed of weak-acid (e.g., carboxylic) functional groups that are negatively charged, the addition of multivalent cations such as magnesium (Mg^{2+}), aluminum (Al^{3+}) and iron (Fe^{3+}) is needed to increase the P binding capacity by forming cationic bridges (Shepherd et al., 2017).

The biochar pyrolysis conditions may also influence its physicochemical characteristics. For instance, production using N_2 flow as a carrier gas has the function of removing the gases formed during pyrolysis to obtain a “cleaner” biochar surface (Chen et al., 2020b). On the other hand, adapted muffle furnace to prevent air flow is also commonly used for biochar production (Tan et al., 2018; Bekiaris et al., 2016), but this method cause a deposition of the gaseous pyrolysis products on the biochar surface. The main reported characteristics that are influenced by the preparation method are porosity, surface area and chemical functional groups (Zhu et al., 2018). These characteristics are expected to influence the transformation of feedstock and P adsorption, consequently influencing P species that are formed.

The use of P K-edge X-ray absorption near-edge spectroscopy (XANES) for speciation in modified biochar samples is poorly reported in the literature (Riddle et al., 2018; Riddle et al., 2019). This technique allows the chemical P speciation in heterogeneous environmental matrices, such as biochar (Sharma and Hesterberg, 2020). The species are identified by changes around the X-ray adsorption edge of the element of interest (the absorber), which is energy-

specific, thus, the spectral characteristics near the edge depends on the coordination environment of the atoms in the absorber element and its closest neighbors (Mobilio et al., 2015).

Although several studies have tested the adsorption capacity of biochar modified with different cations, so far, a deeper understanding of the P species formed after the recovery from aqueous solutions is still lacking. Also, the influence of pyrolysis conditions biochar on the P adsorption capacity and the P speciation remains an open question. Knowing the P species in modified biochars can provide information about the removal mechanisms and allow optimization of the recovery process, as well as the potential performance of the P-loaded biochars as fertilizers when the focus is to be further used in agriculture (Liang et al., 2018).

We hypothesized that impregnation with cations modifies the properties of the biochar forming different species of phosphates after adsorption and that the different pyrolysis conditions will influence the pyrolysis of the feedstock resulting in minerals with different capacities to adsorb P. This study aimed to (1) determine the chemical speciation of P bound to biochars impregnated with different cations (Mg^{2+} , Fe^{3+} and Al^{3+}) and prepared by different pyrolysis conditions (furnace with N_2 flow and muffle furnace), and (2) relate the P speciation to agronomic efficiency of biochar enriched with P by adsorption process.

2. Material and methods

2.1 Biomass preparation

Pig manure was collected in a farm near Lavras, Minas Gerais state, Brazil ($21^{\circ}13'34''$ S and $44^{\circ}58'31''$ W). The feedstock was oven dried at $50^{\circ}C$ until constant weight, ground in a mill equipped with a 10-mesh sieve (<0.25 mm), and stored in plastic recipients. Macro and micronutrients contents in biomass was determined in ICP-OES after nitric-perchloric acid digestion. The nitrogen was determined for Kjeldahl method after sulfuric acid digestion (Malavolta et al. 1997). Later, the material was impregnated with magnesium chloride ($MgCl_2 \cdot 6H_2O$), (Synth, 98%) iron chloride ($FeCl_3 \cdot 6H_2O$) (Vetec, 98%) and aluminum chloride ($AlCl_3 \cdot 6H_2O$) (Merk, 97%) solutions aiming to reach 20% of Mg, Fe and Al in the biochar, according to Li et al. (2016) with modifications. For this, 50 g of pig manure was mixed with 150 mL of $MgCl_2$, $FeCl_3$ and $AlCl_3$ solution, separately, by shaking for 24 h at 120 oscillations

per minute in a shaker (TE 240/1 Tecnal) and oven dried at 80 °C to constant weight. After, the material was crushed and sieved (< 0.25 mm) again.

2.2 Biochar production

The biochar samples were produced under two different atmospheres. Firstly, pig manure without and with Mg²⁺, Fe³⁺ and Al³⁺ impregnation were tightly accommodated in porcelain crucibles, which were overlapped to inhibited O₂ flow and allow pyrolysis in a muffle furnace (Bekiaris et al. 2016). The same materials were pyrolyzed in a horizontal furnace EDG/FT-HI series under N₂ atmosphere (200 mL min⁻¹). In both furnaces, materials were subjected to a heating rate of ~10 °C min⁻¹ up to reach 500 °C, with 2 h of holding time (Lustosa Filho et al. 2017). After pyrolysis, the samples were slowly cooled to room temperature inside the furnaces, ground in a porcelain mortar, and sieved to <0.25 mm. The pig manure biochar samples are herein identified with a code comprising the feedstock (PMB), the pyrolysis conditions (M – muffle furnace or N₂ – horizontal furnace under N₂ flow), and the impregnated cation (Mg, Fe, Al). The materials produced were named as: PMB-M, PMB-N₂, PMB-M-Mg, PMB-N₂-Mg, PMB-M-Al, PMB-N₂-Al, PMB-M-Fe and PMB-N₂-Fe

2.3 Biochar characterization

The characterization of the biochar samples was detailed described in the previous chapter of this thesis. The characterization of biochar samples presented in this work included chemical and physical measurements. Electrical conductivity (EC) and pH value were determined according to Singh et al. (2017). Ash contents were determined using a standard method ASTM D1762-84 (ASTM, 2007), and total nutrients contents were determined according to Enders and Lehmann (2012). The C content was determined in an elemental analyzer (model Vario TOC cube, Elementar, Germany). All analyses were performed in triplicate, except the C analysis that was in duplicate. The data were subjected to analysis of T-student (significant - $p < 0.05$) using software R 3.4.1. (R Core Team, 2017).

2.4 Phosphate removal study

Phosphate removal experiments were performed using biochar samples that were crushed, air dried, and sieved to $<50\ \mu\text{m}$. Briefly, 5 g of biochar samples were added in 1000 mL of phosphate solution (KH_2PO_4) (i.e. $5.0\ \text{g L}^{-1}$ of adsorbent dose) containing $500\ \text{mg L}^{-1}$ of P, which were prepared using $0.01\ \text{mol L}^{-1}$ $\text{Ca}(\text{NO}_3)_2$ as a background electrolyte solution. The mixture was stirred for 24 h at 120 oscillations per minute at room temperature. After this period, the extracts were filtered in membranes ($<0.45\ \mu\text{m}$, Millex HP) and P concentration in the filtrate was measured by ICP-OES (Li et al., 2016). All reagents were of analytical grade and used without further purification.

The amount of P uptake by different biochars was calculated by the equation (1):

$$R (\%) = \frac{(C_i - C_e)}{C_i} \times 100 \quad (1)$$

where $R (\%)$ is the removal percentage C_i and C_e are the initial and equilibrium P concentrations measured in the aqueous solution (mg L^{-1}), respectively.

2.5 Phosphorus K-edge XANES spectroscopy

XANES spectrum data were collected at the soft X-ray spectroscopy (SXS) beamline of the Brazilian Synchrotron Light Laboratory (LNLS) in Campinas-SP, Brazil. For the P K-edge XANES analysis the pristine and P-loaded biochar samples were air dried, ground and passed through a $150\ \mu\text{m}$ screen. Samples were diluted to $\sim 0.15\%$ (w/w) P concentrations with boron nitride in order to diminish self-absorption and a thin layer was uniformly spread on double-sided carbon tape and mounted on a stainless-steel sample holder, which was inserted into a chamber operated under vacuum conditions ($\sim 10^{-7}$ mbar). The beamline was equipped with a double crystal Si (111) monochromator, and data were collected in fluorescence mode using an AMPTEK® X-ray Spectrometer Detector (model X-123) to record the X-ray fluorescence. For energy calibration, a calcium phosphate standard was used (E_0 set at 2150.7 eV) and scans were collected in the energy range of 2120 to 2220 eV. The step size was 1.0 eV from 2120 to 2145 eV; 0.2 eV from 2145 to 2180 and 0.5 eV from 2181 to 2220 eV, and time of 1.0 s per step. About eight scans per sample were measured to obtain a lower signal-noise ratio.

XANES data analysis was performed using Athena software, version 0.9.25 (Ravel and Newville, 2005). Data preprocessing consisted in visual evaluation of the spectrum for

inconsistency (e.g., glitches, drifts, and noise) between replicates of the same spectra and merging of the scans. Was performed the background subtraction, normalization and linear combination fitting (LCF) in the energy range 2140-2180 eV (Gustafsson et al., 2020). The LCF was a combination of four standards grouped and analyzed for visual similarity and analysis of the best R-factor.

A set of standards was obtained from D. Hesterberg (personal collection) and Hurtarte et al. (2019), as follows: calcium phosphates [octacalcium phosphate – $\text{Ca}_8\text{H}_2(\text{PO}_4)_6 \cdot 5\text{H}_2\text{O}$; hydroxyapatite – $\text{Ca}_5(\text{PO}_4)_3(\text{OH})$]; brushite – $\text{CaHPO}_4 \cdot 2\text{H}_2\text{O}$; monetite – CaHPO_4 ; β -tricalcium phosphate – $\beta\text{-Ca}_3(\text{PO}_4)_2$], magnesium phosphate ($\text{MgHPO}_4 \cdot 3\text{H}_2\text{O}$), iron phosphate [strengite – $\text{FePO}_4 \cdot 2\text{H}_2\text{O}$; FePO_4 amorphous; FePO_4 ; P_ferrihydrite – P adsorption in $\text{Fe}_2^{3+}\text{O}_3 \cdot 0.5\text{H}_2\text{O}$] and aluminum phosphate [variscite - $\text{AlPO}_4 \cdot 2\text{H}_2\text{O}$, variscite_amorphous, AlPO_4 ; P-gibbsite – P adsorption in $\text{Al}(\text{OH})_3$, P_caulinite – P adsorption in $\text{Al}_2\text{Si}_2\text{O}_5(\text{OH})_4$] and organic phosphate (phosphonate – $\text{CH}_2 - \text{PO}_3\text{OH}_2$).

3. Results and discussion

3.1 Biochars characterization

Both the impregnation and the pyrolysis conditions influenced the basic characteristics of the biochars (Table 1). The pH values were in the alkaline range for the non-impregnated biochars and Mg-impregnated biochars, while the Al-impregnated biochars were slightly acid and the Fe-impregnated biochars were highly acid, which are in agreement with others (Micháleková-Richveisová et al., 2017). The impregnation increased considerably the content of the impregnated elements as expected, while Ca was the predominant nutrient in the non-impregnated biochar (Table1).

Table 1. Chemical properties of the pristine and cation-impregnated biochar produced in muffle furnace (M) or under N₂ flow (N₂).

Properties	Biochar							
	PMB-M	PMB-N ₂	PMB-M-Mg	PMB-N ₂ -Mg	PMB-M-Al	PMB-N ₂ -Al	PMB-M-Fe	PMB-N ₂ -Fe
Yield (%)	30* ± 0.9	40* ± 0.2	39* ± 0.3	55* ± 0.6	68* ± 0.6	39* ± 0.0	55* ± 0.3	59* ± 0.3
pH _(Water)	9.77 ^{ns} ± 0.01	9.68 ^{ns} ± 0.03	9.25 ^{ns} ± 0.01	9.25 ^{ns} ± 0.01	5.23* ± 0.06	5.64* ± 0.05	1.66* ± 0.01	1.70* ± 0.01
CE (mS cm ⁻¹)	0.76* ± 0.0	0.06* ± 0.0	4.79* ± 0.03	4.54* ± 0.01	1.76* ± 0.03	2.17* ± 0.02	4.24* ± 0.01	5.01* ± 0.02
C (%)	57.9 ^{ns} ± 2.80	44.8 ^{ns} ± 0.70	25.5 ^{ns} ± 0.05	26.9 ^{ns} ± 0.25	24.9* ± 0.20	23.4* ± 0.20	18.5 ^{ns} ± 0.05	18.8 ^{ns} ± 0.25
Ash (%)	39.2* ± 0.9	36.4* ± 0.1	47.9 ^{ns} ± 0.5	44.2 ^{ns} ± 0.8	47.5* ± 0.3	45.4* ± 0.1	47.8 ^{ns} ± 0.1	47.0 ^{ns} ± 0.3
Ca (g kg ⁻¹)	65.7* ± 0.5	95.8* ± 0.7	22.0* ± 0.3	14.4* ± 0.1	32.2 ^{ns} ± 0.3	32.0 ^{ns} ± 0.1	32.7 ^{ns} ± 0.3	32.9 ^{ns} ± 0.3
Mg (g kg ⁻¹)	4.70 ^{ns} ± 0.04	4.83 ^{ns} ± 0.05	169* ± 2	149* ± 5	2.02 ^{ns} ± 0.02	2.31 ^{ns} ± 0.11	2.07* ± 0.01	2.44* ± 0.01
Fe (g kg ⁻¹)	3.99 ^{ns} ± 0.08	5.89 ^{ns} ± 0.48	0.63 ^{ns} ± 0.19	0.44 ^{ns} ± 0.09	5.57* ± 0.14	3.82* ± 0.12	115 ^{ns} ± 2	113 ^{ns} ± 3
Al (g kg ⁻¹)	3.77 ^{ns} ± 0.21	4.81 ^{ns} ± 0.44	0.69 ^{ns} ± 0.09	0.52 ^{ns} ± 0.09	168 ^{ns} ± 2	171 ^{ns} ± 1	0.48 ^{ns} ± 0.06	0.42 ^{ns} ± 0.03

Notes: ns - not significant. * Significant at 5% probability (p < 0.05) by the T-student test. The test compares the pyrolysis conditions (M-muffle and N₂- with N₂ flow), inside each impregnated cation. Values are the mean ± standard error (n=3).

Except for the biochar impregnated with Mg, the C content and ash content followed the same trend for pyrolysis conditions, with the highest values found in biochar produced in muffle furnace. This difference in pyrolysis conditions is probably related to the temperature variation in the core of the feedstock (Spokas, 2010). This oscillation generates a differentiation in the dehydration of hydroxyl groups and also in the degradation of lignocellulose that occurs at high temperatures (Gonzaga et al., 2017).

At temperatures below 300 °C the degradation of lignocellulose promotes the release of radicals by homolytic cleavage of bonds induced by the thermal action of structural O and inorganic impurities present in the raw material. Another source of free radicals may be the presence of low amounts of atmospheric O₂. Water loss also occurs because of dehydration reactions. Finally, these free radicals break down and the biochar forms (Amonette and Joseph, 2009).

As the pyrolysis temperature increases, such as from 300 °C to 600 °C, greater liquid, and bio-oil (tar) formation occurs, and the biochar yield is lower. This is because the tar formed from cellulose is composed of anhydrosugars that are less reactive than the free radicals generated by the homolytic cleavage. Higher temperatures increase heat and mass transfer rates with increased volatile production, further reducing yield (Amonette and Joseph, 2009).

The impregnation with different cations caused an increase in the ash content and a decrease in the C content of the biochar, which is consistent since the ash content reflects the measure of the inorganic compounds of the biochar. The ash contents were close among the cation-impregnated biochars and the pyrolysis conditions cause a small or no difference in this characteristic. However, the Fe-impregnated biochar caused the highest decrease in the C content among the cations-impregnated biochars. The amount of Fe used in the impregnation behaved as a powerful catalyst that favored the loss of C as a gas during pyrolysis (Zheng et al., 2020). The impregnation with salts increased the production of ash because these function as acidic or basic catalysts that promote reactions of dehydration and fission of anhydrosugars. This process results in biochars extremely reactive to oxidation with consequent lower C content (Amonette and Joseph, 2009).

3.2) Phosphorus removal using cation-modified biochars

The highest P removal capacity was obtained for PMB-N₂-Mg, followed by the sequence of PMB-M-Mg>PMB-N₂-Al>PMB-N₂-Fe>PMB-M-Al>PMB-M-Fe (Figure 1). The higher P removal of the Mg-impregnated biochars samples is due to the fact that Mg creates high PZC biochars (Zhu et al., 2020) and thus is able to maintain a positively charged biochar surface (pH of the medium below the pHPZC) over a wide pH range in aqueous medium and consequently adsorbing larger amounts of P (Yao et al. 2011). The pyrolysis conditions influenced the P removal capacity in all biochars, with greater removal in those produced under N₂ flow. The use of an inert gas in the production of the biochar is important because it influences characteristics such as surface area and porosity, which are important to coordinate adsorption (Chen et al., 2020b). Aspects of the adsorption behavior, mechanisms, and characterization of biochars are detailed in the former chapter.

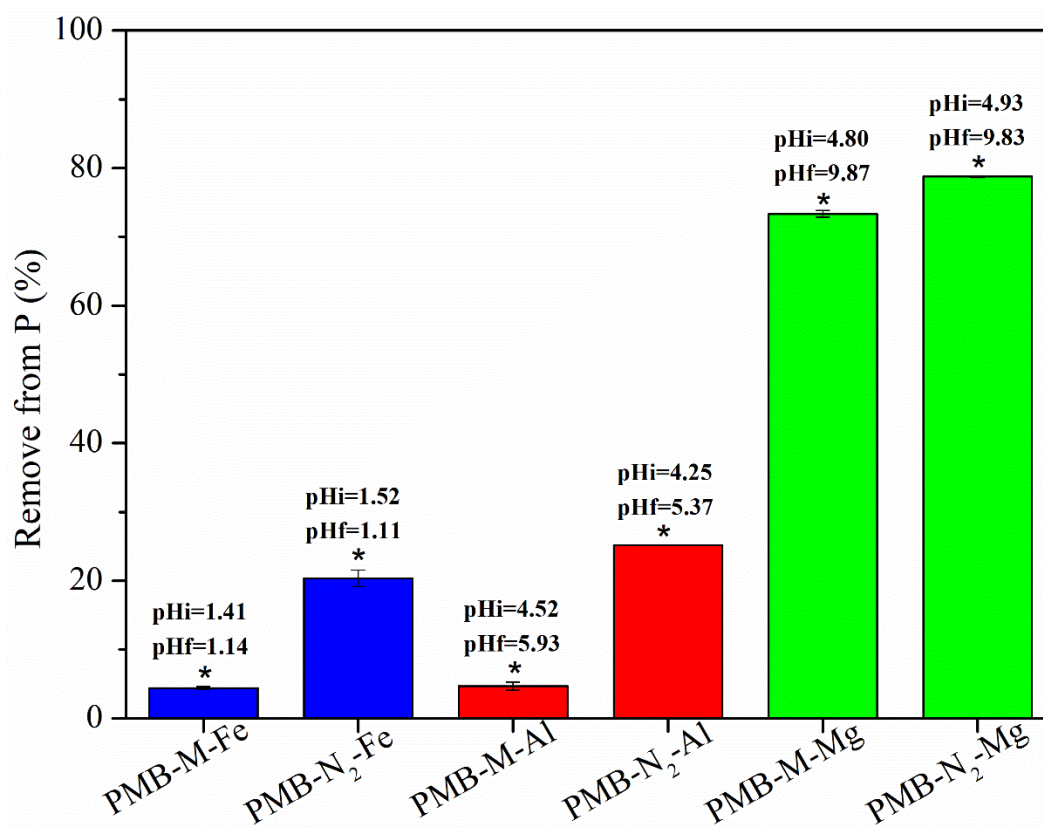


Figure 1. Percentage of phosphorus removal in cation-modified biochar samples. pHi- pH initial; pHf- pH final. Experimental conditions: 5 g L⁻¹ of adsorbent dose and 1000 mL of solution with 500 mg L⁻¹ of P (adsorbate).

Notes: ns - not significant ($p > 0.05$). * Significant at 5% probability by the T-student test ($p < 0.05$). The test compares the pyrolysis conditions (M-muffle and N₂- with N₂ flow), inside each cation-impregnated biochar. Bars are the mean \pm standard error of 2 replicates.

3.3) Phosphorus K-edge XANES analysis

Figure 2 shows the P K-edge X-ray absorption near edge spectra (XANES) obtained from cation-modified and pristine biochar samples. Each XANES spectrum has a striking characteristic used to identify the analyzed material as a “fingerprint” for each neighboring element. The peak of P absorption (maximum peak observed in the spectra of Figure 3) occurs at around 2151 eV, in which an electron is transferred from the innermost 1s orbital to the $t2^*$ orbital with greater energy (Brandes et al., 2007). In fluorescence mode, after excitation of this electron, it decays with the highest energy to the unoccupied orbital 1s and there is the release of photons that are collected by the detector (Vicentin et al., 1999).

The identification and differentiation of the mineral and organic phases that make up the analyzed biochar samples was done by the linear combination fitting (LCF) through the combination of different P standards, that in this study are all in +5 oxidation state. The differentiation of P species is done by identifying specific aspects that may appear in pre-edge or post-edge in relation to the absorption edge (maximum peak of the spectrum) (Ingall et al., 2011).

In almost all biochar samples, P-Ca species (Table 2) were identified, mainly in non-impregnated biochar. Calcium is generally the element that makes up the largest amount of waste and consequently results in biochars rich in this nutrient (Rose et al., 2019). In the pristine biochar samples, the highest P fraction (~60%) was in the form of hydroxyapatite (HA), which is a result of the high Ca content the pig manure (Table S1).

The pyrolysis conditions influenced the P species formed (Figure 2), for instance in the PMB-M only HA and brushite were identified, while in the PMB-N₂ it was found the formation of HA, monetite and P-organic (phosphonate). The carbonization process of the biomass by different methods causes a different transformation of lignocellulose in stable C compounds (Amonette and Joseph, 2009). Inorganic compounds of the feedstock during the pyrolysis process may undergo volatilization during thermal degradation, but most are either incorporated as part of the carbonaceous structure or retained as mineral phases (Chan and Xu, 2009).

The conditions of the pyrolysis process such as temperature, heating rate, residence time of the raw material, gas purging rate, presence of atmospheric O₂, composition of the feedstock,

pressure, cooling rate and heat distribution in the cavity of pyrolysis, cause an initial fractionation in the carbonaceous material releasing gases and forming tar during the thermal degradation in a different way (Schnitzer et al., 2007a; 2007b). The N₂ flow probably changed the internal temperature of pyrolysis during heating or cooling resulting in less condensed C forms like phosphonate (CH₂ – PO₃OH₂).

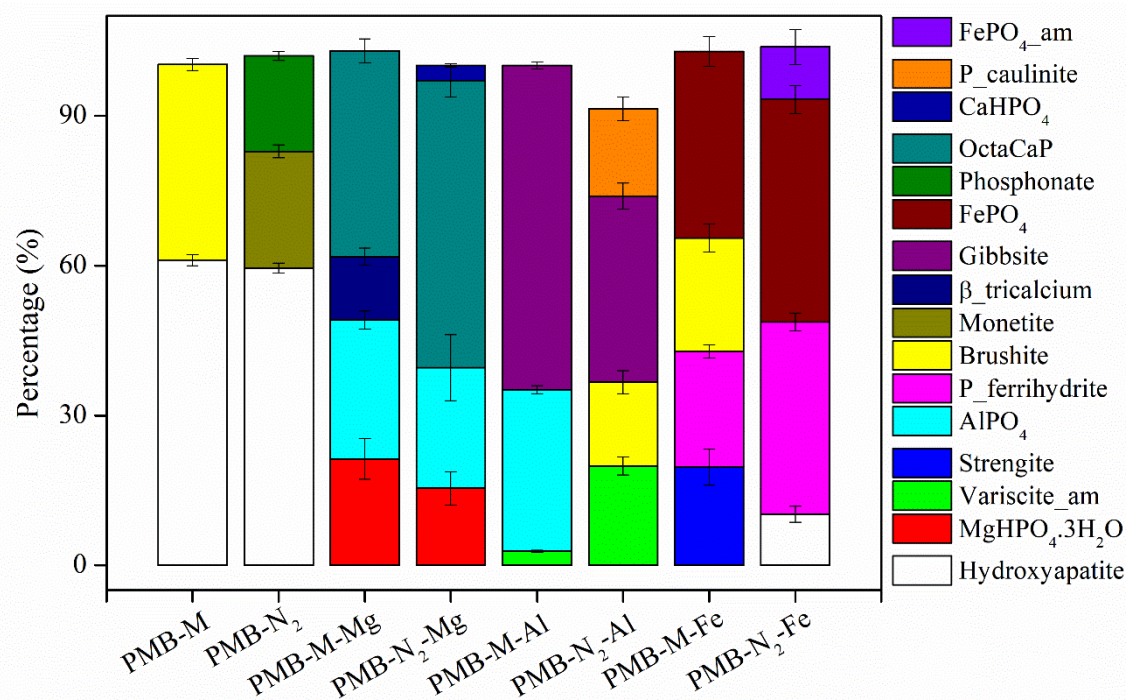


Figure 2. Major P species determined by linear combination fitting of XANES spectra of standards to XANES spectra of biochars from different biochar samples.

The identification of P-Ca compounds is due to the presence of a shoulder in the absorption energy of 2153 eV, and this shoulder is more pronounced in more crystalline phases and lower in amorphous samples (Eveborn et al., 2009). In both PMB-M and PMB-N₂ samples is possible to observe the characteristic shoulder of Ca-containing samples, and the appearance of the spectrum was similar to the hydroxyapatite pattern (Figure 3A and B).

Samples containing Fe in the composition are identified by the presence of a significant pre-white line peak around 2146 eV (Eveborn et al., 2009). This feature was observed only in samples impregnated with Fe (Figure 3E and F). The P-Fe species identified in the PMB-M-Fe were strengite (19%), P sorbed on ferrihydrite (23%) and FePO₄ (37%). It was also identified a Ca-P compound as brushite (22%). For PMB-N₂-Fe, the main P-Fe species were P sorbed on ferrihydrite (38%), FePO₄ (44%) and FePO₄_amorphous (10%). A P-Ca compound was also identified as a minor phase of hydroxyapatite (10%).

Table 2- linear combination fitting results showing proportions of (% of standards) giving the best fit to spectra from biochar samples. Chi² and R-factor values indicate goodness of fit.

Standards	Biochar							
	PMB-M	PMB-N ₂	PMB-M-Mg	PMB-N ₂ -Mg	PMB-M-Al	PMB-N ₂ -Al	PMB-M-Fe	PMB-N ₂ -Fe
Hydroxyapatite	61.1±1.1	59.5±1.0	-	-	-	-	-	10.2±1.6
MgHPO ₄ ·3H ₂ O	-	-	21.3±4.1	15.4±3.3	-	-	-	-
Variscite_amorphous	-	-	-	-	3.3±0.2	19.9±1.8	-	-
Strengite	-	-	-	-	-	-	19.6±3.6	-
AlPO ₄	-	-	27.8±1.8	24.2±6.6	32.4±0.8	-	-	-
P_ferrihydrite	-	-	-	-	-	-	23.2±1.3	38.5±1.8
Brushite	39.2±1.2	-	-	-	-	16.8±2.3	22.7±2.8	-
Monetite	-	23.4±1.3	-	-	-	-	-	-
B_tricalcium	-	-	12.7±1.7	-	-	-	-	-
Gibbsite	-	-	-	-	64.9±0.7	37.2±2.6	-	-
FePO ₄	-	-	-	-	-	-	37.4±3.0	44.6±2.8
Phosphonate	-	19.1±0.9	-	-	-	-	-	-
OctaCaP	-	-	41.2±2.4	57.5±3.3	-	-	-	-
CaHPO ₄	-	-	-	3.0±0.3	-	-	-	-
P_caulinite	-	-	-	-	-	17.5±2.4	-	-
FePO ₄ _amorphous	-	-	-	-	-	-	-	10.5±3.5
R-factor	0.000945	0.001101	0.002253	0.000861	0.001318	0.000555	0.001757	0.0011896
Red-Chi ²	0.0008596	0.0008671	0.0018933	0.0331508	0.0016377	0.0008525	0.0014951	0.0014220

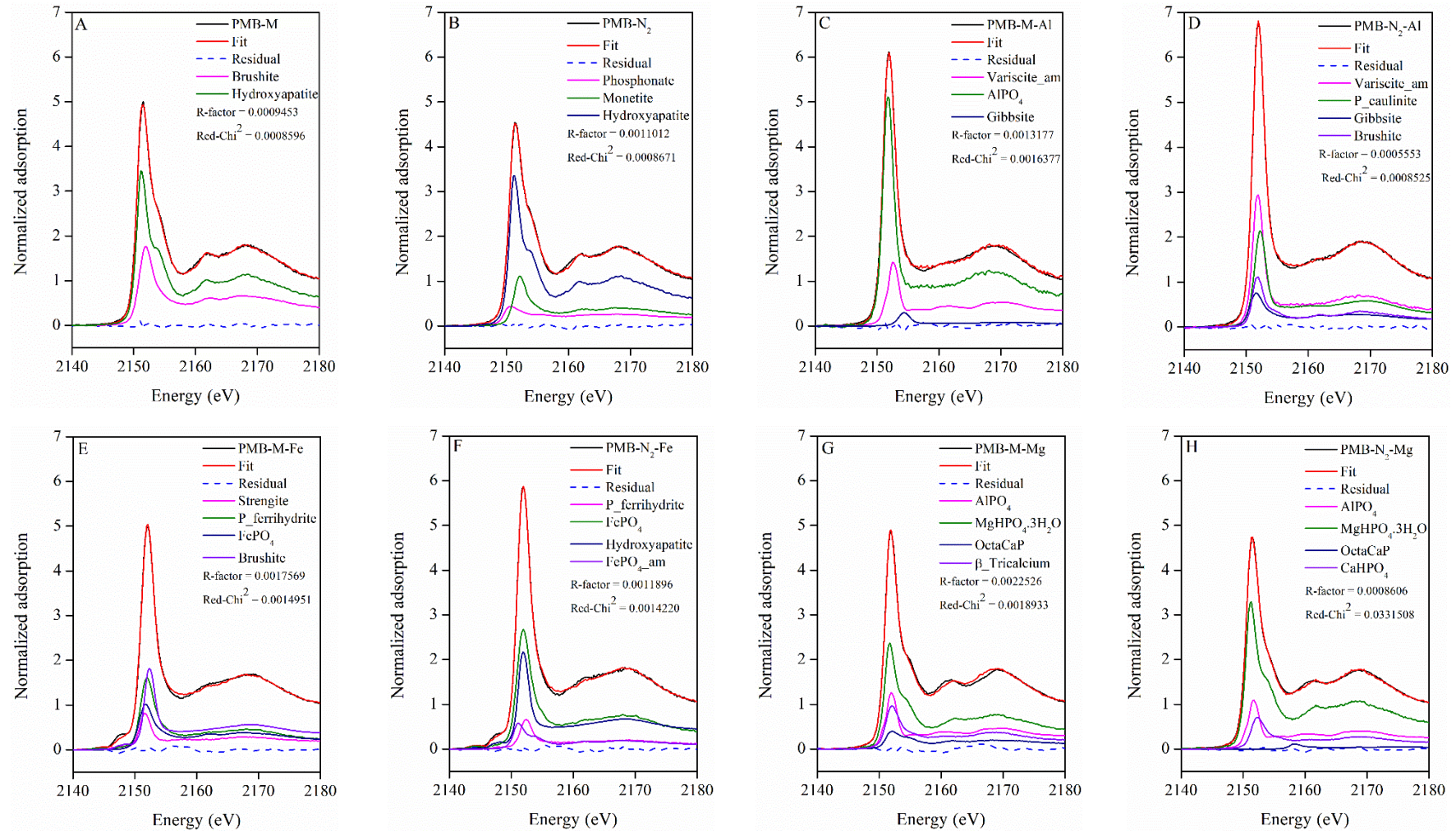


Figure 3- Phosphorus (P) K-edge X-ray absorption near-edge structure (XANES) spectra and best fit from linear combination fitting for biochar samples with the reference compounds. Chi² and R-factor values indicate goodness of fit.

In Al-containing samples, the spectra do not have specific features either in pre- or post-white line that clear distinct the Al-treated samples. Most of the P species associated to Al in PMB-M-Al was observed as P sorbed on gibbsite-like compounds [Al(OH)₃] (64%), followed by AlPO₄ (32%) and a minor amount (3%) of variscite_amorphous. In PMB-N₂-Al, the main species observed were also of P sorbed on gibbsite-like compounds (37%), P sorbed on ferrihydrite (23%), P sorbed on kaolinite (17%) and P-Ca as brushite (16%). For the Al-impregnated samples, the biochar produced in the furnace under N₂ flow resulted in a product with a greater variety of minerals compared to that produced in muffle in which a large portion of the P was adsorbed on gibbsite-like compound.

Finally, although the Ca:Mg ratio was low in Mg-impregnated samples (Table 1), the feature of spectra are similar to P-Ca compounds. There was a widening at the base of the post edge at 2155 eV that is characteristic of compounds analogous to non-crystalline HA (Hilger et al., 2020). The main specie formed was octa-calcium phosphate (OctaCaP - Ca₈H₂(PO₄)₆.5H₂O) (41% in PMB-M-Mg e 57% in PMB-N₂-Mg). As observed by others, in high pH systems, even in the presence of high Mg content and lower amounts of Ca in solution favors the formation of short-range order amorphous P-Ca species, such as OctaCaP (Hilger et al., 2020). Thus, the formation of P-Mg compounds in the presence of Ca is unlikely due to the high solubility of magnesium phosphate minerals. There was a higher percentage of MgHPO₄.3H₂O in PMB-M-Mg (21%) than in PMB-N₂-Mg (15%) (Table 2). Spectra of Mg phosphates (newberite and bobierite) are identified by the intensity of the white line that is shifted +0.5 eV and does not show any post edge characteristics at 2162 eV. A very slight peak can also be observed at 2155 eV (Ingall et al., 2011).

The percentages of the compounds in the samples are obtained by the linear combination fitting (LCF), in which the sample analyzed is modeled with a combination of patterns with known composition and structure (Gustafsson et al., 2020). The analysis of environmental samples using techniques such as XANES has been increasing in recent years, but often due to the complexity of these matrices (e.g. biochars from manure) there are uncertainties regarding the LCF result, especially when the spectrum does not have a characteristic that makes it clearly distinguishable. The more complex a geochemical matrix is the less specific the spectroscopic techniques such as XANES and XRD are to characterize the structure of these matrices (Hesterberg, 2019).

In the former chapter of this thesis, the XRD diffractograms of the same set of samples presented confirm the P species identified by the XANES analysis. However, other mineral phases identified by the XRD are lacking in the XANES technique, since only a limited number of standards can be accurately included in the LCF (Gustafsson et al., 2020).

A question asked by soil scientists using XANES spectroscopy techniques is how to differentiate Ca-phosphate minerals in complex matrix studies, since the appearance of the spectra is very similar (Chien, 2019). X-ray diffraction (XRD) is a technique that is already well founded to define each mineral and allow this differentiation. The identification of crystalline phases is made from angles and beam intensities that, when interacting with the sample, are diffracted in different directions. From this information it is possible to obtain the arrangement of atoms within a crystal and to identify the interplanar spacings (d -spacing) that are specific to each crystalline structure. The length scale of the crystalline structure that is repeated for phase identification is from the scale of tens to hundreds of nanometers. The XANES technique, on the other hand, identify the molecular coordination around P atoms on a scale of several angstroms (Hesterberg, 2019). Another limitation of the XRD technique is that it is not possible to differentiate the adsorbed P from the crystalline P, as well as P-organic forms.

3.4) Phosphorus speciation and agronomic efficiency of biochar

Knowing the destination of the P added to the soil-plant system is important to outline strategies that aim to optimize agricultural production with less environmental impacts. Phosphorus is essential for plant growth and sources to produce soluble phosphate fertilizers are restricted to a few countries. As a result, it is necessary to improve the technologies for recovering P from wastes and wastewaters, since these are in general P-rich matrices and can be optimized for the use in agriculture.

The interest of biochar addition to soil has grown in recent years aiming to increase the carbon sequestration, reduce greenhouse gas emissions, stabilize contaminants in the soil, reduce waste volume, among others (Oni et al., 2019). Biochar mainly influences soil pH, C content, cation exchange capacity and nutrient cycling that directly influence plant growth (Ding et al., 2016). The application of unmodified biochars for the supply of nutrients requires very large amounts to be applied, which makes the process costly and of low efficiency (Bach et al., 2016).

The use of modified biochars with the objective of recovering P from wastewater has grown as well as its application as a phosphate fertilizer (Nardis et al., 2020; Riddle et al., 2019; Riddle et al., 2018). In acidic tropical soils like most Brazilian soils, the application of phosphate fertilizer together with an organic matrix can reduce the adsorption of P in Fe and Al (hydro) oxides (Gerke, 2010).

The biochars produced in this study can be applied to soil to provide P to plants, especially those impregnated with Mg since they had showed the highest P adsorption capacity and can efficiently supply P and Mg to plants (Nardis et al., 2020). The P-loaded Mg-impregnated biochar samples have greater solubility than the Al- or Fe-impregnated ones, which agrees with the species identified by the XANES analysis in the PMB-M-Mg and PMB-N₂-Mg. The main species identified are formed by bases (Mg and Ca) that cause these biochars to have high pH values (9.25). For this reason, these biochars would be recommended for application in tropical acidic soils rich in Fe and Al (hydro)oxides.

Biochars impregnated with Al and Fe, despite not having a high P adsorption capacity, compared to those impregnated with Mg, could be applied in alkaline soils because they are more acidic (Table 1). Although these biochars are not as efficient at removing P, they can function as a stable recalcitrant matrix in which the impregnated metals can be stabilized and reduce leaching of P in alkaline soils or reduce specific adsorption in tropical soils, improving the efficiency of phosphate fertilizers.

Riddle et al. (2018) observed that the application of a magnetite-coated biochar in a column experiment (containing washed sand) delayed the movement of the phosphate through the column. They also observed that only a small proportion of the phosphate (~ 7%) was permanently retained in the biochar.

In effluent treatment plants, Fe and Al salts are used as flocculants to recover nutrients, mainly P. Several materials have been studied in order to improve the efficiency of removing and / or replacing these salts with compounds that can be reused (Xu et al., 2012). The use of these modified biochars can be an alternative to the use of salts and a strategy for the recovery of P in wastewater treatment plants (Pokharel et al., 2020), recovering P that can be reapplied to the soil, favoring a P circular economy and increasing P use sustainability.

Conclusions

The highest phosphate removal in cation-impregnated biochars occurred with Mg, followed by Al, while Fe-impregnated biochar was extremely limited in our study. The XANES results showed that in non-modified biochar Ca-phosphate compounds (mainly hydroxyapatite) prevailed in both PMB-M and PMB-N₂. In the biochars impregnated with Al, there was a predominance of Al-phosphate compounds most being identified as P sorbed on gibbsite or gibbsite-like compounds [Al (OH)₃]. In biochars impregnated with Fe, P-Fe compounds (ferrihydrite and FePO₄) were identified. For the biochars impregnated with Mg, although Mg was in greater quantity than Ca, there was a predominance of P-Ca species such as octacalcium phosphate (OctaCaP) with lesser amounts of P-Mg compounds. The pyrolysis condition influenced both the removal efficiency (greater for those produced under N₂ flow) and the phosphate species formed. This fact was due to the temperature in the biomass core, which resulted in a differentiated degradation of lignocellulose, affecting the mineral and organic content. In conclusion, Mg-impregnated biochar is a sustainable option to add value to organic residues and to recycle P to be reused as enhanced efficiency fertilizer.

Acknowledgements

This research used resources of the Brazilian Synchrotron Light Laboratory (LNLS), an open national facility operated by the Brazilian Centre for Research in Energy and Materials (CNPEM) for the Brazilian Ministry for Science, Technology, Innovations and Communications (MCTIC). The SXS beamline staff is acknowledged for the assistance during the experiments.

References

- Amonette, J.E., Joseph, S., 2009. Characteristics of Biochar : Microchemical Properties, in: Lehmann, J., Joseph, S. (Eds.), *Biochar for Environmental Management: Science and Technology*. pp. 33–85.
- Bach, M., Wilske, B., Breuer, L., 2016. Current economic obstacles to biochar use in agriculture and climate change mitigation. *Carbon Manag.* 7, 183–190. <https://doi.org/10.1080/17583004.2016.1213608>
- Bekiaris, G., Peltre, C., Jensen, L.S., Bruun, S., 2016. Using FTIR-photoacoustic spectroscopy for phosphorus speciation analysis of biochars. *Spectrochim. Acta - Part A Mol. Biomol. Spectrosc.* 168, 29–36. <https://doi.org/10.1016/j.saa.2016.05.049>
- Bradford, S.A., Segal, E., Zheng, W., Wang, Q., Hutchins, S.R., 2008. Reuse of Concentrated

- Animal Feeding Operation Wastewater on Agricultural Lands. *J. Environ. Qual.* 37, 97–115. <https://doi.org/10.2134/jeq2007.0393>
- Brandes, J.A., Ingall, E., Paterson, D., 2007. Characterization of minerals and organic phosphorus species in marine sediments using soft X-ray fluorescence spectromicroscopy 103, 250–265. <https://doi.org/10.1016/j.marchem.2006.09.004>
- Chan, Y., Xu, Z., 2009. Biochar : Nutrient Properties and Their Enhancement, in: Lehmann, J., Joseph, S. (Eds.), *Biochar for Environmental Management Science and Technology*. London, pp. 67–84.
- Chen, W., Ding, Shuya, Lin, Zerui, Peng, Yuanzhen, Ni, Jinzhi, Ding, S, Lin, Z, Peng, Y, Ni, J, 2020. Different effects of N₂-flow and air-limited pyrolysis on bamboo-derived biochars' nitrogen and phosphorus release and sorption characteristics. *Sci. Total Environ.* 711, 134828. <https://doi.org/https://doi.org/10.1016/j.scitotenv.2019.134828>
- Chien, S.H., 2019. Geoderma Letter to the editor on synchrotron-based identification of reaction products in phosphorus fertilized alkaline soils. *Geoderma* 337, 42–43. <https://doi.org/10.1016/j.geoderma.2018.09.013>
- Colocho Hurtarte, L.C., Francisco, S.-F.L., Oliveira, S.W., Vergütz, L., Prietzel, J., Hesterberg, D., 2019. Optimization of Data Processing Minimizes Impact of Self-Absorption on Phosphorus Speciation Results by P K-Edge XANES. *Soil Syst.* 3, 61file:///C:/Users/Barbara/Google Drive/Bárbara Ol. <https://doi.org/10.3390/soilsystems3030061>
- Cui, X., Dai, X., Khan, K.Y., Li, T., Yang, X., He, Z., 2016. Removal of phosphate from aqueous solution using magnesium-alginate/chitosan modified biochar microspheres derived from *Thalia dealbata*. *Bioresour. Technol.* 218, 1123–1132. <https://doi.org/10.1016/j.biortech.2016.07.072>
- Ding, Y., Liu, Y., Liu, S., Li, Z., Tan, X., Huang, X., Zeng, G., Zhou, L., Zheng, B., 2016. Biochar to improve soil fertility. A review. *Agron. Sustain. Dev.* 36, 1–18. <https://doi.org/10.1007/s13593-016-0372-z>
- Enders, A., Lehmann, J., 2012. Comparison of Wet-Digestion and Dry-Ashing Methods for Total Elemental Analysis of Biochar. *Commun. Soil Sci. Plant Anal.* 43, 1042–1052. <https://doi.org/10.1080/00103624.2012.656167>
- Eveborn, D., Gustafsson, J.P., Hesterberg, D., Hillier, S., 2009. XANES speciation of P in environmental samples: An assessment of filter media for on-site wastewater treatment. *Environ. Sci. Technol.* 43, 6515–6521. <https://doi.org/10.1021/es901084z>
- Gerke, J., 2010. Humic (Organic Matter)-Al(Fe)-Phosphate Complexes : An Underestimated Phosphate Form in Soils and Source of Plant-Available Phosphate. *Soil Sci.* 175, 417–425. <https://doi.org/10.1097/SS.0b013e3181f1b4dd>
- Gonzaga, M.I.S., Mackowiak, C.L., Comerford, N.B., Moline, E.F. da V., Shirley, J.P., Guimaraes, D.V., 2017. Soil & Tillage Research Pyrolysis methods impact biosolids-derived biochar composition , maize growth and nutrition. *Soil Tillage Res.* 165, 59–65. <https://doi.org/10.1016/j.still.2016.07.009>
- Gustafsson, J.P., Braun, S., Tuyishime, J.R.M., Adediran, G.A., Warrinnier, R., Hesterberg,

- D., 2020. A Probabilistic Approach to Phosphorus Speciation of Soils Using P K-edge XANES Spectroscopy with Linear Combination Fitting 1–17. <https://doi.org/10.3390/soilsystems4020026>
- Hesterberg, D., 2019. *Geoderma*. *Geoderma* 337, 150–151. <https://doi.org/10.1016/j.geoderma.2018.09.014>
- Hilger, D.M., Hamilton, J.G., Peak, D., 2020. The Influences of Magnesium upon Calcium Phosphate Mineral Formation and Structure as Monitored by X-ray and Vibrational Spectroscopy. *Soil Syst.* 5, 1–13. <https://doi.org/10.3390/soilsystems4010008>
- Ingall, E.D., Brandes, J.A., Diaz, J.M., De Jonge, M.D., Paterson, D., McNulty, I., Elliott, W.C., Northrup, P., 2011. Phosphorus K-edge XANES spectroscopy of mineral standards. *J. Synchrotron Radiat.* 18, 189–197. <https://doi.org/10.1107/S0909049510045322>
- Li, R., Wang, J.J., Zhou, B., Awasthi, M.K., Ali, A., Zhang, Z., Lahori, A.H., Mahar, A., 2016. Recovery of phosphate from aqueous solution by magnesium oxide decorated magnetic biochar and its potential as phosphate-based fertilizer substitute. *Bioresour. Technol.* 215, 209–214. <https://doi.org/10.1016/j.biortech.2016.02.125>
- Liang, X., Jin, Y., He, M., Niyungeko, C., Zhang, J., Liu, C., Tian, G., Arai, Y., 2018. Phosphorus speciation and release kinetics of swine manure biochar under various pyrolysis temperatures. *Environ. Sci. Pollut. Res.* 25, 25780–25788. <https://doi.org/10.1007/s11356-017-0640-8>
- Liu, Y., Chen, J., 2008. Phosphorus Cycle. *Enycl. Ecol. Five-Volume Set* 5, 2715–2724. <https://doi.org/10.1016/B978-008045405-4.00754-0>
- Lustosa Filho, J.F., Penido, E.S., Castro, P.P., Silva, C.A., Melo, L.C.A., 2017. Co-Pyrolysis of Poultry Litter and Phosphate and Magnesium Generates Alternative Slow-Release Fertilizer Suitable for Tropical Soils. *ACS Sustain. Chem. Eng.* 5, 9043–9052. <https://doi.org/10.1021/acssuschemeng.7b01935>
- Malavolta, E., Vitti, G.C., Oliveira, S.A., 1997. *Avaliação do estado nutricional das plantas: princípios e aplicações*, 2nd ed. Potafos, Piracicaba.
- Micháleková-Richveisová, B., Fri, V., Pipí, M., Frišták, V., Pipíška, M., Ďuriška, L., Moreno-Jimenez, E., Soja, G., 2017. Iron-impregnated biochars as effective phosphate sorption materials. *Environ. Sci. Pollut. Res.* 24, 463–475. <https://doi.org/10.1007/s11356-016-7820-9>
- Mobilio, S., Boscherini, F., Meneghini, C., 2015. *Synchrotron Radiation: Basics, Methods and Applications*, 1st ed. Springer, Berlin, Heidelberg. <https://doi.org/https://doi.org/10.1007/978-3-642-55315-8>
- Nardis, B.O., Santana Da Silva Carneiro, J., Souza, I.M.G. De, Barros, R.G. De, Azevedo Melo, L.C., 2020. Phosphorus recovery using magnesium-enriched biochar and its potential use as fertilizer. *Arch. Agron. Soil Sci.* 1–17. <https://doi.org/10.1080/03650340.2020.1771699>
- Ngatia, L., Taylor, R., 2019. Phosphorus Eutrophication and Mitigation Strategies, in: Ohtake, H., Tsuneda, S.. (Eds.), *Phosphorus - Recovery and Recycling*. Singapore, pp. 45–61.

- <https://doi.org/10.5772/intechopen.79173>
- ONI, B.A., OZIEGBE, O., OLAWOLE, O.O., 2019. Significance of biochar application to the environment and economy. *Ann. Agric. Sci.* 64, 222–236. <https://doi.org/10.1016/j.aoas.2019.12.006>
- Pokharel, A., Acharya, B., Farooque, A., 2020. Biochar-Assisted Wastewater Treatment and Waste Valorization, in: Abdelhafez, A.A., Abbas., M.H. (Eds.), *Applications of Biochar for Environmental Safety*. pp. 1–19. <https://doi.org/10.5772/intechopen.92288>
- Ravel, B., Newville, M., 2005. ATHENA, ARTEMIS, HEPHAESTUS: Data analysis for X-ray absorption spectroscopy using IFEFFIT. *J. Synchrotron Radiat.* 12, 537–541. <https://doi.org/10.1107/S0909049505012719>
- Riddle, M., Bergström, L., Schmieder, F., Lundberg, D., Condrón, L., Cederlund, H., 2019. Impact of biochar coated with magnesium (hydr)oxide on phosphorus leaching from organic and mineral soils. *J. Soils Sediments* 19, 1875–1889. <https://doi.org/10.1007/s11368-018-2197-7>
- Riddle, M., Cederlund, H., Schmieder, F., Bergström, L., 2018. Magnetite-coated biochar as a soil phosphate filter: From laboratory to field lysimeter. *Geoderma* 327, 45–54. <https://doi.org/10.1016/j.geoderma.2018.04.025>
- Rose, T.J., Scheffe, C., Weng, Z.H. (Han), Rose, M.T., Zwieten, L. Van, Liu, L., Rose, A.L., van Zwieten, L., Liu, L., Rose, A.L., 2019. Phosphorus speciation and bioavailability in diverse biochars. *Plant Soil* 443, 233–244. <https://doi.org/10.1007/s11104-019-04219-2>
- Schnitzer, M.I., Monreal, C.M., Facey, G.A., Fransham, P.B., 2007a. The conversion of chicken manure to biooil by fast pyrolysis I. Analyses of chicken manure, biooils and char by ¹³C and ¹H NMR and FTIR spectrophotometry. *J. Environ. Sci. Heal., Part B* 42, 71–77. <https://doi.org/10.1080/03601230601020894>
- Schnitzer, M.I., Monreal, C.M., Jandl, G., Leinweber, P., Peter, B., 2007b. The conversion of chicken manure to biooil by fastpyrolysis II. Analysis of chicken manure, biooils, andchar by curie-point pyrolysis-gas chromatography/massspectrometry (Cp Py-GC/MS). *J. Environ. Sci. Heal., Part B* 42, 79–95. <https://doi.org/10.1080/03601230601020944>
- Sharma, A., Hesterberg, D., 2020. 9 - Synchrotron radiation-based spatial methods in environmental biogeochemistry, *Multidimensional Analytical Techniques in Environmental Research*. Elsevier Inc. <https://doi.org/10.1016/B978-0-12-818896-5.00009-0>
- Shepherd, J.G., Joseph, S., Sohi, S.P., Heal, K. V, 2017. Biochar and enhanced phosphate capture: Mapping mechanisms to functional properties. *Chemosphere* 179, 57–74. <https://doi.org/10.1016/j.chemosphere.2017.02.123>
- Singh, B., Camps-Arbestain, M., Lehmann, J., CSIRO (Australia), 2017. *Biochar: A Guide to Analytical Methods*, Csiro publishing.
- Spokas, K.A., 2010. Review of the stability of biochar in soils: Predictability of O:C molar ratios. *Carbon Manag.* 1, 289–303. <https://doi.org/10.4155/cmt.10.32>
- Tan, G., Liu, Y., Xiao, D., 2018. Influence of different pyrolysis methods on the sorption

- property of rice straw biochar. *Sep. Sci. Technol.* 00, 1–10.
<https://doi.org/10.1080/01496395.2018.1553981>
- Vicentin, F.C., Rocha, M.C., Tolentino, H.C.N., 1999. The soft X-ray spectroscopy beamline at the LNLS : Technical description and commissioning results The soft X-ray spectroscopy beamline at the LNLS : technical description and commissioning results.
<https://doi.org/10.1107/S0909049599008122>
- Xu, P., Ming, G., Lian, D., Ling, C., Hu, S., Hua, M., 2012. Use of iron oxide nanomaterials in wastewater treatment : A review. *Sci. Total Environ.* 424, 1–10.
<https://doi.org/10.1016/j.scitotenv.2012.02.023>
- Yao, Y., Gao, B., Inyang, M., Zimmerman, A.R., Cao, X., Pullammanappallil, P., Yang, L., 2011. Removal of phosphate from aqueous solution by biochar derived from anaerobically digested sugar beet tailings. *J. Hazard. Mater.* 190, 501–507.
<https://doi.org/10.1016/j.jhazmat.2011.03.083>
- Zheng, Y., Zimmerman, A.R., Gao, B., 2020. Comparative investigation of characteristics and phosphate removal by engineered biochars with different loadings of magnesium, aluminum, or iron. *Sci. Total Environ.* 747, 141277.
<https://doi.org/10.1016/j.scitotenv.2020.141277>
- Zhu, D., Chen, Y., Yang, H., Wang, S., Wang, X., Zhang, S., Chen, H., 2020a. Synthesis and characterization of magnesium oxide nanoparticle-containing biochar composites for efficient phosphorus removal from aqueous solution. *Chemosphere* 247, 125847.
<https://doi.org/10.1016/j.chemosphere.2020.125847>

CONCLUDING REMARKS

The recovery of P from wastes and wastewaters is a necessity in the current and future scenarios. The implementation of technology aimed at removing P from waste before disposal is already a reality in some European countries, that have launched in 2013 the European Sustainable Phosphorus Platform (ESPP), among other P initiatives worldwide. These initiatives started from the fact that the mineral sources of P are finite and generated discussions on the subject, which consist of studying the extraction capacity, extension of reserves and geographic concentration restricted to a few countries.

Improving sustainability in the use of P is a challenge that must be faced by the whole world, especially in Brazil, since our agriculture is highly dependent on the import of phosphate fertilizers. Moreover, most Brazilian soils under intensive crop cultivation systems are rich in Fe and Al oxyhydroxides, which strongly adsorb P by inner-sphere complex, considerably reducing the P availability for plants.

In this sense, this thesis brings a contribution to better understand the potential of cations-modified biochars to recover P from aqueous solution, the P products formed and their value as a fertilizer. The use of these biochars as P adsorbents has the advantages of being produced from different residues generated on a large scale in the world, such as swine manure, among other waste materials that are difficult to manage and have high environmental pollution potential. They are easy to produce compared to activated carbon that often require sophisticated equipments for activation and their use in agriculture contributes to the circular economy concept. Additionally, we showed that Mg impregnation is more efficient among the studied cations, having a high P adsorption capacity.

Another aspect elucidated in this thesis was the influence of pyrolysis conditions on the modified biochars. It was observed that it is possible to produce efficient biochars without the need for sophisticated equipment or the use of carrier gas, which makes the process less costly and more sustainable. It was also shown that despite having low solubility in water, the modified biochars were able to supply P to maize plants in amounts similar to those grown with conventional sources of soluble phosphates, in addition to providing Mg more efficiently that synergistically increased P uptake.

The use of techniques such as X-ray absorption (XAS) provided important information about the speciation P loaded biochars. This information helps to understand the behavior of P-enriched biochar as fertilizers. The study also showed the difficulty faced by many researchers

when analyzing complex environmental matrices such as biochars. The use of this technique requires expertise and experience by the researcher. Yet, Brazil has excelled in research using synchrotron light and is making a great leap forward with the inauguration of Sirius last year. Sirius will be the second fourth generation light source in the world. However, the techniques available in this facility are not yet widespread in the Brazilian academic community, especially in geosciences and agricultural areas, due mainly to the difficulty for data analysis and processing. In this way, this work is important to increase the community of users qualified to use Sirius and produce high quality research in Brazil.

Additional investigations applying these biochars to the soil should be carried out both in pot and field experiments, in order to assess *in situ* the release of P in tropical soils and what effects they will have on the adsorption of P. It is still necessary to calibrate adequate doses, explore the synergism of P with Mg in plants and the effect of biochars impregnated with Fe and Al in tropical soils.

The results shown here reinforce the Brazil's need to start practicing the circular economy in the recovery of P. We are a continental country with a strong agriculture that produces countless residues that can be reused in agriculture as biochar, being a sustainable way of using nutrients.